DOCTORAL THESIS

Development of Electrospun Nanostructured Electrochemical Double-Layer Capacitor Electrodes

Siret Malmberg

TALLINNA TEHNIKAÜLIKOOL
TALLINN UNIVERSITY OF TECHNOLOGY
TALLINN 2021

TALLINN UNIVERSITY OF TECHNOLOGY
DOCTORAL THESIS
39/2021

Development of Electrospun Nanostructured Electrochemical Double-Layer Capacitor Electrodes

SIRET MALMBERG

TAL TECH PRESS

TALLINN UNIVERSITY OF TECHNOLOGY
School of Engineering
Department of Materials and Environmental Technology
This dissertation was accepted for the defence of the degree 29/06/2021

Supervisor: Prof. Dr. Andres Krumme
School of Engineering
Tallinn University of Technology
Tallinn, Estonia

Co-supervisor: Dr. Mati Arulepp
Skeleton Technologies OÜ
Tallinn, Estonia

Opponents: Prof. Dr. Elzbieta Frackowiak
Institute of Chemistry and Technical Electrochemistry
Poznan University of Technology
Poznan, Poland

Dr. Tarmo Tamm
Faculty of Science and Technology
Institute of Technology
University of Tartu
Tartu, Estonia

Defence of the thesis: 24/08/2021, Tallinn

Declaration:

Hereby, I declare that this doctoral thesis, which is my original investigation and achievement, has been submitted for the doctoral degree at Tallinn University of Technology. It has not been submitted to any other institute for a doctoral degree or an equivalent academic degree.

Siret Malmberg

---
signature

European Union
European Regional
Development Fund

Investing
in your future

ISSN 2585-6898 (publication)
ISBN 978-9949-83-722-9 (publication)
ISSN 2585-6901 (PDF)
ISBN 978-9949-83-723-6 (PDF)
Printed by Koopia Niini & Rauam

TALLINNA TEHNIKAÜLIKOOL
DOKTORITÖÖ
39/2021

Elektrilise kaksikkihi kondensaatori elektrokedratud nanostruktuursete elektroodide arendus

SIRET MALMBERG

Contents

List of Publications 6
Author's Contribution to the Publications 7
Introduction 8
Abbreviations 10
1 Literature review 11
1.1 Introduction 11
1.2 Supercapacitors 11
1.3 Carbon materials for supercapacitors 13
1.4 Carbide-derived carbon 15
1.5 Polymers 16
1.6 Electrolytes for supercapacitors 17
1.7 Electrospinning 19
1.7.1 Grinding of carbon materials 20
1.7.2 Electrospinning of conductive and filler materials 21
1.7.3 Electrospun supercapacitors 22
1.8 Electrochemical evaluation methods for supercapacitors 23
1.9 Summary of literature review and aim of the study 25
2 Experimental section 27
2.1 Materials 28
2.2 Methods 28
2.2.1 Solution and electrode preparation 28
2.2.2 Electrospinning process 29
2.2.3 Characterisation of electrospun CDC-based fibrous electrodes 29
2.2.4 Electrochemical evaluation 30
3 Results and discussion 32
3.1 Development of electrospun fibrous electrode 32
3.2 Stability study of fibrous CDC-based electrodes in various electrolytes 35
3.2.1 Electrochemical stability study of aqueous electrolytes 35
3.2.2 Electrochemical stability of organic electrolytes 38
3.2.3 Electrochemical characteristics of various electrolytes 40
3.3 Electrochemical evaluation of symmetrical cells 43
3.3.1 Electrochemical specification of symmetrical cells 43
3.3.2 Lifetime analysis of symmetrical EDL cells 44
Conclusions 46
List of Figures 47
List of Tables 48
References 49
Acknowledgements 60
Abstract 61
Lühikokkuvõte 63
Appendix 65
Curriculum vitae 111
Elulookirjeldus 112

List of Publications

The list of publications based on which the thesis has been prepared:

I **Malmberg, S**., Arulepp, M., Savest, N., Tarasova, E., Vassiljeva, E., Krasnou, I., Käärik, M., Mikli, V., Krumme, A. (2020) Directly electrospun electrodes for electrical double-layer capacitors from carbide-derived carbon. *Journal of Electrostatics*, vol 103, 103396

II **Malmberg, S**., Arulepp, M., Tarasova, E., Vassiljeva, E., Krasnou, I., Krumme, A. (2020) Electrochemical evaluation of directly electrospun Carbide-derived carbon-based electrodes in different nonaqueous electrolytes for energy storage applications. *C - Journal of Carbon Research*, vol 6 (4), 59

III **Malmberg, S.**, Arulepp, A., Laanemets, K., Käärik, M., Laheäär, A., Tarasova, E., Vassiljeva, E., Krasnou, I., Krumme, A. (2021) The Performance of Fibrous CDC Electrodes in Aqueous and Non-Aqueous Electrolytes. *C - Journal of Carbon Research*, vol 7 (2), 46

Author's Contribution to the Publications

The author's contributions to the three papers in this thesis are as follows:

I. Milling study, solution preparation, electrospinning, preparation of the electrochemical test cells, electrochemical evaluation, and writing of the paper.

II. Preparation of the electrochemical test cells, electrochemical evaluation, and writing of the paper.

III. Preparation of electrochemical test cells, electrochemical evaluation of three-electrode test cells, analysis of three-electrode test cells, and writing of the paper.

Introduction

Renewable energy has gained increasing attention owing to the growing problem of greenhouse gases in recent decades. Several attempts have been made to substitute carbon-containing energy sources with more eco-friendly options, such as wind, solar, and hydro and etc. However, these alternatives cannot meet the overall demand for energy storage. Transportation is one of the most energy-demanding industries; therefore, it is important to substitute combustion engines for EVs at the personal transportation level in order to decrease emissions (Burke & Zhao, 2015; Radu et al., 2019; Stan et al., 2014). Alternative energy sources are constantly being developed to meet the overall demands of the energy storage market. Among the chemical and physical energy storage systems, three systems are considered as potential alternatives for transportation: lithium-ion batteries, fuel cells, and supercapacitors (Winter & Brodd, 2004).

Supercapacitors, which are also known as electrochemical double-layer (EDL) capacitors or ultracapacitors, possess superior properties to those of conventional capacitors, such as a higher energy density over a wide range of power values while exhibiting a long cycle life (Conway, 1999; Y. Wang et al., 2016; A. Yu et al., 2017). Supercapacitors were discovered by General Electric engineers in 1957, while performing tests with porous carbon electrodes in a fuel cell (Becker, 1957). EDL capacitors were commercialised in 1978 by NEC (Conway, 1999). Currently, EDL capacitor electrodes are used as cast electrodes or aqueous slurries. However, in recent years, fibre-based electrodes have been increasingly researched. Fibrous electrodes are useful because of their improved mechanical properties and relatively low electrode thicknesses (≈20 µm), which are several times lower than those of commercial electrodes.

One of the simplest ways to produce fibrous electrodes is electrospinning, which has drawn significant attention for energy storage devices. During the last decade, researchers have proposed several polymer/solvent and polymer/solvent/carbon combinations for energy storage applications (Guo et al., 2009; He et al., 2018; X. Li et al., 2017). However, high EDL capacitance from electrospun nanoporous carbide-derived carbon (CDC) and polymer electrodes has not yet been achieved without applying further post carbonization processes. The purpose of this study was to develop a thin-layered CDC-based fibrous electrode material with the highest possible capacitance and the longest cycle life for energy storage applications.

For this purpose, various combinations of polymer/solvent/carbon, with the addition of ionic liquids (ILs), were tested in electrospinning solutions. The fibrous electrode preparation process was fully optimised to achieve high capacitance in EDL applications with excellent mechanical properties. Furthermore, to improve the electrochemical properties of the electrospun electrodes and to find the best combination of CDC and electrolyte ions, a variety of organic, inorganic, and ionic-liquid-based electrolytes were also tested.

The results of this thesis have been presented additionally to scientific papers at several scientific conferences:

Malmberg, S.; Arulepp, M.; Savest, N.; Käärik, M.; Krumme, A.; (2018). Baltic Polymer symposium, Jurmala, Latvia.

Malmberg, S.; Tarasova, E.; Vassiljeva, V.; Krasnou, I.; Arulepp, M.; Krumme, A. (2018). EDLC Durable Electrodes and Capacitor for High Frequency Applications. SPCD 2018 3rd Space Passive Components Days International Symposium, Noordwijk, Netherlands, 9 - 12 October 2018. EPCI.

Krasonu, I.; Tarasova, E.; Malmberg, S.; Vassiljeva, V.; Krumme, A. (2019). Preparation of fibrous electrospun membranes with activated carbon filler. IOP Conference Series: Materials Science and Engineering, 500, 012022.10.1088/1757-899X/500/1/012022.

Abbreviations

AC	Alternative current
ACN	Acetonitrile
BET	Brunauer–Emmet–Teller
CB	Carbon black
CDC	Carbide-derived carbon
CE	Counter electrode
CNT	Carbon nanotube
CV	Cyclic voltammetry
DMAc	*N*,*N*-dimethylacetamide
DMF	Dimethylformamide
DMSO	Dimethyl sulphoxide
EDL	Electrical double-layer
EIS	Electrochemical impedance spectroscopy
EMIm-BF_4	1-ethyl-3-methylimidazolium tetrafluoroborate
EOL	End of Life
ESR	Equivalent series resistance
EV	Electrical vehicle
GC	Galvanostatic cycling
IL	Ionic liquid
MWNT	Multi-walled carbon nanotube
PAN	Polyacrylonitrile
PANi	Polyaniline
PC	Propylene carbonate
PEO	Poly(ethylene oxide)
PI	Polyimide
PMMA	Poly(methyl methacrylate)
PS	Polystyrene
PSD	Particle size distribution
PVA	Poly(vinyl alcohol)
PVDF	Poly(vinylidene fluoride)
Ref	Reference electrode
SEM	Scanning electron microscopy
SWNT	Single-walled carbon nanotube
TGA	Thermal gravimetric analysis
WE	Working electrode
wt%	Weight percentage

1 Literature review

1.1 Introduction

Nanotechnology has the potential to address global challenges through the design and fabrication of functional nanofibers for energy and environmental applications. The key fabrication method is electrospinning, which is a versatile technique that allows for the preparation of continuous, thin fibres with diameters of a few hundred nanometres (Ding & Yu, 2014). Electrostatic attraction of a liquid was first reported by William Gilbert in the 17th century, and the electrospinning technique was first patented in 1900 by John Francis Cooley (Cooley, 1902; Nascimento et al., 2015; Tucker et al., 2012). The advantages of electrospun fibres are their high surface area, flexibility, and good mechanical properties, thereby rendering them desirable materials for many applications (Ramakrishna, 2005). Owing to the unique properties of electrospun fibres, they have also gained attention in the energy storage industry.

Supercapacitors are energy storage devices that provide fast charge–discharge capability and are considered to be alternative energy sources to combustion engines (Hester & Harrison, 2018). During the last decade, there have been several reports on various combinations of fibrous supercapacitor electrodes; however, none have utilized high-capacity carbide-derived carbon (CDC) and polymer solutions without applying external processing, such as pyrolysis and carbonisation (He et al., 2018; X. Li et al., 2017). Therefore, the present work focuses on the development of electrospun, fibrous, CDC-based electrodes for electrical double-layer capacitor applications in organic and aqueous electrolytes.

1.2 Supercapacitors

Rechargeable batteries are considered promising candidates for electric vehicles; however, the charge-storage mechanism of existing rechargeable batteries is mainly dependent on the intercalation of cations within the crystalline structure of the electrode. Intercalations are regulated by the diffusion of cations within the crystalline framework. In supercapacitors, energy storage is based on surface reactions in the electrode; therefore, they provide a much higher power density than that of batteries (Y. Wang et al., 2016). An EDL was first described and modelled by Von Helmholtz in the 19th century. The Helmholtz double-layer model comprised two layers of opposite charge that form at the electrode–electrolyte interface and are separated by an atomic distance (Helmholtz, 1853; L. L. Zhang & Zhao, 2009). The Helmholtz model was further developed by Gouy and Chapman while considering the continuous distribution of electrolyte ions in the electrolyte solution (Chapman, 1913; Gouy, 1910; L. L. Zhang & Zhao, 2009). In 1991, Brian Evans Conway described the difference between the energy storage mechanisms of supercapacitors and batteries (Conway, 1999).

The high capacitance of EDL capacitors is in the order of hundreds of farads to kilofarads, which is several orders of magnitude larger than those of traditional electrolytic capacitors, whose capacitance is measured in microfarads. With EDL capacitors, high capacitance is possible because of the short charge-separation distance at the electrode–electrolyte interface and the high surface area of the carbon material (Helmholtz, 1853; Ji et al., 2014). The high surface area of the carbon originates from the presence of very small pores on the carbon surface (Figure 1A). The porous matrix of carbon arises from the activation processes. It is very important that the pore size of the

carbon matches the ion size of the electrolyte for sufficient electrolyte ion penetration into the carbon pores (Garche et al., 2013).

The electrochemical device is composed of two electrodes, a separator, and an electrolyte (Figure 1B); the electrolyte can be in either the solid or liquid phase. A solid-state electrolyte has two functions: conduction of ions and separation of the positive and negative electrodes. Liquid electrolyte solutions also conduct ions; however, for the separation of positive and negative electrodes, a porous separator sheet is required (Yu et al., 2017).

Energy storage is created when the polarisation of the electrode ions is absorbed in the double-layer area.

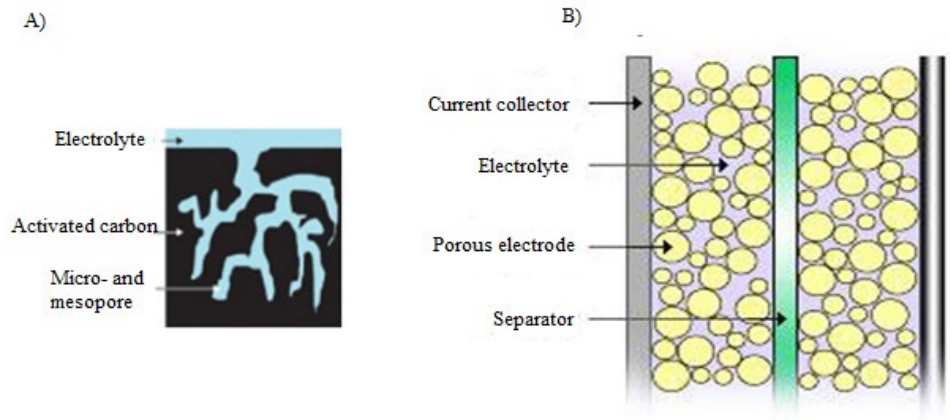

Figure 1. Mechanism of electrical double-layer capacitors (Endo et al., 2001; Frackowiak, 2007; Garche et al., 2013; Pohlmann, n.d.).

In practical applications, supercapacitors are used in the form of a coin-shaped, cylindrical, or prismatic cell and are combined in series into larger modules. Full cells are filled with organic or aqueous electrolytes and are used in high-power applications; however, the cell voltage is limited due to electrolyte decomposition. Organic electrolyte-based cells can provide higher working voltages, but the current is limited by their low ionic conductivity (Garche et al., 2013; Pohlmann, n.d.).

Supercapacitors exhibit superior properties such as long cycle life, low resistance, high power density, and a wide operating temperature range. Although batteries exhibit a higher energy density than that of supercapacitors, their power density does not reach the level of EDL capacitors, as shown in Figure 2. Therefore, an increasing number of investigations have been performed in the last decade to maximize the energy density of supercapacitors.

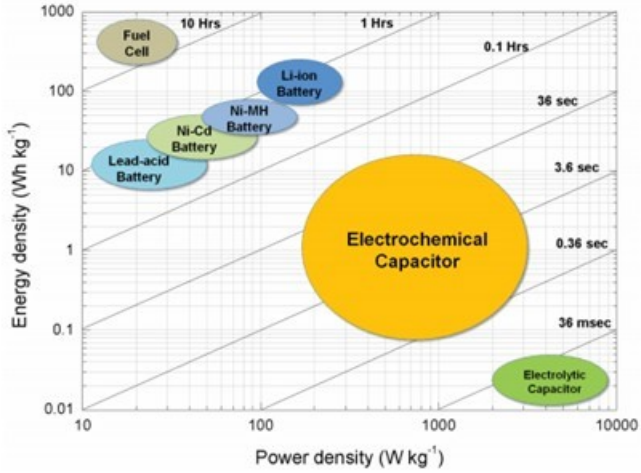

Figure 2. Specific energy vs specific power for energy storage devices (Kumar Panda et al., 2020; S. Zhang & Pan, 2015).

1.3 Carbon materials for supercapacitors

The electrode material is a key element for EDL capacitor performance. Carbon materials have exceptional properties such as a high surface area, good electrical conductivity, low density, high stability, and relatively low cost. Carbon materials have been widely used as electrodes for energy-storage devices. Furthermore, the porosity and morphology of carbon materials can be modified by activation processes (Endo et al., 2001; Frackowiak & Béguin, 2001; Leis et al., 2001; Li et al., 2019). The different structures of carbon materials for supercapacitors are presented in Figure 3.

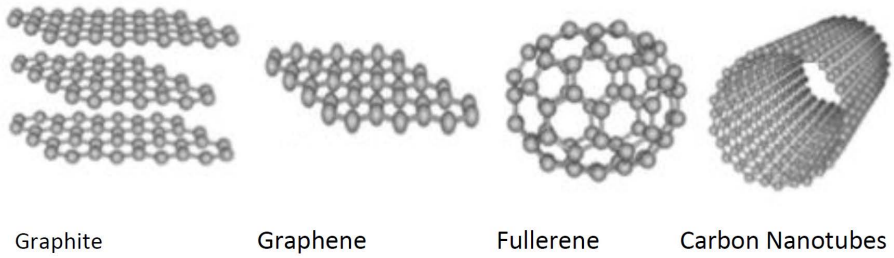

Figure 3. Carbon allotropes used in supercapacitors (Giubileo et al., 2018).

Activated carbon is one of the oldest and most studied porous carbon materials (Sadashiv Bubanale et al., 2017). The basic structural unit of activated carbon is the hexagonal structure of graphite, which occurs in the form of numerous small graphite platelets. The process of activating carbon was discovered in the early 1800s (Sadashiv Bubanale et al., 2017). In today's energy storage industry, most commercial EDL capacitors are based on activated carbon materials owing to their well-known manufacturing processes. The properties of activated carbon rely on its simple, large-scale production and relatively low cost. Activated carbon is produced from nutshells, wood, starch, sucrose, cellulose, corn grain, banana fibre, coffee grounds, and sugar cane bagasse, among other materials. Furthermore, the synthesis of activated carbon enables

well-controlled properties, suitable pore size distribution, and greatly enhanced capacitive characteristics. Carbon can be activated by either physical or chemical activation. In the case of physical activation, carbon materials are first pyrolyzed at high temperatures (600–900 °C) to remove non-carbon elements, and subsequently treated with oxidising atmospheres such as steam, CO_2, or a mixture of the two. Activation by chemical treatment involves impregnation of the carbon precursor with chemicals such as KOH, NaOH, H_3PO_4, $ZnCl_2$, and H_2SO_4, which is followed by carbonisation at 450–900 °C (Sevilla & Mokaya, 2014; L. Wei & Yushin, 2012a).

Activated carbon is commonly used in combination with quaternary ammonium salts in acetonitrile or propylene carbonate solutions. The capacitance of activated carbon reaches 35–250 F g^{-1} in organic electrolytes, 60–150 F g^{-1} in ionic liquids (at high temperatures), and 300 F g^{-1} in aqueous electrolytes (at lower voltages due to water decomposition).

Graphene affords an extremely high electrical conductivity, accessibility to electrolyte ions, relatively low costs, an excellent mechanical strength, and a high surface area (2699 m^2 g^{-1}), rendering it suitable for energy storage devices (Khalid et al., 2018). The existence of graphene was first reported by P. R. Wallace in 1947 (Wallace, 1947); however, it was rediscovered at the beginning of the 21st century. Graphene is a flat, one-layer-thick material comprising sp^2- bonded carbons with a fully conjugated structure of C–C and C=C bonds. However, graphene often requires molecular-level functionalization for most electronic applications. Other forms of graphene such as fullerene, carbon nanotubes (CNTs), and graphite exhibit a similar hexagonal ring structure to that of graphene; however, various orientations are observed in space, giving each form its own unique properties (Khalid et al., 2018).

Fullerenes consist of carbon balls composed of hexagonal and pentagonal carbon rings. The first fullerene was discovered in 1985 by Sir Harold W. Kroto of the United Kingdom and Richard E. Smalley and Robert F. Curl, Jr. of the United States (Kroto, 1997). The small band gaps inside the carbon rings enable fast charge transfer owing to their high conductivity. Using fullerenes as electrode materials enhances the diffusion of ions because of their very high surface area and cage-like structure (Ali et al., 2020a). However, studies on the large-scale production of these materials are still in progress (Ali et al., 2020b; Keypour et al., 2013). Finally, it has been concluded that graphene-based electrode materials usually suffer from poor control of particle size distribution (PSD) with a lack of macropores or large mesopores, which are commonly present in activated carbon or CDC materials (L. Wei & Yushin, 2012a).

CNTs afford good mechanical properties such as high strengths and low weights (Zaharaddeen et al., 2016). They are formed when a graphite sheet is curled up into cylinders and can either be single-walled (SWNT) or multi-walled (MWNTs) (Pan et al., 2010). CNT applications have been widely investigated since their discovery in 1995 (Rinzler et al., 1995). They have been used as electrode materials for supercapacitors, achieving specific capacitances of up to 102 F g^{-1} and 180 F g^{-1} for MWNTs and SWNTs, respectively (Lu & Dai, 2010). However, carbon nanotubes are too expensive for large-scale production, and their long-term stability has not yet been achieved (Wei & Yushin, 2012b; Weinstein & Dash, 2013).

1.4 Carbide-derived carbon

The production of carbide-derived carbon (CDC) using high-temperature chlorine gas and silicon carbide was first described in a patent by O. Hutchins in 1918 (Hutchins, 1918). Larger-scale production was developed in 1956 (Andersen 1956).

In more detail, CDCs are produced by the extraction of metals from carbide precursors at high temperatures. The unique properties of porous CDCs, such as high specific surface area and tuneable pore size with a narrow size distribution, make it an ideal material for supercapacitor electrodes (Gogotsi, 2006; Arulepp et al., 2010; Presser et al., 2011). The advantage of CDC materials is the narrower pore size distribution compared to that of activated carbon.

CDC fabrication is typically used as chlorination at high temperatures. The chlorination of metal or non-metal precursors is described by the following reaction:

$$MC + xCl_2 \rightarrow MCl_{2x} + C$$

In this reaction, the carbon layer is formed by inward growth, usually while retaining the original shape and volume of the precursor. If the remaining reaction products, such as residual chlorides, are trapped in the pores, they can be removed by treatments such as hydrogenation or vacuum annealing. In general, hydrogenation is carried out after chlorination with a temperature equal to or lower than the synthesis temperature. (Presser et al., 2011). For the synthesis of CDC materials, various metal and metalloid precursors, such as TiC, SiC, ZrC, WC, VC, Al_4C_3 and Mo_2C have been used (Ariyanto et al., 2019; Dash et al., 2005; Gudavalli & Dhakal, 2018; Maletin et al., 2004; Leis et al., 2001, 2002, 2010; Yushin et al., 2006).

The characteristics of the synthesised CDC materials are dependent on the chlorination temperature and carbide precursor, which allow for tuning of the pore sizes to 0.6–2 nm (Gogotsi, 2006; Gudavalli & Dhakal, 2018). The model (Zhan et al., 2017) and the structure of the CDC particle, as determined by transmission electron microscopy (TEM) image, are presented in Figure 4. The surface area of CDC can reach up to 2200 $m^2 g^{-1}$ (Leis et al., 2002; Gogotsi et al., 2003; Maletin et al., 2004).

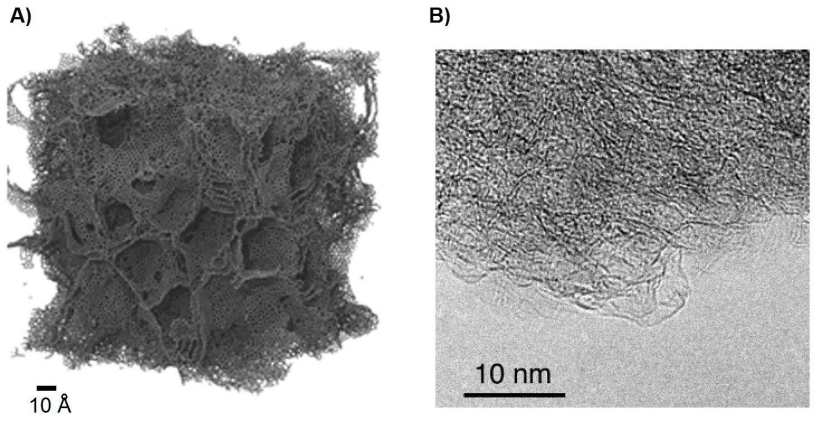

Figure 4. A) Model of the CDC structure (Zhan et al., 2017) and B) TEM image of TiC-CDC (Leis et al., 2002).

The porosity of the CDC is determined by the carbide structure, and the structure of the formed CDC is strongly influenced by the distribution of carbon atoms in the carbide lattice (Presser et al., 2011).

Furthermore, to improve the EDL properties of CDC materials, post-modification processes similar to those of activated carbon are employed (Käärik et al., 2018). In addition, chemical activation by KOH is the most common activation process for CDC. Unfortunately, with chemical activation, relatively high oxygen content occurs inside the material compared to physical processes such as CO_2, steam activation, and a mixture of both. The high oxygen content leads to additional functional groups on the carbon surface, and, in turn, unfavourable Faradaic reactions can occur in parallel with the EDL. The benefits of using CO_2 and H_2O steam are the cleaner production, cost-efficiency, and endothermic nature of their reactions, which allows for better process control. Previously, E. Tee et al. showed that gas-phase activation doubles the Brunauer–Emmett–Teller (BET) surface area and increases the pore size of SiC CDC (Tee et al., 2015). The theoretical capacitance for two-electrode configurations of CDC materials ranges from 60 to 320 F g^{-1} (Inamuddi et al., 2019; Vatamanu et al., 2013; Käärik et al., 2018, 2020). Furthermore, recently Käärik et al. presented mathematical model for characterizing and predicting physical parameters of porous carbon using experiment-derived structure descriptors (Käärik et al., 2018).

1.5 Polymers

Polymers for electrospinning can be categorised into natural and synthetic polymers (Zahmatkeshan et al., 2018). Natural polymers such as collagen, gelatine, and silk are preferred over synthetic polymers in medical and biological applications because of their low immunogenicity and higher biocompatibility (Li et al., 2019). Synthetic polymers are more beneficial than natural polymers because of their superior mechanical properties (Zahmatkeshan et al., 2018). In general, over 100 different types of polymers have been electrospun into nanofibers (Xue et al., 2019).

Poly(ethylene oxide) (PEO, $C_{2n}H_{4n}2O_{n+1}$) is the most commonly used water-soluble polymer. However, of the water-insoluble polymers, polyacrylonitrile (PAN, $(C_3H_3N)_n$), which is soluble in dimethyl sulphoxide (DMSO, C_2H_6OS) and dimethylformamide (DMF, C_3H_7NO), is mainly used. PAN is gaining increasing interest because of its potential as a precursor material for electrospun carbon materials for a variety of applications (Wortmann et al., 2019).

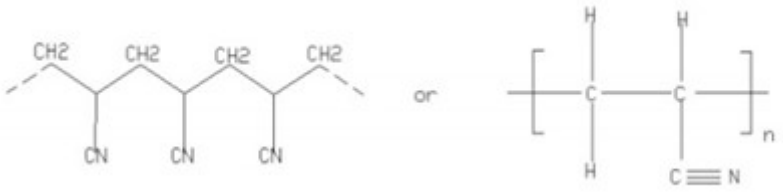

Figure 5. Molecular structure of PAN (Saufi & Ismail, 2002).

PAN is a semicrystalline polymer with a relatively high glass-transition temperature of 100 °C (Sada et al., 2014). The molecular weight of PAN used for electrospinning was 150 000 g mol^{-1}. Regarding its stability against chemical reagents, the nitrile group of PAN

has relatively low reactivity, and thermal oxidation causes the degradation of PAN to carbon fibres (Sada et al., 2014).

As mentioned above, the most important function of PAN as a raw material is to act as a precursor for carbon fibres (Huang, 2009; Liu & Kumar, 2012; Sada et al., 2014). PAN-based carbon nanofibers have remarkable properties such as high tensile strength, low density (less than 2.0 g cm^{-3}), high thermal- and chemical stability, good electrical- and thermal conductivity, and creep resistance. The preparation of PAN-based carbon nanofibers includes four steps: fibre formation by electrospinning, thermal stabilisation at high temperatures (180–300 °C) under an oxidative atmosphere, carbonisation in an inert atmosphere (350–1700 °C) to remove non-carbon particles, and graphitisation at 2000 °C to create a graphitic structure. Currently, 90% of commercial nanofibers are produced from PAN (Sada et al., 2014). PAN-based carbon fibres are used in several applications such as military aircraft, automobiles, and high-grade sporting goods (Sada et al., 2014).

Several aprotic solvents can be used for the electrospinning of PAN-based fibres: DMF, DMSO, *N*,*N*-dimethylacetamide (DMAc, C_4H_9NO), and dimethyl sulphone ($C_6H_{12}O_2S$). Compared with other possible production methods such as vapour growth, arc discharge, laser ablation, and chemical vapour deposition, electrospinning can easily generate nanofibers with diameters ranging from 10 nm to several millimetres by applying an electrostatic force to the polymer solution. PAN-based nanofibers can also be combined with composite materials incorporating CNTs (Song et al., 2013), metal salts (Park et al., 2005), metal complexes (Parekh et al., 2018), and metal oxides (Drew et al., 2005).

1.6 Electrolytes for supercapacitors

Electrolytes are important components in supercapacitor applications and play a crucial role in transferring charges between positively and negatively charged electrodes (Pal et al., 2019). Electrolytes are categorised into various classes, such as organic, aqueous, ionic liquids, solid-state or quasi-solid-state, and redox-active; more specifically, their categorisation is depicted in Figure 6 (Pal et al., 2019; Zhong et al., 2015). The selection of the electrolyte plays a key role in further supercapacitor performance. In addition to its impact on the operating voltage, the electrolyte has a significant influence on the power density, cycling stability, operating temperature, equivalent series resistance (ESR), lifetime, and self-discharge of the capacitor (Wang, 2017). In addition, aqueous-electrolyte-based EDL capacitors have high conductivity and -capacitance; however, they possess low energy density and cycling stability (Zhong et al., 2015). In the case of organic- and IL-electrolyte-based supercapacitors, the operating voltage is significantly higher than that of aqueous electrolytes; however, they suffer from low ionic conductivity and high toxicity (Zhong et al., 2015).

Overall, an ideal electrolyte for EDL applications should exhibit important characteristics: high electrochemical stability, broad electrochemical potential range, wide working-temperature range, high ionic conductivity, high polarity, low viscosity, environmental friendliness, low flammability, and low cost (Pal et al., 2019; F. Wang, 2017). However, in reality, no single electrolyte can meet all these performance requirements. Besides the cycle life (or lifetime), energy density and power density are the two most crucial properties in the evaluation of electrochemical energy devices and are also strongly influenced by the selection of the electrolyte (Zhong et al., 2015). Because both the energy and power densities of a supercapacitor depend on the square

of the cell voltage (see equations 1 and 2), the development of electrolytes proceeds in the direction of increasing operating voltage (Suresh et al., 2017; Zhong et al., 2015).

$$E = \frac{CU^2}{2}, \quad (1)$$

where *C* is the capacitance and U is the cell voltage.

$$P = \frac{E}{t}, \quad (2)$$

where *E* is the energy and *t* is the time (Wu and Cao, 2018).

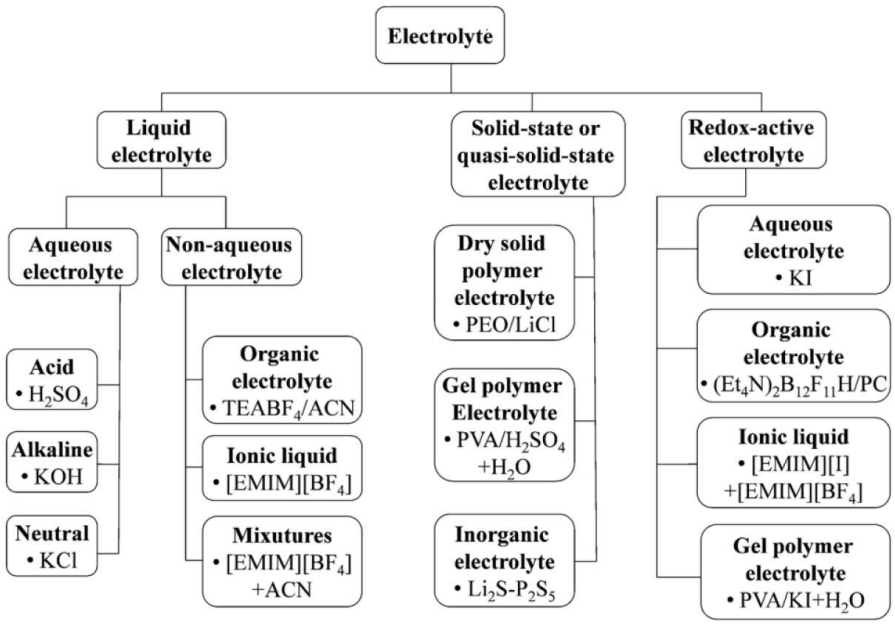

Figure 6. Categorization of electrolytes (Zhong et al., 2015).

Aqueous electrolytes are appealing because of their low cost and simple manipulation (no need for a controlled environment). Typically, three types of aqueous electrolytes are used: acidic (H_2SO_4, etc), neutral salt (Na_2SO_4, etc), and alkaline (KOH, etc) (Béguin et al., 2014; Frackowiak, 2007; Ibukun & Jeong*, 2019; Zhong et al., 2015). The specific capacitance of carbon in aqueous electrolytes ranges from 100–300 F g^{-1} and is highly influenced by the size of the electrolyte ions inserted into the pores of carbon (Ibukun & Jeong*, 2019). Depending on the electrolyte type, the ionic radius of the electrolyte can vary significantly, especially in the case of hydrated ions. In addition, the hydrated ionic radius of H^+ in H_2SO_4 is the smallest (2.80 Å), and that of K^+ in KOH is the largest (3.31 Å) (Jeong 2019). The major disadvantage of aqueous electrolytes is their narrow electrochemical stability window of 0 – 1.23 V as a result of water decomposition (Balducci et al., 2007; Inamuddin et al., 2019; Stan et al., 2014; Vatamanu et al., 2013).

Organic electrolytes mostly consist of quaternary ammonium salts mixed with organic solvents such as acetonitrile (ACN) or polycarbonate (PC) (Arulepp et al., 2004; Brazis et al., 2010; Libich et al., 2018; Ue et al., 1994). Acetonitrile-based electrolytes are known to have higher conductivity and lower viscosity than PC-based electrolytes (Balducci et al., 2007). Although PC-based electrolytes have lower levels of toxicity and higher flash points,

ACN-based electrolytes are preferred because they have a much higher power density (Arulepp et al., 2004; Béguin et al., 2014). Furthermore, because of the wider operating voltage (maximum operative voltage between 2.5–3.0 V) compared to aqueous electrolytes, organic electrolytes are mostly used in commercial products (Brazis et al., 2010; Libich et al., 2018). The capacitance range for carbon materials in organic electrolytes is 50–190 F g^{-1} (Béguin et al., 2014; Käärik et al., 2020). The major disadvantage of organic electrolytes is the complex manipulation process required to protect them from moisture.

ILs are organic salts composed of asymmetric cations, which are usually bulkier than anions. ILs occur in liquid form over a broad range of temperatures, including room temperature and below. As electrolytes, they operate under a wide working potential, ranging from 2 to 6 V (Mishra et al., 2020). Despite their wide potential window, ILs are expensive, and because of their relatively high viscosity, they tend to outperform at low capacitance and high resistance. However, recent developments have shown that the high viscosity of ILs can be mitigated by using ILs in solution with organic electrolytes (Mishra et al., 2020). Similar to organic electrolytes, IL-based electrolytes are also extremely sensitive to moisture, which can drastically affect their stability and conductivity (Pohlmann et al., 2013; Shahzad et al., 2019; L. Yu & Chen, 2019).

1.7 Electrospinning

Electrospinning is a versatile and efficient process for producing continuous nanofibers with diameters ranging from submicron to nanometre by applying a high-potential electric field (Karakaş, n.d.). The advantages of electrospun nanofibers are high flexibility, higher surface area compared to regular fibres, and outstanding mechanical properties (Ding & Yu, 2014; Karakaş, n.d.; Ramakrishna et al., 2006). With electrospinning, it is possible to produce nanofibers of different materials in various fibrous assemblies (Ramakrishna et al., 2006). Electrospinning is highly attractive both at the lab scale and at the industry level owing to the simplicity of its setup (Karakaş, n.d.; Ramakrishna et al., 2006). In the electrospinning process, a variety of nanofibers can be fabricated for applications in energy storage (Malmberg et al., 2020; A. Yu et al., 2017), healthcare (Babitha et al., 2017), biotechnology (Doyle et al., 2013), and environmental engineering (Doyle et al., 2013).

Electrospinning and electrospraying processes are based on the same physical and electrical mechanisms. However, the main difference is that continuous fibres are formed in electrospinning, whereas small droplets are produced by electrospraying (Karakaş, n.d.). The electrospinning setup at the lab scale consists of a syringe, syringe pump, power supply, and current collector, where the current collector can either be static or rotating. One electrode of power supply is connected to the needle tip of the syringe containing the polymer solution, and the second electrode is attached to the rotating and grounded collector. When a DC voltage is applied, the charge repulsion on the fluid surface causes a force directly opposite to the surface tension of the fluid itself. After the increase of the electric field, the hemispherical surface of the fluid at the tip of the syringe elongates and assumes a conical shape known as the “Taylor cone”. Afterwards, a charged fluid jet is ejected from the tip of the cone. Solvent evaporation takes place on the rotating collector, and fibre formation occurs on the conducting substrate (Aussawasathien, 2006; Karakaş, n.d.; Y. Wang et al., 2016). The electrospinning process (Figure 5) is influenced by several parameters, such as applied voltage, distance between the syringe tip and collector,

solution pumping rate, temperature, solution viscosity, and polymer molecular weight (Korycka et al., 2018).

When the viscosity of the solution is too low, electrospray can occur, causing polymer particles to form instead of fibres. Furthermore, the formation of the beaded fibres tends to occur more often in the case of low solution viscosity ('Electrospinning Archives', n.d.).

The applied voltage has a significant influence on the jet stability and fibre morphology, and the solution conductivity is influenced by the polymer type, solvent, and availability of ionisable salts. With an increase in the electrical conductivity of the solution, a significant decrease in the fibre diameter of the electrospun nanofibers occurs ('Electrospinning Archives', n.d.; Karakaş, n.d.).

Furthermore, the electrospinning process is affected by the distance between the syringe tip and collector. The distance has a significant influence on the deposition time, evaporation rate, and instability interval. It has been shown that a sufficient distance is needed to allow time to stretch and dry the electrospinning solution before its deposition onto the substrate, since beads or liquid films would appear if the distance is too short or too long ('Electrospinning Archives', n.d.; Junoh et al., 2015; Karakaş, n.d.).

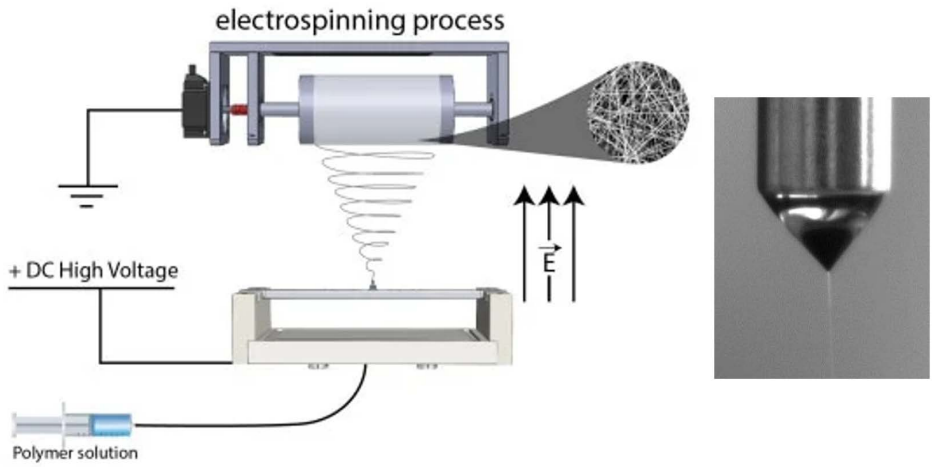

*Figure 7. (Left center) Scheme of electrospinning process (Junoh et al., 2015). (Right) Formation of a Taylor cone (*Electrospinning - CEST - Laboratory Equipment*, n.d.).*

1.7.1 Grinding of carbon materials

For EDL fibrous electrode fabrication, it is important to use carbon with a small particle size (<1 µm). The grinding process of carbon materials improves the formation of conductive networks among carbon particles, binders, and current collectors. The initial particle size of the TiC-based CDC is approximately 1–5 µm. Prolonged milling and sieving are options for producing micron-sized TiC powders (Dyatkin et al., 2016). Various grinding methods exist for carbon materials, such as jet-milling, ball-milling (Dyatkin et al., 2016), planetary ball-milling (Lyu et al., 2017), and others.

Ball-milling is an efficient approach for reducing the particle size of solids to the nanoscale and is widely used in large-scale production processes owing to its low cost, flexibility, and effectiveness (Lyu et al., 2017). In a planetary mill, the vessels are placed on a rotating disk and rotate around their own axes. The size of the vessels is an important parameter for the efficiency of the process, as a higher distance allows for a higher kinetic

energy and thus stronger impacts (Piras et al., 2019). The ball-milling process and its methodology are presented in Figure 4. The conditions of the milling process have a significant influence on the surface area and pore structure of the obtained carbon material (Welham et al., 2002).

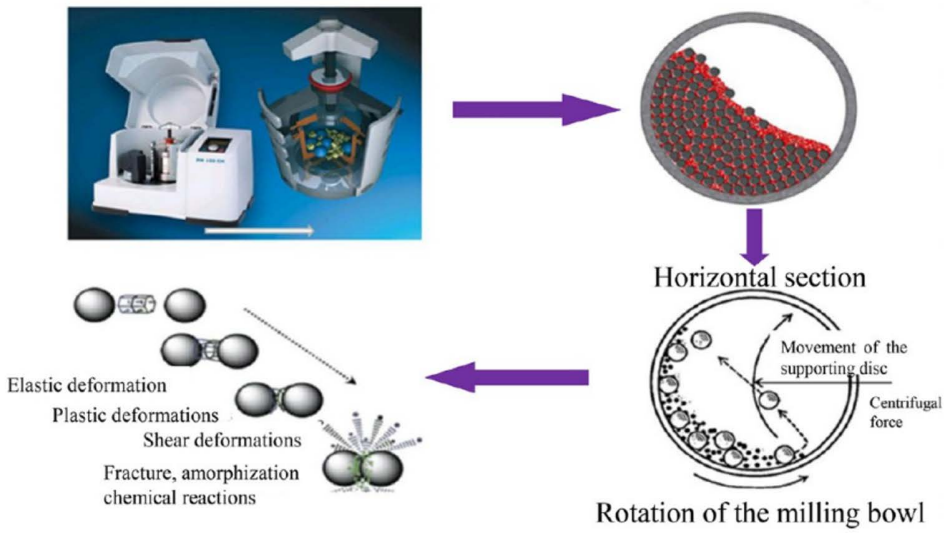

Figure 8. Principle of the ball-milling method (Lyu et al., 2017).

1.7.2 Electrospinning of conductive and filler materials

Electrospun fibres can be functionalized by applying additives and nanosized fillers to the electrospinning solution. Solution-based electrospinning is preferred for the electrospinning of filler materials because greater amounts of filler can be injected by wet electrospinning compared to melt spinning, and dispersion can be achieved in a variety of ways for wet processes (Ahn et al., 2020). CNTs are often used as filler materials in PAN-based nanofibers (Heikkila & Harlin, 2009; Wan et al., 2007; Ye et al., 2004). Generally, CNTs are used as reinforcement components; however, they can also be used to modify the electrical properties of the produced nanomaterials (Jeong et al., 2006; Seoul et al., 2003).

The use of filler materials in the electrospinning solution may influence the fibre-forming process. In addition, fillers can act as charge carriers in the electrospinning solution, causing an increase in the conductivity of the solution, which in turn increases the charge density of the jet and enhances instability during the electrospinning process (Heikkila & Harlin, 2009). Overall, the increase in solution conductivity is reflected in two opposite ways: first, it can cause an increase in the solution flow rate, which leads to a larger fibre diameter; and second, an increase in the net charge density may occur, leading to instabilities, enhancing the whipping stability, and decreasing the fibre diameter (Heikkila & Harlin, 2009; Qin et al., 2007; Zheng et al., 2014).

The effects of fillers and additives on fibre properties vary from system to system depending on the polymer, solvent, and additive (Heikkila & Harlin, 2009).

Additionally, carbon black (CB) is used to form conductive nanofibers. CB is a polycrystalline material in which spherical carbon particles are obtained by the incomplete combustion or pyrolysis of hydrocarbons entangled in grape-like clusters. CB has the advantages of high dispersibility, good processability in mixtures, and low cost (Ahn et al.,

2020; Donnet, 1993). Several studies have focused on the electrospinning of CB fillers using different types of polymer matrices; however, produced fibres tend to have poor mechanical properties due to fibre agglomerates, even if they exhibit high conductivity. Therefore, it is necessary to develop composite nanofibers with high tensile strength and high electrical conductivity (Ahn et al., 2020).

Additionally, CNT and CB filler materials have also been studied using activated carbon or graphene particles in the electrospinning solution. Graphene-based electrospun nanofibers have enhanced mechanical, electrical, and morphological properties with increased diameter and/or porosity. Several studies have demonstrated the successful use of graphene and activated carbon as filler materials for nanofibers (Javed et al., 2019; Tõnurist et al., 2014).

1.7.3 Electrospun supercapacitors

High porosity, low density, and facile incorporation of various components into a single nanofiber can be achieved by electrospinning; therefore, it is an attractive means to produce nanomaterials with high reproducibility and simplicity for energy storage applications (Miao & Liu, 2019, p. 2). The latest developments in electrospun electrodes can be categorised into three groups based on their charge-storage mechanism: EDL capacitive materials, pseudocapacitive materials, and hybrid materials (Miao & Liu, 2019).

Carbon nanofibers with good mechanical, thermal, and electrical properties are suitable for energy storage applications. In the case of CNTs, the main precursor materials are PAN, polyimide (PI), poly(vinylidene fluoride) (PVDF), poly(vinyl alcohol) (PVA), and cellulose, which can be converted into carbon nanofibers by carbonisation at high temperatures. To enhance their properties for energy storage applications, poly(methyl methacrylate) (PMMA) and polystyrene (PS) are used as sacrificial phases and removed after heat treatment to increase the surface area of the microporous and mesoporous structures of the produced nanofibers (Mao et al., 2013; Miao & Liu, 2019). Additionally, other activation processes through various gaseous species, such as carbon dioxide, carbon monoxide, and methane, can be carried out during the high-temperature carbonisation of carbon nanofibers to enhance their properties. In general, carbon nanofibers exhibit a surface area of 1000–2000 $m^2\ g^{-1}$ and pore size distribution in the range of 2–5 nm, with a gravimetric capacitance of 100–120 F g^{-1} in organic electrolytes (K. Wei & Kim, 2014).

CNTs are often used to increase specific capacitance and energy. By applying mechanical reinforcement materials to carbon nanofiber/CNT composites, the properties of such electrode materials become suitable for energy storage applications. Guo et al. showed that hybrid carbon nanofibers containing CNTs produced by electrospinning, followed by carbonisation and activation using mixed hydrogenperoxide/water steam at 650 °C, reached a capacitance of up to 310 F g^{-1} in aqueous 1.0 M H_2SO_4 electrolyte (Guo et al., 2009). Additionally, CNT-activated carbon materials can also be used as filler or capacitive components in nanofibers for energy storage applications. However, there are only a few studies on the use of activated carbon in combination with electrospun fibres. Tõnurist et al. successfully proposed a multistep electrode preparation method by electrospinning commercial activated carbon for energy storage applications (Tõnurist et al., 2014).

Composite electrode materials with carbon nanofibers are also composed of conductive polymers, of which polyaniline (PANi) is the most promising. However, one of the main disadvantages of PANi-based fibres in supercapacitor applications is their poor

cyclability, which is generally mitigated by the addition of CNTs, graphene, and carbon aerogels to electrode materials (Miao & Liu, 2019). Yan et al. reported a composite PANi/carbon nanofiber electrode with a specific capacitance of up to 638 F g^{-1} in an aqueous 1.0 M H_2SO_4 electrolyte (Yan et al., 2011).

In addition to carbon composite materials and conductive polymers, electrode materials from nanofibers can also be composed of metal oxides containing Ni, Co, Cu, and Ag. The capacitance level of metal-doped, nanofiber-based electrode materials can reach very high values; for example, that of carbon nanofiber–Co can reach 911 F g^{-1} in aqueous 1.0 M H_2SO_4 electrolyte. However, such composite electrode materials are relatively expensive owing to their large production scale (Miao & Liu, 2019).

1.8 Electrochemical evaluation methods for supercapacitors

An electrochemical double-layer is established whenever an ionically conducting phase, electrolyte solution, and electronically conducting phase, metal, or carbonaceous surface, are brought into contact (Bärtsch et al., n.d.; Ge et al., 2020). To evaluate the performance of the solid/electrolyte interface system, three classical electrochemical evaluation methods are commonly used: cyclic voltammetry (CV), electrochemical impedance spectroscopy (EIS), and galvanostatic cycling (GC).

CV is a technique that measures the current that develops in an electrochemical cell under conditions in which the voltage is in excess of that predicted (Rajendran, 2016). The CV method is generally used to investigate the reduction and oxidation processes of molecular species. In addition, CV enables the investigation of chemical reactions, which includes catalysis (Elgrishi et al., 2018). By applying a constant voltage scan rate dU/dt, an ideal capacitor should provide a constant current in the CV (Bärtsch et al., n.d.).

The output of the electrochemical test method strongly depends on the unit cell configuration, which is divided into two categories: three- or two-electrode configurations (Stoller & Ruoff, 2010). A three-electrode configuration is commonly used to evaluate the performance of an electrode material or electrolyte and consists of a working electrode, reference electrode, and counter electrode. It is important to note that in a three-electrode configuration, only the working electrode is analysed. In a two-electrode configuration, the each electrode is analysed (Stoller & Ruoff, 2010). Examples of CV measurements with three- and two-electrode configurations are shown in Figure 9.

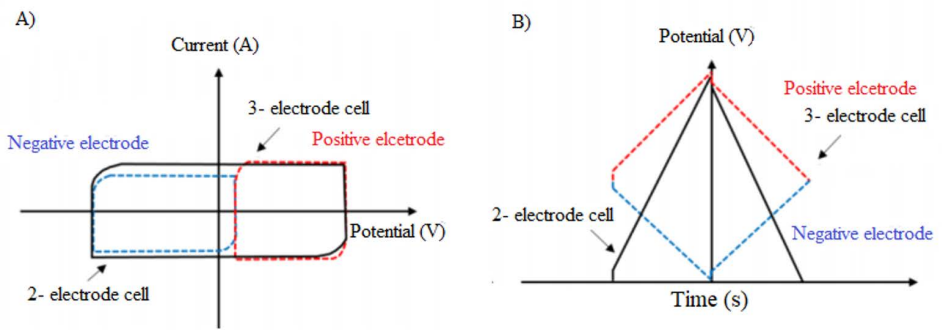

Figure 9. Examples of two- and three- electrode cell configurations: A) current vs. potential and B) potential vs. time performance (Shao et al., 2018).

EIS is a relatively powerful technique for characterising materials and interfaces and is capable of measuring impedance over a wide range of frequencies (between 10^{-6} Hz and 10^{9} Hz). EIS helps to determine the electrical properties of heterogeneous systems, such as membrane–electrolyte or composite membrane systems. It enables the electrical contribution of each sublayer to be estimated separately using impedance plots and equivalent circuits as models, where the different parts of the circuit are related to the structural transport properties. EIS measurement data are analysed by the complex plane method using a Nyquist plot ($-Z_{img}$ vs Z_{real}) (Asaka, 1990; Benavente, 2005; Benavente et al., 1998). For porous electrode materials, Nyquist plots typically consist of three regions: a small, depressed semicircle at higher alternating current (AC) frequencies (R_{AB}); a porous region with a nearly –45° slope (R_{BC}); and a double-layer capacitance region with a slope of −90° (R_C in Figure 10). The semicircle describes the electrolyte resistance, which consists of the contact resistance of the carbon/metal collector and the electrolyte resistance in the separator. The porous region describes double-layer charging in mesopores, and the double-layer region describes the charging of the carbon micropores (Mei et al., 2018). An example of a Nyquist plot is shown in Figure 10.

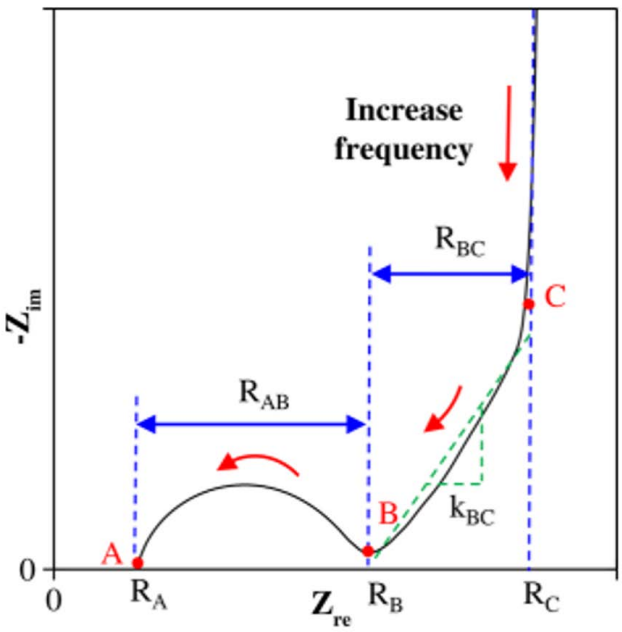

Figure 10. Nyquist plot of typical EDL device (Mei et al., 2018).

Galvanostatic cycling is the accepted measurement method for determining the capacitance of commercial supercapacitors and is thus more closely related to how applications typically apply an electrical load to the supercapacitor. In the GC method, after charging the capacitor with a power source, the capacitor is discharged over a known resistor or with a power supply, and the evolution of the current and voltage is monitored (Bärtsch et al., n.d.; Stoller & Ruoff, 2010). An example of a galvanostatic curve describing the dependence of the current and voltage behaviour during cycling is presented in Figure 11.

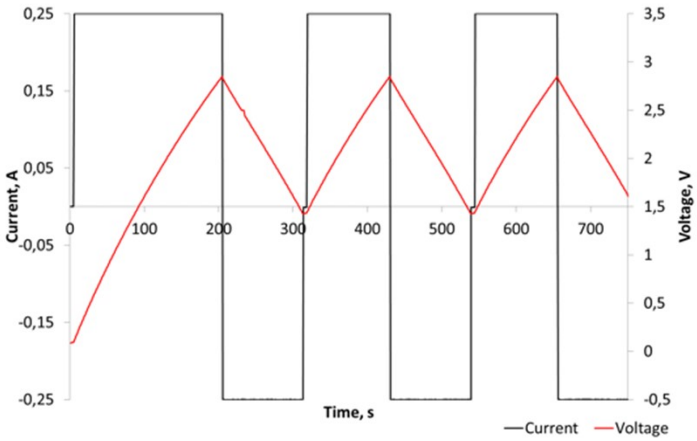

Figure 11. Current and voltage curves of EDL capacitors during constant current charge–discharge.

1.9 Summary of literature review and aim of the study

Supercapacitors are energy storage devices with a long cycle life and fast charge–discharge capability. Traditional supercapacitor electrodes are fabricated in the form of films, activated carbon slurries, or carbon fabrics. In recent years, thin-layered electrodes have gained increasing interest and importance. Such materials have profound benefits in mechanically demanding applications, such as wearable devices, smart textiles, and space applications. Therefore, a targeted balance must be achieved between the mechanical, electrical, and electrochemical properties of the electrodes. Existing commercial electrode technologies lack compatibility in such applications because of their limited mechanical properties and high cost.

Electrospinning is a powerful method for producing nanofibers with versatile properties. The electrospinning process has strong potential not only for lab applications but also for larger production scales. Parameters such as solution properties, processing, and ambient parameters of electrospinning play a crucial role in achieving a stable and uniform fibre-forming process. Various polymers and additives can be used to achieve the desired properties of electrospun fibres. PAN is one of the most commonly used polymers for electrospinning owing to its versatility. Recently, PAN has gained interest because of its potential as a precursor material for the electrospinning of carbon materials for applications such as energy storage. For energy storage, one of the most important properties is the high surface area of the electrodes used. Carbonaceous additives such as CDC, CNTS, and graphene have been used to increase the surface area of electrospun fibres. CDC is known for its versatile properties, such as a narrow pore-size distribution and high surface area (>1000 $m^2 g^{-1}$). For EDL applications, it is important to match the carbon pore size with the ion size of the electrolyte, ensuring access to the carbon surface by having a sufficient amount of transport channels, and, with decreasing distance between charges, in the double layer.

The aim of this study was to develop a thin-layered, CDC-based fibrous electrode material with the highest possible capacitance and long cycle life suitable for energy storage applications, without the use of any destructive post-treatment processes. To accomplish this, it was important to determine the balance between the capacitance

and the mechanical properties of thin-layered fibrous electrodes. The following objectives were set:

- To develop a new procedure for the preparation of directly electrospun, CDC-based fibrous electrodes with improved mechanical properties without further processing (etc pyrolysis, carbonization).
- To determine the optimum electrode composition for achieving a balance between the electrochemical and mechanical properties of the nanofiber-based electrodes.
- To determine the influence of aqueous and organic electrolytes on the capacitance and ESR of the electrospun fibrous electrodes.
- To understand the influence of aqueous and organic electrolytes on the power and energy densities of the fibrous electrodes.

The following activities were performed to accomplish these objectives:

- The effects of various ratios of CDC/CB were studied in terms of the composition of electrospun fibrous electrodes.
- The effects of mechanical densification of electrospun fibrous mats were studied.
- The morphology, porosity, and mechanical, thermal, and other properties of electrospun fibrous electrodes were studied.
- The electrochemical performance of fibrous electrodes in aqueous and non-aqueous electrolytes was studied in three- and two-electrode configurations.

2 Experimental section

This chapter provides an overview of the materials used in the present work, as well as the processing and analysis methods applied to evaluate the properties of the CDC-based fibrous electrospun electrodes. As previously stated, the main purpose was to develop thin-layered, durable, CDC-based composite fibrous electrodes without applying any destructive carbonization processes, which change the composition of the fibres or diminish their mechanical properties. Various electrode compositions and their mechanical properties were studied before the optimum fibre composition was achieved. In addition, various electrode–electrolyte combinations were investigated for developing a thin-layered, durable EDL. An overview of the materials and methods used in this PhD thesis is presented in Table 1.

Table 1. Materials and methods (used in the work)

Materials	Studied aspects	Characterisation methods	Aim of the paper	Paper
Polymer: PAN *Solvent*: DMF *Additives*: CDC, CB, $EMImBF_4$ *Electrolyte*: $TEMABF_4$/ACN	CDC/CB content variation, densification of fibrous electrode material	SEM, N_2 - adsorption, BET, mechanical testing, CV, EIS	Development of electrospun fibrous DC-based electrode	Paper I
Polymer: PAN *Solvent*: DMF *Additives*: CDC, CB, $EMImBF_4$ *Electrolytes*: $TEMABF_4$/ACN, $TEABF_4$/ACN, $SBPBF_4$/ACN, $EMImBF_4$/ACN, EMImTFSI/ACN	Physical analysis of selected optimal electrode material, Influence of organic electrolytes to electrochemical performance: quaternary ammonium, ionic liquids	SEM, TGA, N_2 adsorption, BET, mechanical testing, CV, GC, EIS	Study the effect of organic electrolytes on the electrochemical performance of electrospun fibrous CDC-based electrodes	Paper II
Polymer: PAN *Solvent*: DMF *Additives*: CDC, CB, $EMImBF_4$ *Electrolytes*: $NaNO_3/H_2O$, KNO_3/H_2O, Na_2SO_4/H_2O, $SBPBF_4$/ACN, EMImTFSI/ACN	Physical analysis of selected optimal electrode material, Influence of aqueous electrolytes to electrochemical performance:	SEM, thermal analysis (TGA), N_2 adsorption, BET, mechanical testing, FTIR, CV, GC, EIS	Study the effect of aq.electrolytes on the electro-chemical perfor-mance of electro-spun electrodes. The cycle-life study of electro-spun EDL capaci-tors.	Paper III

2.1 Materials

Polyacrylonitrile (Sigma Aldrich, M_w = 150 000 g mol^{-1}) was chosen as the polymer and dimethylformamide (≥99.9% purity, Sigma Aldrich) as the solvent for the electrospinning process. Carbide-derived carbon, synthesised from titanium carbide by Skeleton Technologies OÜ, was used as the main EDL capacitive material in electrode formation due to its highly porous structure and narrow pore size distribution. For this purpose, the TiC precursor was converted to CDC by Cl_2 treatment at 900 °C. To remove chlorine residues, a hydrogen gas purification step at 800 °C was applied. The specific surface area of the synthesised CDC was 1580 m^2 g^{-1}, with an initial particle size of 1–5 µm. Carbon black (Timcal) was used as a conductive additive to improve the contact between the CDC particles. The ionic liquid EMIm-BF_4 (≥99.0% purity, Sigma Aldrich) was used to increase the conductivity of the electrospinning solution, which is required to achieve a stable fibre-forming process during electrospinning.

2.2 Methods

2.2.1 Solution and electrode preparation

Prior to the preparation of the electrospinning solution PAN + CDC/CB + DMF + EMIm-BF_4, the CDC powder (≈1 – 5 µm) was milled using a planetary ball mill (Retch PM 100) under an N_2 atmosphere for 1 h. The milling process was applied to reduce the initial particle size of the CDC to less than 0.8 µm.

For electrospinning solution preparation, the dispersion of CB, CDC, and DMF was prepared through ultrasonic treatment (Node ultrasonic homogeniser from Bandelin Sonoplus, Germany, with a 1 cm diameter nozzle) for 2 h. To avoid overheating of the solution, the glass vessel was placed in an ice bath. The weight ratio between CB/CDC was varied at 80/20, 85/15, 90/10, and 100/0 in Paper I (for Papers II and III, the ratio between CDC/CB was kept constant at 80/20, respectively). Thereafter, 7 wt% of PAN was added to the carbon dispersion and dissolved by mechanical stirring for another 24 h at 40 °C. The ratio between PAN and carbon was kept constant at 50/50 throughout the study. Prior to electrospinning, 15 wt% (by weight of the entire solution) of IL (EMIm-BF_4) was added to the solution, and additional mechanical stirring (0.5 h) was applied at 40 °C. A schematic diagram of the solution preparation is shown in Figure 7.

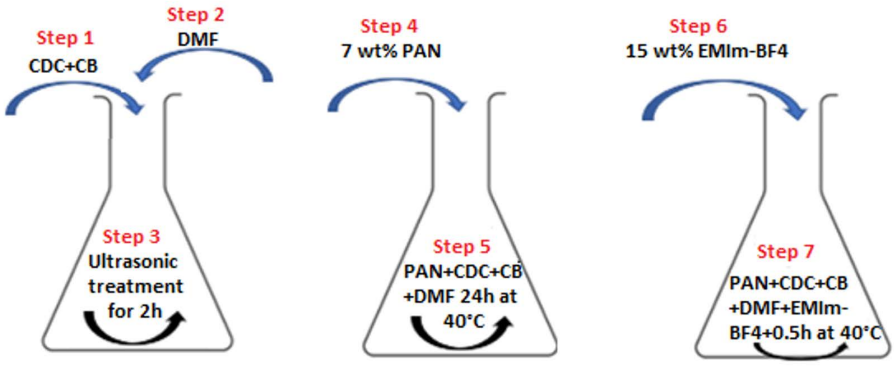

Figure 12. Solution preparation process.

2.2.2 Electrospinning process

Electrospinning was carried out using an in-house-built horizontal electrospinning setup (see Figure 13) with a cylindrical rotating, grounded drum covered with carbon-precoated aluminium foil (Toyal Aluminium K.K). A syringe pump from the New Area Pump System was used for continuous solution flow. The solution feed rate was between 0.3 and 1.5 ml h^{-1}. The choice of the feed rate depended upon the solution viscosity (for Papers II and III, the pumping rate was 0.5 ml h^{-1}). The solutions were electrospun in a voltage range of 15–18 kV with a distance range of 8–10 cm between the spinneret (needle of the syringe) and rotating drum collector. After electrospinning, electrode densification was carried out using a hydraulic mechanical press (Scamia) to increase the conductivity of the fibrous electrode.

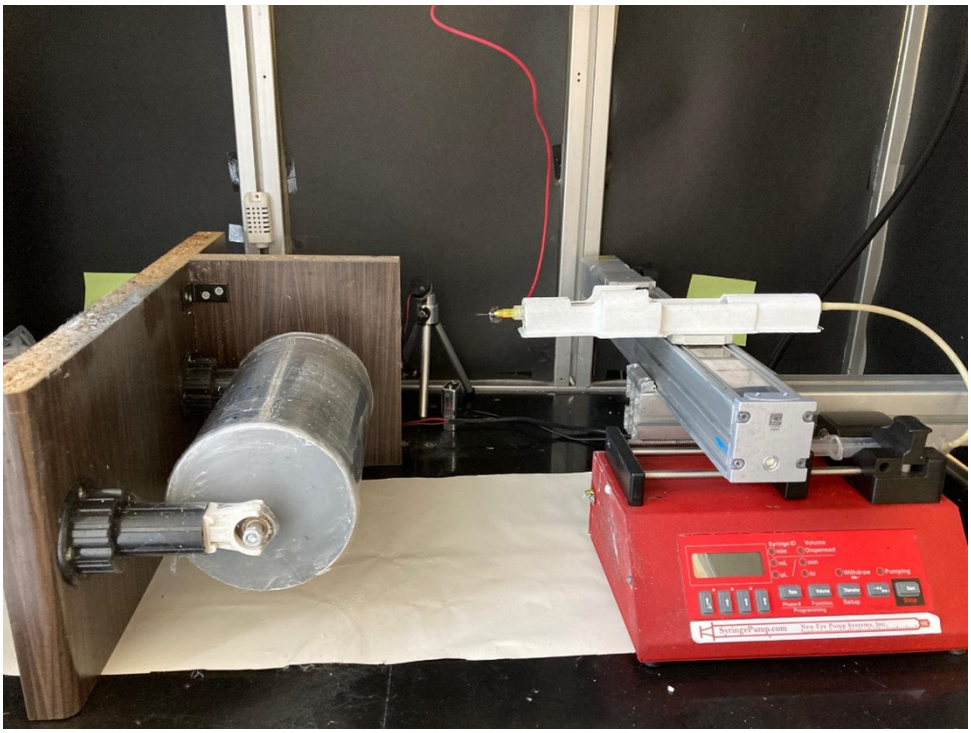

Figure 13. Electrospinning setup.

2.2.3 Characterisation of electrospun CDC-based fibrous electrodes

The morphology of the electrospun CDC-based fibrous electrodes was analysed by scanning electron microscopy (SEM; Gemini Zeiss Ultra 55). No conductive coating was deposited on the samples.

The thermal stability of the electrospun fibrous electrodes was evaluated by thermal gravimetric analysis (TGA, Labsys Evo TG DTA Omni Star). The fibrous electrode samples were torn into small pieces to achieve a uniform sample structure and placed in a crucible. Thermal analysis was performed in an artificial air atmosphere (21% O_2 and 79% Ar). The total gas flow was set to 30 mL h^{-1}. The temperature increase rate was set to 5 °C min^{-1}, and the sample was heated to 600 °C (see Figure 2 in Paper II).

The porosities of the carbon constituent and the electrospun fibrous electrodes were determined from N_2 adsorption at −196 °C using a surface area and porosity analyser

(NOVA touch LX2, Quantachrome Instruments). The specific surface area (S_{BET}) of the carbon samples was calculated according to the Brunauer–Emmett–Teller theory in the P/P_0 pressure interval of 0.02–0.2, and the total pore volume (V_{tot}) was calculated at a P/P_0 of 0.97. The calculations of the pore size distribution (PSD) were performed using a quenched solid density functional theory (QSDFT) and equilibria model for slit-type pores. Before measurement, the carbon samples were degassed under vacuum at 300 °C for 12 h. In the case of the fibrous electrode materials, the temperature was reduced to 100 °C.

The mechanical properties of the fibrous electrodes were tested using an Instron 5866 tensile-testing machine. For this approach, sample ribbons (five specimens of each sample) were cut into rectangular shapes with dimensions 10.0 × 4.5 mm. The strength of the electrospun CDC-based electrodes was evaluated based on the specific stress at maximum load. To calculate the specific stress, the density ρ of each specimen was calculated according to Equation (3):

$$\rho = \frac{m}{V}, \quad (3)$$

where *m* is the weight of the electrode, and *V* is the volume of the electrode.

Thereafter, the specific stress σ_{sp} was calculated using Equation (4):

$$\sigma_{sp} = \frac{F}{A}\frac{1}{\rho}, \quad (4)$$

where *F* is the force, and A is the width of the sample (Ko and Wan, 2014).

The interactions within the polymer and electrolyte in fibrous mats treated with several aqueous electrolytes were analysed by Fourier-transform infrared spectroscopy (FTIR; Interspec 200-X). To evaluate the influence of the electrolytes on the intermolecular interactions in the PAN/DMF fibres, the specimens were submerged in the electrolyte for 48 h. The treated specimens were then washed several times with distilled water to remove the electrolyte salt residues. The specimens were dried under vacuum at 95 °C for 24 h to remove the water.

2.2.4 Electrochemical evaluation

In the present study, three-electrode (asymmetric) and two-electrode (symmetric) test cells were used to analyse the EDL properties of the studied materials. In the case of three-electrode cells, a counter electrode (CE) with a diameter of 15 mm was constructed from a high-surface-area carbon film attached to an aluminium (used with organic electrolytes) or gold collector (used with aqueous electrolytes). Reference electrodes (Ref) were selected according to the type of electrolyte: the organic electrolyte had a carbon reference, and the aqueous solution had a Ag|AgCl reference. A working electrode (WE) with a diameter of 6 mm was used as the fibrous electrospun CDC-based electrode with an average coat weight 1.86 g m^{-2}. The WE and CE were interleaved using a 1 mm thick glass fibre separator membrane (Whatman). For the two-electrode configuration, two symmetrical electrodes (15 mm diameter) separated by a cellulose separator (Nippon Kodoshi) were used. Prior to the assembly of both types of electrochemical test cells, electrodes were dried at 100 °C for 24 h under vacuum (≈1 mbar) to remove moisture and obtain the dry weight of the electrode material. After assembly, the cells were vacuumed

and filled with non-aqueous electrolyte (further details can be found in Papers I and II) or with aqueous electrolytes (Paper III).

Cyclic voltammetry, galvanostatic cycling, and electrochemical impedance spectroscopy tests were performed to evaluate the electrochemical performance of the electrospun CDC-based fibrous electrodes. Electrochemical measurements were carried out at room temperature using a VMP3 (BioLogic Science Instruments; Paper I) and Gamry Interface 1010 E equipment (Papers II and III).

The differential capacitance (C) was calculated from the CV measurements according to Equation (5):

$$C_{CV}(C_i^+; C_i^-) = \frac{i\,(i^+; i^-)}{v}, \quad (5)$$

where C_i^+ is the positively charged electrode capacitance; C_i^- is the negatively charged electrode capacitance; i is the current, read at fixed electrode potentials; and v is the applied voltage scan rate. All current values were obtained from the third CV discharge cycle.

The integrated capacitance (C_{GC}) of the electrodes was calculated by performing constant current experiments according to Equation (6) (Conway, 1999; Stojanovska et al., 2019):

$$C_{GC}\,(C_i^+; C_i^-) = \int_{E_{max}}^{0} \frac{Idt}{\Delta E}, \quad (6)$$

where I is the current, dt is the discharge time, and ΔE is the potential range of the positively or negatively charged electrodes. To calculate the specific capacitance (in F g^{-1} or F cm^3) of the CDC and electrode, Equation (7) was used:

$$C_{specific} = \frac{C_{GC}\,;\, C_{CV}}{m;\,(V)}, \quad (7)$$

where m is the weight of the carbon in electrode, and V is the volume of the electrode.

The resistance and ESR were evaluated using the EIS method. EIS spectra were measured in the various AC frequency ranges at the amplitude of the sinusoidal voltage of 5 mV (details can be found in Papers II and III). The total impedance (Z) of the RC circuits is described by Equation (8):

$$Z = Z' + Z'' = R + \frac{1}{j\omega C_s}, \quad (8)$$

where Z' is the real impedance, Z' is the imaginary impedance, j is the imaginary number $\sqrt{-1}$, ω is the angular frequency ω=2πf, $and\ C_s$ is the series capacitance.

Rs values were determined by frequency response analysis and were equal to the real impedance (see Equation (9)).

$$Rs = Z', \quad (9)$$

The series capacitance (C_S) values from EIS were calculated according to Equation (10) (Torop et al., 2011).

$$C_s = -\frac{1/Z''}{\omega}, \quad (10).$$

3 Results and discussion

3.1 Development of electrospun fibrous electrode

The electrospun fibrous CDC-based electrodes were optimised in Paper I. Mechanical densification was applied to improve the contact between each fibre in the electrospun electrode because the fibres tend to accumulate in relatively fluffy stacks on the collector during the electrospinning process. The hypothesis was that by decreasing the physical free space between fibres, the conductivity of the fibrous electrode will improve, thereby decreasing the resistance and increasing the capacitance. The basis for the high conductivity and capacitance of the electrode material is the good electrical contact between the carbon particles. Conductive additives and calendaring processes are also commonly used in conventional supercapacitor electrodes (Mitchell et al., 2013). A study on the densification pressure and temperature was carried out to clarify the influence of densification on the electrochemical performance of the fibrous supercapacitor electrodes. To analyse the effect of various densification parameters on the electrochemical performance of the fibrous electrodes, symmetrical test cells were assembled using a 1.8 M TEMA-BF_4/ACN electrolyte solution. CV and EIS measurements were performed to evaluate the capacitance and resistance values. The electrochemical characteristics obtained from the densification pressure and temperature studies are presented in Table 2.

Table 2. Electrochemical characteristics of densification studies (two-electrode measurements).

CDC/CB	Densification		Conductivity of fibrous membrane	Density of electrode	C by CV (5 mV s^{-1} 0–2 V)	R_s (at 1 kHz)	Specific energy
	Pressure	Temperature			Specific Capacitance	Specific Resistance	
	MPa	°C	nS cm^{-1}	g cm^{-3}	F g^{-1}	Ohm cm^2	J g^{-1}
85/15	0	25		0.31	11.3	18.5	7.5
	0.6			0.61	84.3	16.8	55.7
	1.2			0.65	93.5	7.3	61.8
	2.5			**0.70**	**100.6**	8.8	66.6
80/20	2.5	25		0.76	95.3	5.2	63.0
		75		**0.84**	**114.0**	2.4	74.0
		95		0.92	111.9	2.5	75.4
		125		0.94	89.4	5.4	59.1
80/20	2.5	75	30	**0.84**	**114.0**	2.4	74.0
85/15			16	0.70	98.6	4.7	65.2
90/10			10		73.0	4.8	48.3
100/0			10		46.5	17.0	30.7

The investigation of densification pressure showed a significant increase in the specific capacitance of the fibrous-electrode-based symmetric test cells. By increasing the pressure up to 2.5 MPa, the specific capacitance increased by nine fold. At the same time, the resistance value of the fibrous electrodes decreased by approximately 50% compared to the non-densified electrodes. In addition, by increasing the densification pressure to 2.5 MPa, a capacitance comparable to that of commercial carbon-based electrodes was achieved.

Furthermore, to study the effect of the densification temperature on the electrochemical performance, electrodes were densified at a constant pressure of 2.5 MPa in the temperature range of 25–125°C. Based on the electrochemical evaluation, a maximum specific capacitance of 114 F g^{-1} was achieved at a densification temperature of 75 °C; thereafter, a capacitance drop was observed. This is in good correlation with the fibre morphology influenced by the densification temperature, as observed by SEM (see Figure 14). The fibrous structure of the electrospun electrodes remained at a densification temperature of 75 °C (see Figure 14A–D). By increasing the temperature to 95 °C, which is close to the glass transition temperature of PAN (100 °C) (Bashir & Nagar, n.d.), the fibres are partly melted together (see Figure 14E–F). The fibres were melted or destroyed when the glass transition temperature was exceeded, as can be seen in Figure 14G–H and Figure 2, Paper I. Damage to the fibre structure leads to insufficient electrical double-layer performance due to the higher electrical resistance (see Figure 6A, Paper I). The increase in resistance was due to partial bond breakage of the fibres, excessive compaction of the electrode material, and a significant reduction in voids between fibres (reduced electrode porosity), which results in the inhibition of the diffusion of electrolyte ions.

A) B)

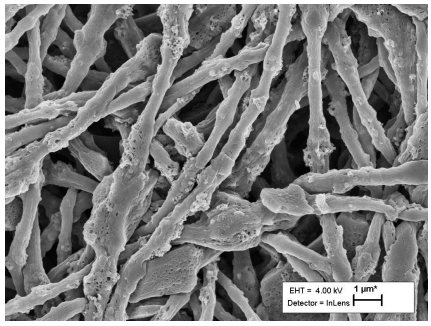

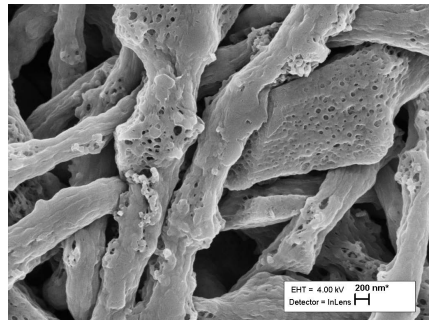

C) D)

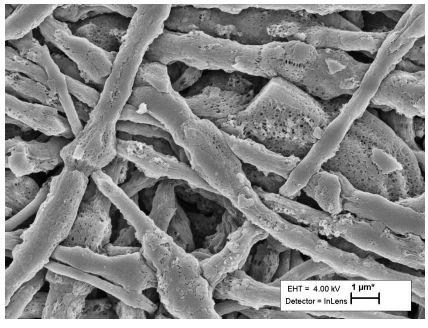

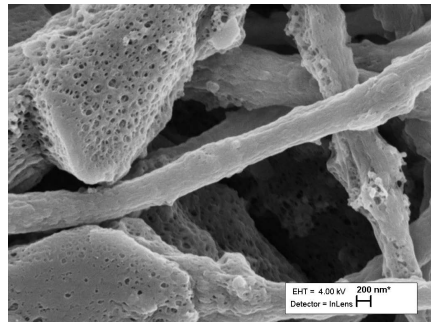

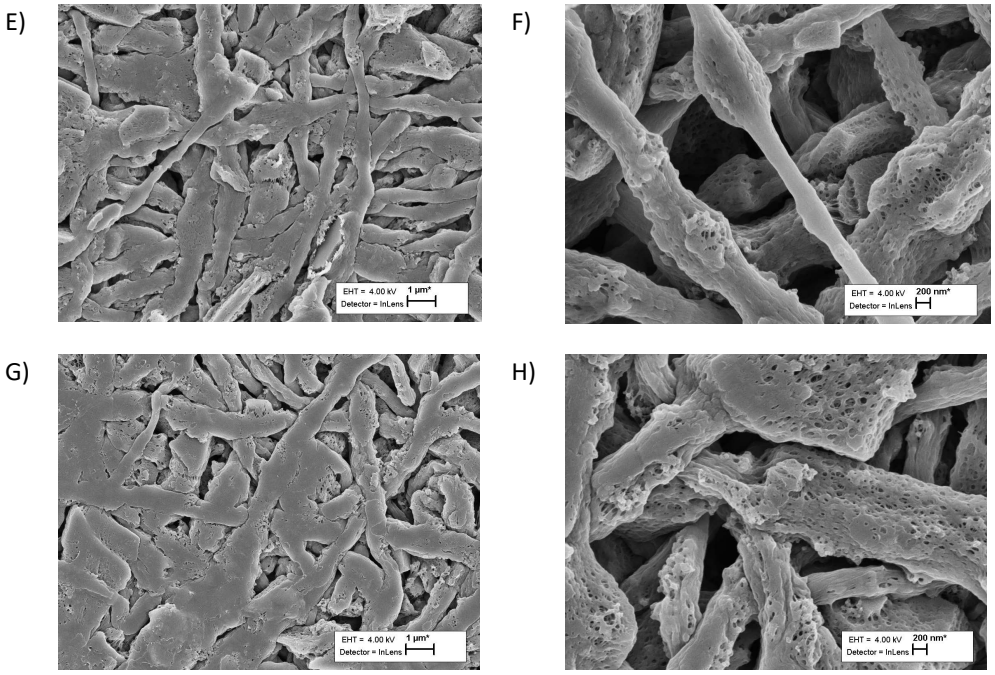

Figure 14. SEM analysis of electrospun samples with two different magnifications and densification temperatures: A,B) 25 °C; C,D) 75 °C; E,F) 95 °C; and G,H) 125 °C.

The observations made by SEM analysis are also supported by the mechanical properties of the obtained fibres. One of the main advantages of the fibrous structure of the studied CDC-based electrospun electrodes is their flexibility and mechanical durability over conventional roll-pressed or casted electrodes. Similar to the morphological analysis, it was indicated that by increasing the densification temperature close to the glass transition temperature of PAN, the specific stress of the fibres significantly decreases (see Figure 3, Paper I). Therefore, the optimum parameters (i.e., those that do not significantly affect mechanical properties of the fibres) were a densification pressure of 2.5 MPa and temperature of 75 °C.

The important parameters for supercapacitors are the electrode conductivity and capacitance. Optimisation of the CDC as the active material and CB as the conductive additive was carried out as discussed in Paper I. For this study, four different weight ratios of CDC and CB were tested: 80/20, 85/15, 90/10, and 100/0, respectively. The hypothesis was that by increasing the CDC content in the fibrous electrodes, the adsorption surface of the electrolyte ions increases, and thus also the EDL capacitance. To characterise the prepared electrode samples with various CDC and CB ratios, the optimum densification pressure (2.5 MPa) and temperature (75 °C) were applied. The characteristics of the tested electrode samples are listed in Table 2. The highest specific capacitance of 114 F g^{-1} and lowest resistance of 2.4 Ω cm^2 were achieved with a CDC/CB ratio of 80/20. The resistance of the material started to increase, and the capacitance began to decrease when the CDC content was increased to over 80%, owing to the lack of a conductive additive that connects the larger CDC particles. Conductive additive bridges are needed to improve the electrical contacts between high-surface-area CDC particles, which also ensures EDL capacitance. This phenomenon can also be seen in the decrease of material conductivity values with decreasing conductive additive content; the conductivity of the electrospun

fibrous electrode is also decreased. However, because the surface area of the CDC is multiple times higher than that of CB (S_{BET} for CDC is ≈1640 $m^2 g^{-1}$ and 63 $m^2 g^{-1}$ for CB), the specific capacitance starts decreasing again upon decreasing the CDC content of the electrode to below 80%. With a CB/CDC ratio of 60/40, the specific capacitance reached only 5.5 F g^{-1}. Therefore, the optimum CDC/CB ratio for fibrous supercapacitor electrodes was selected as 80/20.

Because one of the advantages of supercapacitors is the wide operating temperature range, the thermal properties of the fibrous electrode produced by the optimum parameters (i.e., CDC/CB ratio of 80/20) were investigated by thermal gravimetric analysis (TGA). TGA identified three main stages of weight loss, as presented in Table 3 and Figure 2 of Paper II. The first component of the electrospun CDC-based fibrous electrode, which starts to decompose, is the polymer. The mass loss of the polymer occurs between 247 and 317 °C with an early shoulder at 290 °C. This temperature range refers to several parallel or competing reaction kinetics. In the next mass-loss stage, when the temperature is between and 318–442 °C, IL EMIm-BF_4 degrades. In the last stage, at temperatures above 600 °C, decomposition of the carbon materials occurs.

Table 3. Decomposition characteristics of fibrous electrospun electrode.

	Degradation Temperature	Average mass loss*	Temperature (from the literature)	
	°C	%	°C	Reference
PAN	247–317	5.6	260	(Salles et al., 2010)
EMIm-BF_4	318–442	25	333–445	(Hao & Lin, 2013)
CDC+CB	600	72	≈600	(Sarfraz et al., 2020)

*Mass loss in the degradation temperature range

3.2 Stability study of fibrous CDC-based electrodes in various electrolytes

3.2.1 Electrochemical stability study of aqueous electrolytes

The electrochemical stability of electrospun fibrous electrodes was tested in three different 1.0 M aqueous electrolytes: Na_2SO_4-H_2O, $NaNO_3$-H_2O, and KNO_3-H_2O with asymmetric test-cell configuration vs Ag|AgCl reference electrode. The characteristics of the anions and cations of the electrolytes are listed in Table 4, and their conductivity and pH are listed in Table 2 of Paper III. The potential stability of the fibrous electrodes was tested using the CV method with a potential scan rate of 5 mV s^{-1}. The measured cyclic voltammograms are shown in Figure 15.

Table 4. Characteristics of anions and cations of aqueous electrolytes (Israelachvili, 2011; Pal et al., 2019).

Cation	Ionic radii, Å	Solvated ionic radii, Å	Anion	Ionic radii, Å	Solvated ionic radii, Å	Structural formula
Na^+	0.95	3.59	SO_4^{2-}	2.42	3.79	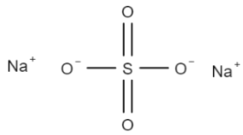
Na^+	0.95	3.59	NO_3^-	1.89	3.4	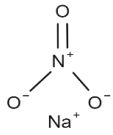
K^+	1.33	3.34	NO_3^-	1.89	3.4	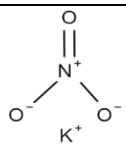

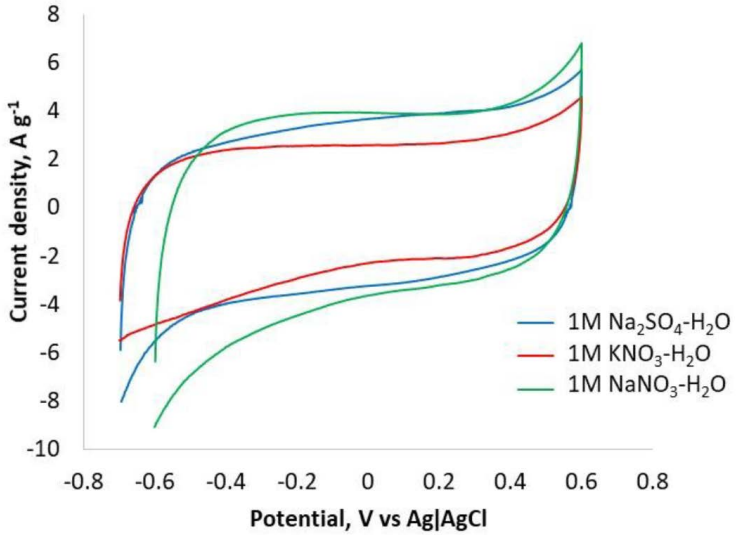

Figure 15. Cyclic voltammograms of measured aqueous electrolytes with fibrous electrodes.

The electrochemical potential stability of the fibrous electrodes was observed by replacing the Na^+ cation with K^+ and the SO_4^{2-} anion with NO_3^-. With aqueous electrolytes, hydrogen reduction and water oxidation reactions are well-known processes that take place on the negative or positive electrode potential limits, respectively. The previously mentioned processes are more pronounced with sodium-based electrolytes than with

potassium-based electrolytes, where the potential limits have not yet been achieved. With replacement of K^+ with Na^+, an exponential current increase at negative electrode potentials was observed, indicating parallel hydrogen and sodium adsorption processes, while no exponential increase in current was observed with replacement of SO_4^{2-} with NO_3^-.

Higher current density values were achieved with sodium-based electrolytes at negative electrode potentials compared to potassium-based electrolytes. The achieved current density difference can be explained by the approximately 30% smaller dehydrated ion size of sodium ions compared to potassium ions. It should be noted that the difference in ion sizes is smaller in the case of hydrate ions; however, it must be taken into account that ions move and may be adsorbed in hydrated or partially hydrated form (Ghrib, 2018). Surprisingly, with positive electrode potentials, no difference in the current response was observed between sulphate and nitrate anions despite the difference in ion sizes.

Furthermore, to analyse the stability of the fibrous electrode in aqueous electrolytes, FTIR analysis was performed on electrode samples treated with the same aqueous electrolyte solutions studied in the electrochemical analysis (ATR measurements with diamond crystal peaks in the 2300 – 1900 $1cm^{-1}$ region). To understand the intermolecular interactions within the nanofibrous electrodes, the samples were soaked in the studied aqueous electrolytes. Sample preparation is described in detail in Paper III. The IR absorption spectra comparison between the treated and non-treated electrode samples is presented in Figure 16.

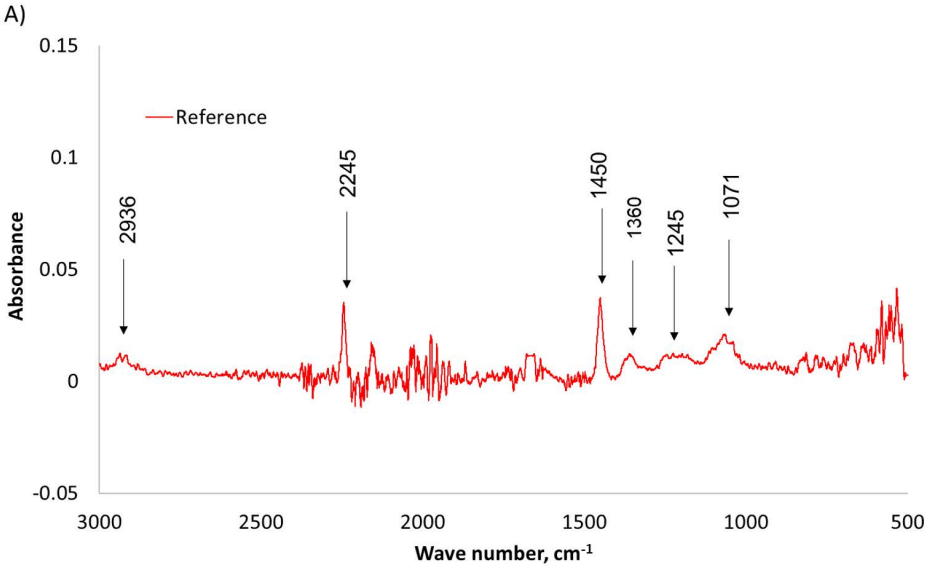

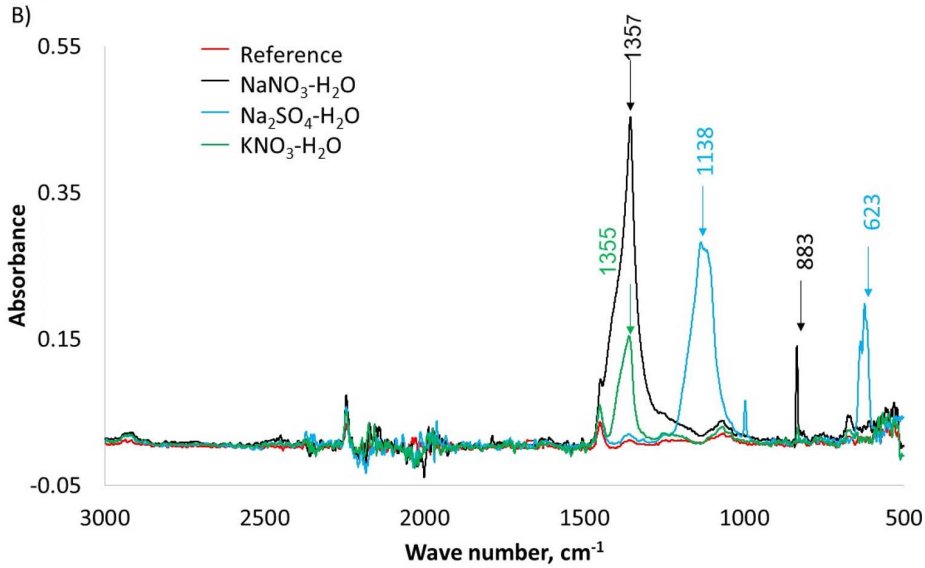

Figure 16. IR absorption spectrum: A) PAN fibre and B) PAN fibres soaked in aqueous electrolytes Na_2SO_4-H_2O, $NaNO_3$-H_2O, and KNO_3-H_2O.

The reference data in Figure 16A show the main peaks of the pure electrospun PAN fibres. The strong adsorption peak at 2245 cm^{-1} corresponds to the nitrile group, C≡N. Furthermore, three band groups attributed to main chain are located at 1245 cm^{-1} (C–C stretching vibrations), 2936/1360 cm^{-1} (C–H symmetric stretch) and at 1450/1071 cm^{-1} (in-plane and out-of-plane bending, respectively) (Conley & Bieron, 1963; Lee et al., 2012; J. Li et al., 2013). When the PAN fibres were exposed to various aqueous electrolytes, there were no evident changes in the main peak intensities or areas, indicating a stable electrode material (see Figure 16B). However, in the IR spectra of the treated fibre samples, peaks corresponding to the anions of the used electrolytes were observed due to strong salt anion adsorption to the fibre surface. As in the case of nitrate-based electrolyte fibre samples, peaks indicating asymmetric and symmetric stretching of the NO_3^- group were evident at 1356 cm^{-1} and 835 cm^{-1}, respectively (Lee et al., 2012). With sulphate-based electrolyte fibre samples, asymmetric stretching of SO_4^{2-} anions was observed at 1123 cm^{-1} and 615 cm^{-1} (Surianarayanan et al., 1998). A more detailed analysis of the FTIR spectra can be found in Paper III.

3.2.2 Electrochemical stability of organic electrolytes

The electrochemical stability of electrospun fibrous electrodes was tested in two quaternary-ammonium-based and two IL-based electrolytes: 1.5 M spiro-(1,10)-bipyrrolidinium tetrafluoroborate in acetonitrile (SBP-BF_4/ACN) and 1.8M triethylmethyl-ammonium tetrafluoroborate in acetonitrile (TEMA-BF_4/ACN) were selected as quaternary ammonium-based electrolytes; and 1.5 M 1-ethyl-3-methylimidazoliumbis(trifluoromethylsulphonyl)imide in acetonitrile (EMIm-TFSI/ACN) and 1.5 M 1-ethyl-3-methylimidazolium tetrafluoroborate in acetonitrile (EMIm-BF_4/ACN) were selected as IL-based electrolytes. All four electrolytes were tested with an asymmetric test cell configuration versus a carbon reference electrode. The characteristics of the anions and cations in the electrolytes are listed in Table 5. The electrochemical potential stability

of the fibrous electrodes in organic electrolytes was tested using the CV method with a potential scan rate of 1 mV s^{-1}. The positive and negative potential limits were evaluated according to the methods described by Xu (Xu, 1999) and Weingarth (Weingarth et al. (2013). The measured cyclic voltammograms are shown in Fig. 17.

At negative electrode potentials, where cation adsorption occurs, wider potential limits and higher Coulombic efficiencies are observed for both organic and IL-based electrolytes. The widest potential window of 3 V was achieved with fibrous electrodes in SBP-BF_4/ACN electrolyte, where the negative and positive potential limit were determined at –1.7 V and 1.3 V (vs Ref), respectively. A lower electrochemical stability was observed with the TEMA-BF_4/ACN electrolyte, in which a Columbic efficiency of <90% was recorded with both positive and negative electrode potentials. This surprisingly low efficiency can be explained by exceeding the EDL limits of the electrode potentials of such systems when recording voltammograms. Therefore, possible side reactions upon the adsorption of ions into the carbon pores were also included.

As expected, IL-based electrolytes have a wider potential window compared to quaternary-ammonium-based electrolytes. In general, the widest potential window of 3.5 V was achieved using the EMIm-TFSI/ACN electrolyte with negative and positive electrode potential limits of up to –2 V and +1.5 V (vs Ref), respectively, without a rapid decrease in Columbic efficiency. For the negative electrode potentials of the EMIm-BF_4/ACN, an exponential increase in current was observed already at –1.6 V with an additional reproducible peak at –0.5 V. The appearance of such an extra peak in the EDL region indicates the formation of surface functional groups on the carbon electrode surface. Furthermore, the formation of surface functional groups on the carbon surface can block the carbon pores, resulting in insufficient adsorption of electrolyte ions and lower electrochemical stability. This can lead to a decrease in the capacitance because electrolyte adsorption can occur not only in the case of solvated ions, but also in a partially or entirely solvated state, which doubles the size of the electrolyte ion in acetonitrile solution (see Table 5). The solvated electrolyte ion includes salt ions as well as the solvent interface (Ghrib, 2018).

Table 5. Characteristics of anions and cations of organic electrolytes.

Cation	Ionic radii, Å	Solvated ionic radii, Å	Anion	Ionic radii, Å	Solvated ionic radii, Å	Structural formula
SBP^+	4.20	8.40	BF_4^-	4.6	11.6	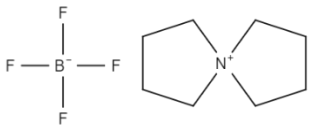
$TEMA^+$	3.27	6.54	BF_4^-	4.6	11.6	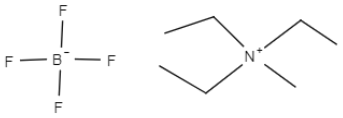
$EMIm^+$	3.26	6.52	$TFSI^-$	2.27	4.54	
$EMIm^+$	3.26	6.52	BF_4^-	4.6	11.6	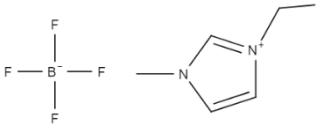

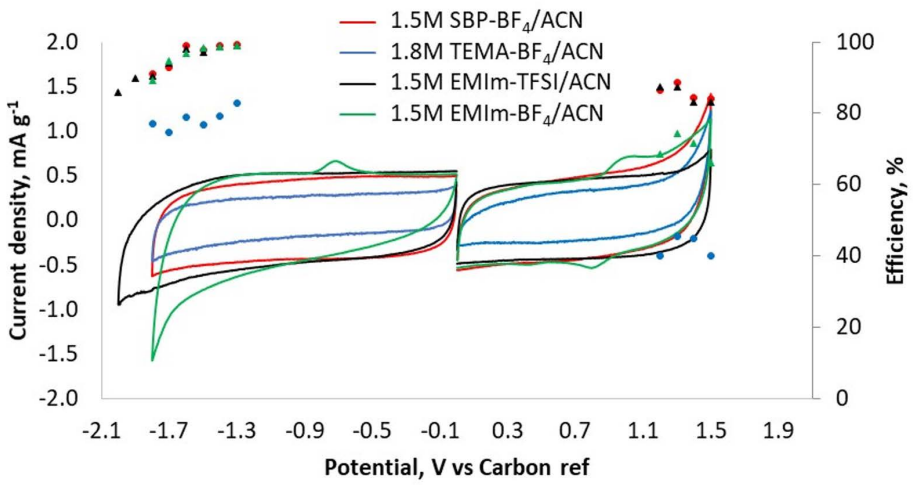

Figure 17. Cyclic voltammograms of measured organic electrolytes with fibrous electrodes.

3.2.3 Electrochemical characteristics of various electrolytes

The EDL capacitance values of fibrous-CDC-based electrode materials in aqueous and organic electrolytes were evaluated using the galvanostatic cycling method. The potential limits for organic and aqueous electrolytes were selected based on the potential stability

limits determined by the CV method. Therefore, for aqueous electrolytes, the potential limits for positively and negatively charged electrodes were selected as +0.6 V and –0.6 V (vs Ref), respectively. For the organic electrolytes, the limits for positively and negatively charged electrodes were set higher, at +1.2 V and –1.2 V (vs Ref), respectively, due to the wider potential stability, as shown in Figure 17. As mentioned earlier, the narrower potential stability of aqueous electrolytes is caused by water decomposition (Béguin et al., 2014). The current density for both types of electrolytes was selected as 0.5 mA cm^{-2}. The characteristics obtained from the comparison between aqueous and organic electrolytes are presented in Table 6.

Table 6. Comparison of electrochemical characteristics of tested aqueous and organic electrolytes in asymmetric cells.

Cation	Anion	Solvent	Molarity	Potential range	Positively charged electrode			Negatively charged electrode		
			M	V	C, mF	C, mF cm^{-2}	F g^{-1}	C, mF	C, mF cm^{-2}	F g^{-1}
Na^+	NO_3^-	H_2O	1		21.0	9.3	182.8	33.9	15.0	295.1
Na^+	SO_4^{2-}	H_2O	1	0..0.6	34.2	15.1	135.0	42.0	18.6	166.2
K^+	NO_3^-	H_2O	1		29.0	12.8	157.7	38.7	17.1	210.2
$TEMA^+$	BF_4^-	ACN	1.8		6.4	5.7	70.8	5.3	6.9	55.8
SBP^+	BF_4^-	ACN	1.5	0..1.2	16.3	14.4	80.4	19.7	17.5	95.3
$EMIm^+$	BF_4^-	ACN	1.5		27.4	24.2	105.6	19.7	17.5	76.2
$EMIm^+$	$TFSI^-$	ACN	1.5		23.3	20.6	89.8	23.3	20.6	89.8

In all three aqueous electrolyte combinations, it was clear from the CVs that a higher capacitance was reached with the negatively charged electrode. The nitrate-based electrolytes (i.e., $NaNO_3$-H_2O and KNO_3-H_2O) exhibited remarkably high capacitances on the positively (183 F g^{-1} for $NaNO_3$-H_2O and 157 F g^{-1} for KNO_3-H_2O) and negatively charged (295 F g^{-1} for $NaNO_3$-H_2O and 210 F g^{-1} for KNO_3-H_2O) electrodes. To the best of our knowledge, such high capacitances have previously been achieved in the case of acidic or alkaline electrolytes, but not with neutral, salt-based aqueous electrolytes in combination with fibrous electrodes.

Although the quaternary-ammonium-salt- and IL-based electrolytes have somewhat lower capacitances than the aqueous solutions, they exhibit significantly higher energy densities. This observation can be explained by the potential doubling owing to wider electrode potential limits because energy density is not only dependent on the capacitance but also significantly on the applied voltage (U^2), as shown in Equation 1.

Compared to quaternary-ammonium-based electrolytes, ILs are known to have lower conductivity but somewhat higher capacitance, as measured for porous carbon electrodes (Pohlmann, n.d.). A similar effect was observed with the fibrous electrodes. As with IL-based electrolytes, the highest capacitance of 105.6 F g^{-1} was achieved with the EMIm-BF_4/ACN electrolyte for the positively charged electrode; however, a significantly

lower capacitance of 76.2 F g^{-1} was achieved on the negatively charged electrode. In a symmetrical cell configuration, it is known that the lower-capacitance electrode from asymmetric cell performance will also be a limiting factor for full-cell performance. A more stable system was established with the EMIm-TFSI/ACN electrolyte, as shown in the cyclic voltammograms (Figure 17). A uniform capacitance level of 89.8 F g^{-1} was achieved for the positively and negatively charged electrodes with the EMIm-TFSI/ACN electrolyte.

The resistance behaviour of all three electrolyte types in the asymmetric test-cell configuration was evaluated by electrochemical impedance spectroscopy in the AC frequency range of 200 kHz to 5 mHz, at a fixed electrode potential. For the aqueous electrolytes, the electrode potential was chosen to be 0 V vs Ag|AgCl reference, and with organic electrolytes, –0.5 V vs carbon reference. The obtained Nyquist plots are shown in Figure 18.

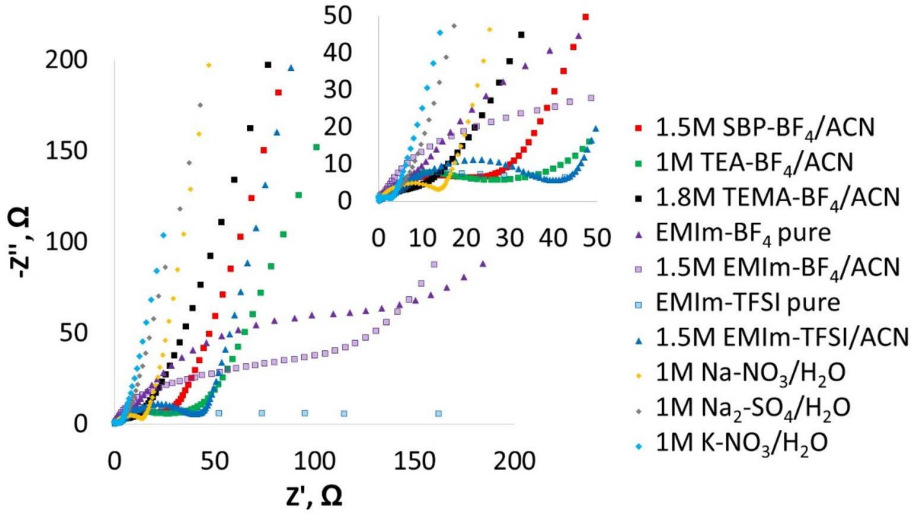

Figure 18. Nyquist plot for the electrolyte–carbon interface.

The performance that most closely resembled that of the EDL fibrous electrodes was achieved using aqueous electrolytes, where a near-vertical line was reached in the low-frequency area. The highest charge-transfer resistance was observed for both IL-based electrolytes in the high-frequency region. The reason for such a high charge-transfer resistance can be explained by the impedance of the interface at the current collector/active material or mass transfer resistance inside the porous electrode fibres at high frequencies. In general, the lowest resistance was observed for aqueous electrolytes and the highest for organic-IL-based electrolytes. This phenomenon can be explained by the higher viscosity and lower conductivity of IL-based electrolytes compared to those of aqueous and quaternary-ammonium-based electrolytes. A more detailed impedance analysis can be found in Papers II and III.

3.3 Electrochemical evaluation of symmetrical cells

3.3.1 Electrochemical specification of symmetrical cells

A two-electrode test-cell configuration was used to analyse the symmetrical full device of the fibrous electrodes. This configuration of the test cell provides the closest performance to the actual prototype cells. Electrolyte selection was based on the results of asymmetric configuration analysis. The best electrolyte candidates were selected from aqueous, organic, and IL-based electrolytes. The energy and power of the fibrous CDC-based materials were analysed for each electrolyte type. The specific capacitance and resistance of the symmetrical cells were evaluated by CV and EIS, respectively. The electrochemical performances of $NaNO_3$-H_2O, SBP-BF_4/ACN, and EMIm-TFSI/ACN in the two-electrode configurations are listed in Table 7.

Table 7. Electrochemical performances of symmetrical cells.

Electrolyte	Molarity M	Voltage range, V	Specific Capacitance of Carbon*, F g^{-1}	Specific Capacitance of Electrode*, F g^{-1}	Specific Resistance R_s at 1 kHz, Ω cm^2	Energy Density*, J g^{-1}	Power Density*, W g^{-1}
$NaNO_3/H_2O$	1.0	0–1.0	127	29.4	7.1	13.3	0.27
SBP-BF_4/ACN	1.5	0–2.3	110	26.5	9.0	72.9	0.63
EMIm-TFSI/ACN	1.5	0–2.3	105	25.3	92.6	69.2	0.60

*Calculated from CV plots at 20 mV s^{-1}

As shown in Table 7, the highest specific capacitance of 127 F g^{-1} and the lowest specific resistance of 7.1 Ω cm^2 was achieved with 1.0 M aqueous $NaNO_3/H_2O$ electrolyte solution. Compared to the studied organic and IL-based electrolytes, $NaNO_3$ also has the smallest solvated anion and cation sizes, which enables and supports better ion absorption of the fibrous electrode into CDC nanopores. In general, the specific capacitance increases in the following order: SBP-BF_4 < EMIm-TFSI < $NaNO_3$, which correlates well with the size of the solvated ions in the electrolytes.

To characterise and compare energy storage devices with different properties, the relationship between the energy and power density is presented through the Ragone plot (see Figure 19), and the respective values were calculated according to Equations 1 and 2. The operating voltages for aqueous and organic electrolytes were chosen to be 1 V and 2.3 V, respectively. The higher operating voltage of the 1.0 M SBP-BF_4/ACN electrolyte has 5.5 times the energy density and 2.3 times the power density of lower-operating-voltage supercapacitors. This can be clearly seen in the Ragone plot in Figure 19. Therefore, increasing the operating voltage is preferred for energy storage applications. The energy and power performances of CDC-based electrospun electrodes were significantly improved by using non-aqueous electrolytes.

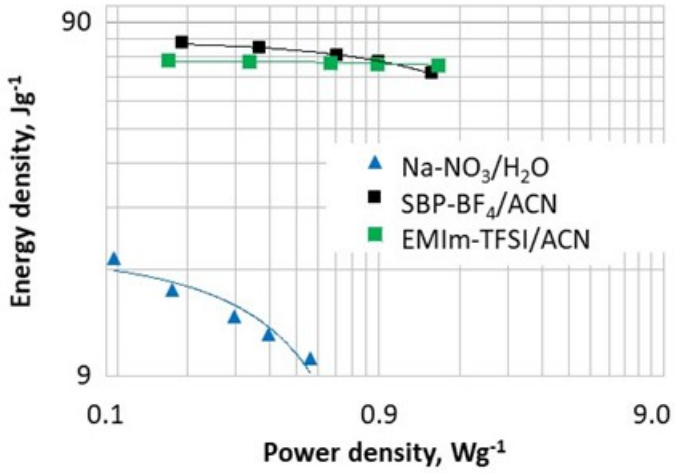

Figure 19. Ragone plot of fibrous symmetrical cells in various electrolytes.

3.3.2 Lifetime analysis of symmetrical EDL cells

The estimation of the ageing of energy storage systems is an important parameter to assess when researching new materials. The growing demand for ageing information stems from an application perspective, as the lifespan of a supercapacitor should be relatively long—for cars, for example. The lifetime expectancy of energy storage systems is approximately 5000 h, corresponding to 750 000 starting/braking cycles (Hammar et al., 2011). The lifespan of supercapacitors can be evaluated using two different methodologies: accelerated lifetime by means of a constant voltage hold or by charge–discharge cycling. The end of life (EOL) criteria are the same for both methods; the EOL is reached when a capacitance decrease of 20% or resistance increase of 100% from the initial values (Murray & Hayes, 2015). In the present study, the charge–discharge cycle method of fibrous electrodes was applied to different electrolyte systems. The applied cycling voltage range was chosen to be 0–1 V for aqueous electrolytes and 0–2.3 V for organic electrolytes; a CV voltage scan rate of 20 mV s^{-1} was used. For the intermediate specification, the capacitance values were calculated by CV and resistance values by the EIS method. The cycle-life performances of the selected electrolytes are presented in Figure 20A, B.

The change in capacitance over the cycles is shown in Figure 20A. The most stable cycle life was achieved with a quaternary-ammonium-salt-based organic electrolyte (SBP-BF_4/ACN), where only a 2% loss of capacitance was observed for the first 1000 cycles. However, with the IL-based electrolyte, 1.5 M EMIm-TFSI/ACN, an exponential decrease in capacitance was observed during the first 800 cycles. Such a rapid capacitance decrease at the beginning of the cycling may be due to the relatively high viscosity of the IL-based electrolyte and the relatively high voltage-scanning rate of 20 mV s^{-1} used to support inefficient ion transfer and adsorption of electrolyte ions to carbon pores (Balbuena, 2014). The resistance and capacitance of the H_2O based KNO_3 capacitor were almost constant over the cycles.

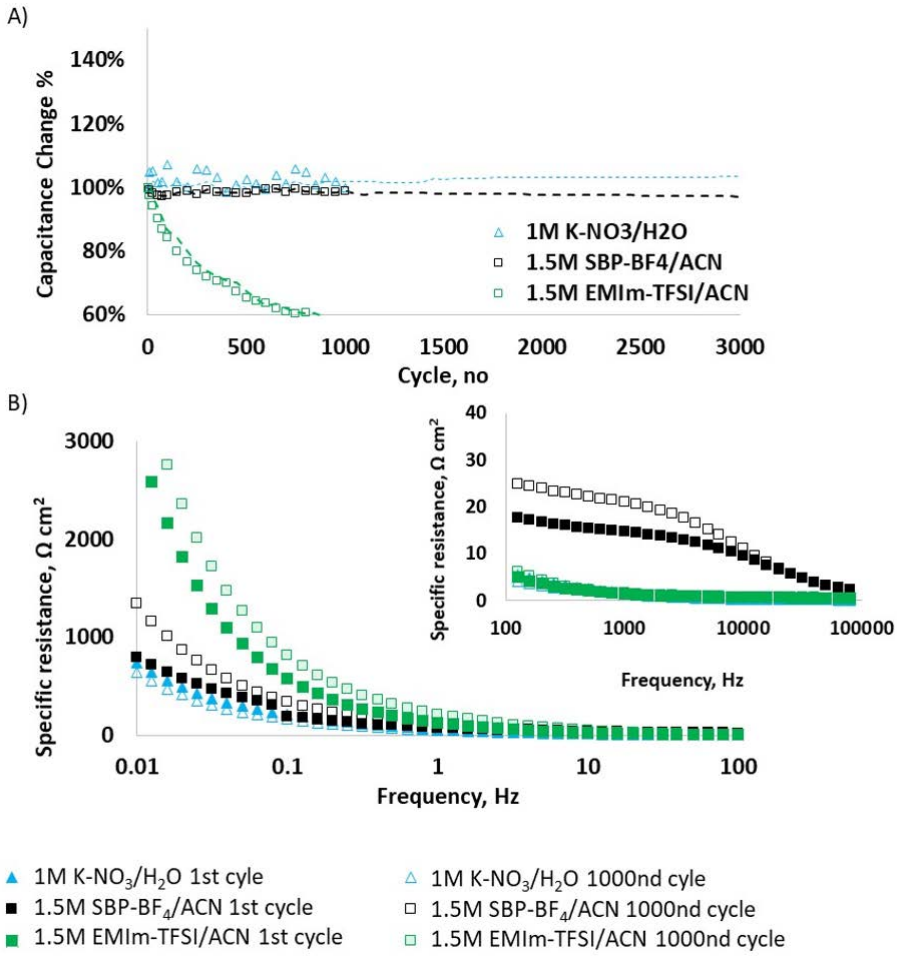

Figure 20. Cycle-life performance of 1.0 M $NaNO_3/H_2O$, 1.5 M SBP-BF_4/ACN, and 1.5 M EMIm-TFSI/ACN: A) capacitance change during cycling and B) resistance change during cycling.

Conclusions

The aim of this study was to develop a new approach for preparing electrospun carbonaceous electrodes for supercapacitors. For this purpose, optimal combinations of CDC and conductive additives were used. The influence of densification temperature and pressure on the mechanical, morphological, and electrochemical properties was studied. Electrochemical evaluation was carried out with aqueous and non-aqueous electrolytes to achieve the highest possible capacitance. The characteristics of the electrospun CDC-based fibrous electrodes were analysed using SEM, BET, and mechanical and thermal testing. For evaluating the electrochemical properties, the three most common techniques were used (CV, GC, and EIS). Based on the study, the following conclusions can be drawn:

1. A novel approach for preparing fibrous electrodes for supercapacitors without post-carbonization was introduced, where CDC was the main capacitive material and CB a conductive additive in electrospun fibres of PAN in DMF solution. The highest specific capacitance of 114 F g^{-1} with acceptable mechanical properties was achieved with a CDC to CB ratio of 80/20.
2. According to the current research, the densification temperature and pressure had a remarkable influence on the mechanical, morphological, and electrochemical properties of fibrous CDC-based electrode materials. The optimal densification parameters were achieved with a pressure of 2.5 MPa and temperature of 75 °C. These parameters were not found to have a negative influence on the structure and morphology of CDC-based fibrous electrodes; however, the capacitance was increased approximately 9-fold compared to the electrode samples for which densification was not applied. Overall, the specific stress for the fibrous electrodes was approximately 20-fold higher than that of the roll-cast electrode.
3. The CDC-based fibrous electrodes tested in aqueous electrolytes showed highest capacitances of 182.8 F g^{-1} and 295.1 F g^{-1} for positively and negatively charged potentials, respectively, in a 1.0 $NaNO_3/H_2O$ electrolyte. This is the highest specific capacitance achieved with fibrous electrodes in neutral aqueous electrolytes, to our knowledge.
4. CDC-based fibrous electrodes tested in organic electrolytes showed a highest capacitance of 89.9 F g^{-1} for positively and negatively charge electrodes and a potential window of 3.5 V in 1.5 M EMIm-TFSI/ACN electrolyte.
5. Electrolyte studies with symmetrical test-cell configuration revealed a highest energy density 72.9 J g^{-1} and power density of 0.63 W g^{-1} with 1.5 M SBP-BF_4/ACN electrolyte. Furthermore, no remarkable loss in cycle stability was observed with the same electrolyte. Previous studies indicated that fibrous electrodes are suitable for high energy density and for mechanically demanding applications.

The results of the current study pave the way for further improvement of the properties of fibrous composite electrodes for energy storage applications. There is a need to explore methods that decrease the polymer content of CDC-based fibrous electrodes and increase the specific capacitance of the elements. Furthermore, it is necessary to find opportunities to increase the power density of CDC-based fibrous electrodes containing supercapacitor elements.

List of Figures

Figure 1. Mechanism of electrical double-layer capacitors. 12
Figure 2. Specific energy vs specific power for energy storage devices. 13
Figure 3. Carbon allotropes used in supercapacitors 13
Figure 4. A) Model of the CDC structure and B) TEM image of TiC-CDC. 15
Figure 5. Molecular structure of PAN 16
Figure 6. Categorization of electrolytes. 18
Figure 7. (Left center) Scheme of electrospinning process (Right) Formation of a Taylor cone 20
Figure 8. Principle of the ball-milling method 21
Figure 9. Examples of two- and three- electrode cell configurations: A) current vs. potential and B) potential vs. time performance. 23
Figure 10. Nyquist plot of typical EDL device. 24
Figure 11. Current and voltage curves of EDL capacitors during constant current charge–discharge. 25
Figure 12. Solution preparation process. 28
Figure 13. Electrospinning setup. 29
Figure 14. SEM analysis of electrospun samples with two different magnifications and densification temperatures: A,B) 25 °C; C,D) 75 °C; E,F) 95 °C; and G,H) 125 °C. 34
Figure 15. Cyclic voltammograms of measured aqueous electrolytes with fibrous electrodes. 36
Figure 16. IR absorption spectrum: A) PAN fibre and B) PAN fibres soaked in aqueous electrolytes Na_2SO_4-H_2O, $NaNO_3$-H_2O, and KNO_3-H_2O. 38
Figure 17. Cyclic voltammograms of measured organic electrolytes with fibrous electrodes. 40
Figure 18. Nyquist plot for the electrolyte–carbon interface. 42
Figure 19. Ragone plot of fibrous symmetrical cells in various electrolytes. 44
Figure 20. Cycle-life performance of 1.0 M $NaNO_3$/H_2O, 1.5 M SBP-BF_4/ACN, and 1.5 M EMIm-TFSI/ACN: A) capacitance change during cycling and B) resistance change during cycling. 45

List of Tables

Table 1. Materials and methods 27
Table 2. Electrochemical characteristics of densification studies (two-electrode measurements). 32
Table 3. Decomposition characteristics of fibrous electrospun electrode. 35
Table 4. Characteristics of anions and cations of aqueous electrolytes 36
Table 5. Characteristics of anions and cations of organic electrolytes 40
Table 6. Comparison of electrochemical characteristics of tested aqueous and organic electrolytes in asymmetric cells. 41
Table 7. Electrochemical performances of symmetrical cells. 43

References

Ahn, D., Choi, H.-J., Kim, H., & Yeo, S. Y. (2020). Properties of Conductive Polyacrylonitrile Fibres Prepared by Using Benzoxazine Modified Carbon Black. *Polymers*, *12*(1), 179. https://doi.org/10.3390/polym12010179

Ali, B. A., Biby, A. H., & Allam, N. K. (2020a). Fullerene C $_{76}$: An Unexplored Superior Electrode Material with Wide Operating Potential Window for High-Performance Supercapacitors. *ChemElectroChem*, *7*(7), 1672–1678. https://doi.org/10.1002/celc.202000192

Ali, B. A., Biby, A. H., & Allam, N. K. (2020b). Fullerene C $_{76}$: An Unexplored Superior Electrode Material with Wide Operating Potential Window for High-Performance Supercapacitors. *ChemElectroChem*, *7*(7), 1672–1678. https://doi.org/10.1002/celc.202000192

Andersen, J. N. (1956). *Silicon tetrachloride manufacture* (United States Patent No. US2739041A). https://patents.google.com/patent/US2739041A/en

Ariyanto, T., Glaesel, J., Kern, A., Zhang, G.-R., & Etzold, B. J. M. (2019). Improving control of carbide-derived carbon microstructure by immobilization of a transition-metal catalyst within the shell of carbide/carbon core–shell structures. *Beilstein Journal of Nanotechnology*, *10*, 419–427. https://doi.org/10.3762/bjnano.10.41

Arulepp, M., Permann, L., Leis, J., Perkson, A., Rumma, K., Jänes, A., & Lust, E. (2004). Influence of the solvent properties on the characteristics of a double layer capacitor. *Journal of Power Sources*, *133*(2), 320–328. https://doi.org/10.1016/j.jpowsour.2004.03.026

Arulepp, M.; Leis, J.; Käärik, M.; Perkson, A. (2010). Carbide-Derived Carbons as Capacitor Materials. Proceedings of the sixth International Symposium on Large EC capacitors Technology and applications: Advanced Automotive Battery and EC Capacitor Conference; Omni Orlando Resort, Orlando, Florida, USA; May 17-21, 2010. Orlando, Florida, USA: Advanced Automotive Batteries, 55−64.

Asaka, K. (1990). Dielectric properties of cellulose acetate reverse osmosis membranes in aqueous salt solutions. *Journal of Membrane Science*, *50*(1), 71–84. https://doi.org/10.1016/S0376-7388(00)80887-X

Aussawasathien, D. (2006). *ELECTROSPUN CONDUCTING NANOFIBRE-BASED MATERIALS AND THEIR CHARACTERIZATIONS: EFFECTS OF FIBRE CHARACTERISTICS ON PROPERTIES AND APPLICATIONS* [University of Akron]. https://etd.ohiolink.edu/pg_10?::NO:10:P10_ETD_SUBID:46497

Babitha, S., Rachita, L., Karthikeyan, K., Shoba, E., Janani, I., Poornima, B., & Purna Sai, K. (2017). Electrospun protein nanofibres in healthcare: A review. *International Journal of Pharmaceutics*, *523*(1), 52–90. https://doi.org/10.1016/j.ijpharm.2017.03.013

Balbuena, P. B. (2014). *Electrolyte materials—Issues and challenges*. 82–97. https://doi.org/10.1063/1.4878481

Balducci, A., Dugas, R., Taberna, P. L., Simon, P., Plée, D., Mastragostino, M., & Passerini, S. (2007). High temperature carbon–carbon supercapacitor using ionic liquid as electrolyte. *Journal of Power Sources*, *165*(2), 922–927. https://doi.org/10.1016/j.jpowsour.2006.12.048

Bärtsch, M., Sauter, J.-C., & Kötz, R. (n.d.). *TESTING OF SUPERCAPACITORS AT PSI*. 3.

Bashir, Z., & Nagar, P. (n.d.). *Polyacrylonitrile, an unusual linear homopolymer with tWo glass transitions*. 9.

Becker, H. I. (1957). *Low voltage electrolytic capacitor* (United States Patent No. US2800616A). https://patents.google.com/patent/US2800616A/en

Béguin, F., Presser, V., Balducci, A., & Frackowiak, E. (2014). Carbons and Electrolytes for Advanced Supercapacitors. *Advanced Materials*, *26*(14), 2219–2251. https://doi.org/10.1002/adma.201304137

Benavente, J. (2005). Electrochemical Impedance Spectroscopy as a Tool for Electrical and Structural Characterizations of Membranes in Contact with Electrolyte Solutions. In *Recent Advances in Multidisciplinary Applied Physics* (pp. 463–471). Elsevier. https://doi.org/10.1016/B978-008044648-6.50074-4

Benavente, J., Ramos-Barrado, J. R., & Heredia, A. (1998). A study of the electrical behaviour of isolated tomato cuticular membranes and cutin by impedance spectroscopy measurements. *Colloids and Surfaces A: Physicochemical and Engineering Aspects*, *140*(1), 333–338. https://doi.org/10.1016/S0927-7757(97)00290-2

Brazis, V., Latkovskis, L., & Grigans, L. (2010). Simulation of Trolleybus Traction Induction Drive with Supercapacitor Energy Storage System. *Latvian Journal of Physics and Technical Sciences*, *47*(5), 33–47. https://doi.org/10.2478/v10047-010-0023-0

Burke, A., & Zhao, H. (2015). *Applications of Supercapacitors in Electric and Hybrid Vehicles*. 15.

Chapman, D. L. (1913). LI. A contribution to the theory of electrocapillarity. *The London, Edinburgh, and Dublin Philosophical Magazine and Journal of Science*, *25*(148), 475–481. https://doi.org/10.1080/14786440408634187

Conley, R. T., & Bieron, J. F. (1963). Examination of the oxidative degradation of polyacrylonitrile using infrared spectroscopy. *Journal of Applied Polymer Science*, *7*(5), 1757–1773. https://doi.org/10.1002/app.1963.070070516

Conway, B. E. (1999). *Electrochemical supercapacitors: Scientific fundamentals and technological applications*. Plenum Press.

Cooley, J. F. (1902). *Apparatus for electrically dispersing fluids* (United States Patent No. US692631A). https://patents.google.com/patent/US692631A/en

C. Piras, C., Fernández-Prieto, S., & Borggraeve, W. M. D. (2019). Ball milling: A green technology for the preparation and functionalisation of nanocellulose derivatives. *Nanoscale Advances*, *1*(3), 937–947. https://doi.org/10.1039/C8NA00238J

Dash, R. K., Yushin, G., & Gogotsi, Y. (2005). Synthesis, structure and porosity analysis of microporous and mesoporous carbon derived from zirconium carbide. *Microporous and Mesoporous Materials*, *86*(1–3), 50–57. https://doi.org/10.1016/j.micromeso.2005.05.047

Ding, B., & Yu, J. (2014). *Electrospun Nanofibres for Energy and Environmental Applications*. Springer Science & Business Media.

Donnet, J.-B. (1993). *Carbon Black: Science and Technology, Second Edition*. CRC Press.

Doyle, J. J., Choudhari, S., Ramakrishna, S., & Babu, R. P. (2013). Electrospun Nanomaterials: Biotechnology, Food, Water, Environment, and Energy. *Conference Papers in Materials Science*, *2013*, 1–14. https://doi.org/10.1155/2013/269313

Drew, C., Wang, X., Bruno, F. F., Samuelson, L. A., & Kumar, J. (2005). Electrospun polymer nanofibres coated with metal oxides by liquid phase deposition. *Composite Interfaces*, *11*(8–9), 711–724. https://doi.org/10.1163/1568554053148744

Dyatkin, B., Gogotsi, O., Malinovskiy, B., Zozulya, Y., Simon, P., & Gogotsi, Y. (2016). High capacitance of coarse-grained carbide derived carbon electrodes. *Journal of Power Sources*, *306*, 32–41. https://doi.org/10.1016/j.jpowsour.2015.11.099

Dyatkin, B., & Gogotsi, Y. (2014). Effects of structural disorder and surface chemistry on electric conductivity and capacitance of porous carbon electrodes. *Faraday Discuss.* https://doi.org/10.1039/C4FD00048J

Electrospinning Archives. (n.d.). *Yflow S.D.* Retrieved 3 August 2020, from http://www.yflow.com/category/electrospinning/

Electrospinning—CEST - Laboratory Equipment. (n.d.). Retrieved 9 November 2020, from https://cest.at/en/laboratory-equipment/electrospinning/

Elgrishi, N., Rountree, K. J., McCarthy, B. D., Rountree, E. S., Eisenhart, T. T., & Dempsey, J. L. (2018). A Practical Beginner's Guide to Cyclic Voltammetry. *Journal of Chemical Education*, *95*(2), 197–206. https://doi.org/10.1021/acs.jchemed.7b00361

Endo, M., Takeda, T., Kim, Y. J., Koshiba, K., & Ishii, K. (2001). *High Power Electric Double Layer Capacitor (EDLC's); from Operating Principle to Pore Size Control in Advanced Activated Carbons*. *1*(3), 13.

Frackowiak, E. (2007). Carbon materials for supercapacitor application. *Physical Chemistry Chemical Physics*, *9*(15), 1774. https://doi.org/10.1039/b618139m

Frackowiak, E., & Béguin, F. (2001). Carbon materials for the electrochemical storage of energy in capacitors. *Carbon*, *39*(6), 937–950. https://doi.org/10.1016/S0008-6223(00)00183-4

Garche, J., Dyer, C. K., Moseley, P. T., Ogumi, Z., Rand, D. A. J., & Scrosati, B. (2013). *Encyclopedia of Electrochemical Power Sources*. Newnes.

Ge, Y., Xie, X., Roscher, J., Holze, R., & Qu, Q. (2020). How to measure and report the capacity of electrochemical double layers, supercapacitors, and their electrode materials. *Journal of Solid State Electrochemistry*, *24*(11), 3215–3230. https://doi.org/10.1007/s10008-020-04804-x

Ghrib, T. (2018). *Porosity: Process, Technologies and Applications*. BoD – Books on Demand.

Giubileo, F., Di Bartolomeo, A., Iemmo, L., Luongo, G., & Urban, F. (2018). Field Emission from Carbon Nanostructures. *Applied Sciences*, *8*(4), 526. https://doi.org/10.3390/app8040526

Gogotsi, Y. (2006). *Nanomaterials Handbook*. CRC Press.

Gogotsi, Y., Nikitin, A., Ye, H., Zhou, W., Fischer, J. E., Yi, B., Foley, H. C., & Barsoum, M. W. (2003). Nanoporous carbide-derived carbon with tunable pore size. *Nature Materials*, *2*(9), 591–594. https://doi.org/10.1038/nmat957

Gouy, M. (1910). Sur la constitution de la charge électrique à la surface d'un électrolyte. *Journal de Physique Théorique et Appliquée*, *9*(1), 457–468. https://doi.org/10.1051/jphystap:019100090045700

Gudavalli, G. S., & Dhakal, T. P. (2018). Simple Parallel-Plate Capacitors to High–Energy Density Future Supercapacitors. In *Emerging Materials for Energy Conversion and Storage* (pp. 247–301). Elsevier. https://doi.org/10.1016/B978-0-12-813794-9.00008-9

Guo, Q., Zhou, X., Li, X., Chen, S., Seema, A., Greiner, A., & Hou, H. (2009). Supercapacitors based on hybrid carbon nanofibres containing multiwalled carbon nanotubes. *Journal of Materials Chemistry*, *19*(18), 2810–2816. https://doi.org/10.1039/B820170F

Hammar, A., Venet, P., Lallemand, R., & Rojat, G. (2011). Study of Accelerated Aging of Supercapacitors for Transport Applications. *Industrial Electronics, IEEE Transactions On*, *57*, 3972–3979. https://doi.org/10.1109/TIE.2010.2048832

Hao, F., & Lin, H. (2013). Recent molecular engineering of room temperature ionic liquid electrolytes for mesoscopic dye-sensitized solar cells. *RSC Advances*, *3*(45), 23521. https://doi.org/10.1039/c3ra44209h

He, T., Fu, Y., Meng, X., Yu, X., & Wang, X. (2018). A novel strategy for the high performance supercapacitor based on polyacrylonitrile-derived porous nanofibres as electrode and separator in ionic liquid electrolyte. *Electrochimica Acta*, *282*, 97–104. https://doi.org/10.1016/j.electacta.2018.06.029

Heikkila, P., & Harlin, A. (2009). Electrospinning of polyacrylonitrile (PAN) solution: Effect of conductive additive and filler on the process. *Express Polymer Letters*, *3*(7), 437–445. https://doi.org/10.3144/expresspolymlett.2009.53

Helmholtz, H. (1853). Ueber einige Gesetze der Vertheilung elektrischer Ströme in körperlichen Leitern mit Anwendung auf die thierisch-elektrischen Versuche. *Annalen Der Physik*, *165*(6), 211–233. https://doi.org/10.1002/andp.18531650603

Hester, R. E., & Harrison, R. M. (2018). *Energy Storage Options and Their Environmental Impact*. Royal Society of Chemistry.

Huang, X. (2009). Fabrication and Properties of Carbon Fibres. *Materials*, *2*(4), 2369–2403. https://doi.org/10.3390/ma2042369

Hutchins, O. (1918). *Method for the production of silicon tetrachlorid* (United States Patent No. US1271713A). https://patents.google.com/patent/US1271713A/en

Ibukun, O., & Jeong*, H. K. (2019). Effects of Aqueous Electrolytes in Supercapacitors. *New Physics: Sae Mulli*, *69*(2), 154–158. https://doi.org/10.3938/NPSM.69.154

Inamuddin, Boddula, R., Ahamed, M. I., & Asiri, A. M. (2019). *Supercapacitor Technology: Materials, Processes and Architectures*. Materials Research Forum LLC.

Inamuddin, Boddula, R., Ahmer, M. F., & Asiri, A. M. (2019). *Morphology Design Paradigms for Supercapacitors*. CRC Press.

Israelachvili, J. N. (2011). 4—Interactions Involving Polar Molecules. In J. N. Israelachvili (Ed.), *Intermolecular and Surface Forces (Third Edition)* (pp. 71–90). Academic Press. https://doi.org/10.1016/B978-0-12-375182-9.10004-1

Javed, K., Oolo, M., Savest, N., & Krumme, A. (2019). A Review on Graphene-Based Electrospun Conductive Nanofibres, Supercapacitors, Anodes, and Cathodes for Lithium-Ion Batteries. *Critical Reviews in Solid State and Materials Sciences*, *44*(5), 427–443. https://doi.org/10.1080/10408436.2018.1492367

Jeong, J. S., Jeon, S. Y., Lee, T. Y., Park, J. H., Shin, J. H., Alegaonkar, P. S., Berdinsky, A. S., & Yoo, J. B. (2006). Fabrication of MWNTs/nylon conductive composite nanofibres by electrospinning. *Diamond and Related Materials*, *15*(11), 1839–1843. https://doi.org/10.1016/j.diamond.2006.08.026

Ji, H., Zhao, X., Qiao, Z., Jung, J., Zhu, Y., Lu, Y., Zhang, L. L., MacDonald, A. H., & Ruoff, R. S. (2014). Capacitance of carbon-based electrical double-layer capacitors. *Nature Communications*, *5*(1), 1–7. https://doi.org/10.1038/ncomms4317

Junoh, H., Jaafar, J., Mohd Norddin, M. N. A., Ismail, A. F., Othman, M. H. D., Rahman, M. A., Yusof, N., Wan Salleh, W. N., & Ilbeygi, H. (2015). A Review on the Fabrication of Electrospun Polymer Electrolyte Membrane for Direct Methanol Fuel Cell. *Journal of Nanomaterials*, *2015*, 1–16. https://doi.org/10.1155/2015/690965

Käärik, M., Arulepp, M., Käärik, M., Maran, U., & Leis, J. (2020). Characterization and prediction of double-layer capacitance of nanoporous carbon materials using the Quantitative nano-Structure-Property Relationship approach based on experimentally determined porosity descriptors. *Carbon 158,* 494–504. https://doi.org/10.1016/j.carbon.2019.11.017

Käärik, M., Arulepp, M., Kook, M., Mäeorg, U., Kozlova, J., Sammelselg, V., Perkson, A., & Leis, J. (2018). Characterisation of steam-treated nanoporous carbide-derived carbon of TiC origin: Structure and enhanced electrochemical performance. *Journal of Porous Materials*, *25*(4), 1057–1070. https://doi.org/10.1007/s10934-017-0517-8

Käärik, M., Maran, U., Arulepp, M., Perkson, A., Leis, J., (2018). Quantitative nano-structure−property relationships for the nanoporous carbon: predicting the performance of energy storage materials. *ACS Applied Energy Materials, 1* (8), 4016−4024. DOI: 10.1021/acsaem.8b00708.

Karakaş, H. (n.d.). *ELECTROSPINNING OF NANOFIBRES AND THEIR APPLICATIONS*. 35.

Keypour, H., Noroozi, M., & Rashidi, A. (2013). An improved method for the purification of fullerene from fullerene soot with activated carbon, celite, and silica gel stationary phases. *Journal of Nanostructure in Chemistry*, *3*(1). https://doi.org/10.1186/2193-8865-3-45

Khalid, M., Bhardwaj, P., & Varela, H. (2018). Carbon-Based Composites for Supercapacitor. *Science, Technology and Advanced Application of Supercapacitors*. https://doi.org/10.5772/intechopen.80393

Ko, F. K., & Wan, Y. (2014). *Introduction to Nanofibre Materials*. Cambridge University Press.

Korycka, P., Mirek, A., Kramek-Romanowska, K., Grzeczkowicz, M., & Lewińska, D. (2018). Effect of electrospinning process variables on the size of polymer fibres and bead-on-string structures established with a 23 factorial design. *Beilstein Journal of Nanotechnology*, *9*, 2466–2478. https://doi.org/10.3762/bjnano.9.231

Kroto, H. (1997). Symmetry, space, stars and C 60. *Reviews of Modern Physics*, *69*(3), 703–722. https://doi.org/10.1103/RevModPhys.69.703

Kumar Panda, P., Grigoriev, A., Kumar Mishra, Y., & Ahuja, R. (2020). Progress in supercapacitors: Roles of two dimensional nanotubular materials. *Nanoscale Advances*, *2*(1), 70–108. https://doi.org/10.1039/C9NA00307J

Lee, S., Kim, J., Ku, B.-C., Kim, J., & Joh, H.-I. (2012). Structural Evolution of Polyacrylonitrile Fibres in Stabilization and Carbonization. *Advances in Chemical Engineering and Science*, *02*(02), 275–282. https://doi.org/10.4236/aces.2012.22032

Leis, J., Perkson, A., Arulepp, M., Käärik, M., & Svensson, G. (2001). Carbon nanostructures produced by chlorinating aluminium carbide. *Carbon*, *39*(13), 2043–2048. https://doi.org/10.1016/S0008-6223(01)00020-3

Leis, J., Perkson, A., Arulepp, M., Nigu, P., Svensson, G. (2002). Catalytic effects of metals of the iron subgroup on the chlorination of titanium carbide to form nanostructural carbon. *Carbon, 40* (9), 1559−1564. https://doi.org/10.1016/S0008-6223(02)00019-2

Leis, J., Arulepp, M., Käärik, M., Perkson, A. (2010) The effect of Mo2C derived carbon pore size on the electrical double-layer characteristics in propylene carbonate-based electrolyte. *Carbon 48*(14), 4001-4008. https://doi.org/10.1016/j.carbon.2010.07.003

Li, J., Su, S., Zhou, L., Kundrát, V., Abbot, A. M., Mushtaq, F., Ouyang, D., James, D., Roberts, D., & Ye, H. (2013). Carbon nanowalls grown by microwave plasma enhanced chemical vapor deposition during the carbonization of polyacrylonitrile fibres. *Journal of Applied Physics*, *113*(2), 024313. https://doi.org/10.1063/1.4774218

Li, X., Zhao, Y., Bai, Y., Zhao, X., Wang, R., Huang, Y., Liang, Q., & Huang, Z. (2017). A Non-Woven Network of Porous Nitrogen-doping Carbon Nanofibres as a Binder-free Electrode for Supercapacitors. *Electrochimica Acta*, *230*, 445–453. https://doi.org/10.1016/j.electacta.2017.02.030

Li, Z., Xu, K., & Pan, Y. (2019). Recent development of Supercapacitor Electrode Based on Carbon Materials. *Nanotechnology Reviews*, *8*(1), 35–49. https://doi.org/10.1515/ntrev-2019-0004

Libich, J., Máca, J., Vondrák, J., Čech, O., & Sedlaříková, M. (2018). Supercapacitors: Properties and applications. *Journal of Energy Storage*, *17*, 224–227. https://doi.org/10.1016/j.est.2018.03.012

Liu, Y., & Kumar, S. (2012). Recent Progress in Fabrication, Structure, and Properties of Carbon Fibres. *Polymer Reviews*, *52*(3), 234–258. https://doi.org/10.1080/15583724.2012.705410

Lu, W., & Dai, L. (2010). Carbon Nanotube Supercapacitors. *Carbon Nanotubes*. https://doi.org/10.5772/39444

Lyu, H., Gao, B., He, F., Ding, C., Tang, J., & Crittenden, J. C. (2017). Ball-Milled Carbon Nanomaterials for Energy and Environmental Applications. *ACS Sustainable Chemistry & Engineering*, *5*(11), 9568–9585. https://doi.org/10.1021/acssuschemeng.7b02170

Maletin, Y., Strizhakova, N., Kozachkov, S., Mironova, A., Podmogilny, S., Danilin, V., Kolotilova, J., Izotov, V., Cederström, J., Konstantinovich, S. G., Aleksandrovna, J. K., Vasilevitj, V. S., Efimovitj, A. K., Perkson, A., Arulepp, M., Leis, J., Wallace, C. L., & Zheng, J. (2004). *Supercapacitor and a method of manufacturing such a supercapacitor* (United States Patent No. US6697249B2). https://patents.google.com/patent/US6697249B2/en

Malmberg, S., Arulepp, M., Savest, N., Tarasova, E., Vassiljeva, V., Krasnou, I., Käärik, M., Mikli, V., & Krumme, A. (2020). Directly electrospun electrodes for electrical double-layer capacitors from carbide-derived carbon. *Journal of Electrostatics*, *103*, 103396. https://doi.org/10.1016/j.elstat.2019.103396

Mao, X., Hatton, T., & Rutledge, G. (2013). A Review of Electrospun Carbon Fibres as Electrode Materials for Energy Storage. *Current Organic Chemistry*, *17*(13), 1390–1401. https://doi.org/10.2174/1385272811317130006

Mei, B.-A., Munteshari, O., Lau, J., Dunn, B., & Pilon, L. (2018). Physical Interpretations of Nyquist Plots for EDLC Electrodes and Devices. *The Journal of Physical Chemistry C*, *122*(1), 194–206. https://doi.org/10.1021/acs.jpcc.7b10582

Miao, Y.-E., & Liu, T. (2019). Electrospun Nanofibre Electrodes. In *Electrospinning: Nanofabrication and Applications* (pp. 641–669). Elsevier. https://doi.org/10.1016/B978-0-323-51270-1.00021-2

Mishra, A., Shetti, N. P., Basu, S., Reddy, K. R., & Aminabhavi, T. M. (2020). Chapter 7—Recent developments in ionic liquid-based electrolytes for energy storage supercapacitors and rechargeable batteries. In Inamuddin, A. M. Asiri, & S. Kanchi (Eds.), *Green Sustainable Process for Chemical and Environmental Engineering and Science* (pp. 199–221). Elsevier. https://doi.org/10.1016/B978-0-12-817386-2.00007-X

Mitchell, P., Xi, X., Zhong, L., & Zou, B. (2013). *Method of manufacturing an electrode* (European Union Patent No. EP2357046B1). https://patents.google.com/patent/EP2357046B1/en

Murray, D. B., & Hayes, J. G. (2015). Cycle Testing of Supercapacitors for Long-Life Robust Applications. *IEEE Transactions on Power Electronics*, *30*(5), 2505–2516. https://doi.org/10.1109/TPEL.2014.2373368

Nascimento, M. L. F., Araújo, E. S., Cordeiro, E. R., de Oliveira, A. H. P., & de Oliveira, H. P. (2015). A Literature Investigation about Electrospinning and Nanofibres: Historical Trends, Current Status and Future Challenges. *Recent Patents on Nanotechnology*, *9*(2), 76–85. https://doi.org/10.2174/1872210509021508191515 32

Pal, B., Yang, S., Ramesh, S., Thangadurai, V., & Jose, R. (2019). Electrolyte selection for supercapacitive devices: A critical review. *Nanoscale Advances*, *1*(10), 3807–3835. https://doi.org/10.1039/C9NA00374F

Pan, H., Li, J., & Feng, Y. P. (2010). Carbon Nanotubes for Supercapacitor. *Nanoscale Research Letters*, *5*(3), 654–668. https://doi.org/10.1007/s11671-009-9508-2

Parekh, S. A., David, R. N., Bannuru, K. K. R., Krishnaswamy, L., & Baji, A. (2018). Electrospun Silver Coated Polyacrylonitrile Membranes for Water Filtration Applications. *Membranes*, *8*(3). https://doi.org/10.3390/membranes8030059

Park, S. H., Jo, S. M., Kim, D. Y., Lee, W. S., & Kim, B. C. (2005). Effects of iron catalyst on the formation of crystalline domain during carbonization of electrospun acrylic nanofibre. *Synthetic Metals*, *150*(3), 265–270. https://doi.org/10.1016/j.synthmet.2005.02.010

Pohlmann, S. (n.d.). *Ionic Liquids and Conductive Salts in Supercapacitors: Investigations on Carbon-Electrolyte Interaction* [PhD Thesis]. Westfälische Wilhelms-University.

Pohlmann, S., Lobato, B., Centeno, T. A., & Balducci, A. (2013). The influence of pore size and surface area of activated carbons on the performance of ionic liquid based supercapacitors. *Physical Chemistry Chemical Physics*, *15*(40), 17287. https://doi.org/10.1039/c3cp52909f

Presser, V., Heon, M., & Gogotsi, Y. (2011). Carbide-Derived Carbons—From Porous Networks to Nanotubes and Graphene. *Advanced Functional Materials*, *21*(5), 810–833. https://doi.org/10.1002/adfm.201002094

Qin, X.-H., Yang, E.-L., Li, N., & Wang, S.-Y. (2007). Effect of different salts on electrospinning of polyacrylonitrile (PAN) polymer solution. *Journal of Applied Polymer Science*, *103*(6), 3865–3870. https://doi.org/10.1002/app.25498

Radu, P., Szelag, A., & Steczek, M. (2019). On-Board Energy Storage Devices with Supercapacitors for Metro Trains—Case Study Analysis of Application Effectiveness. *Energies*, *12*(7), 1291. https://doi.org/10.3390/en12071291

Rajendran, S. (2016). Applications of Cyclic voltammetry in Corrosion inhibition studies Int J Nano Corr Sci and Engg 3(4)(2016) Applications of Cyclic voltammetry Applications of Cyclic voltammetry in Corrosion inhibition studies National Level Seminar on "New Perspective in Science and Technology", St Antony's College of Arts and Sciences for Women, T 3(4)(2016) 166-180 Cyclic voltammetry in Corrosion inhibition studies. *International Journal of Nano Corrosion Science and Engineering*, *3*, 166–180.

Ramakrishna, S. (2005). *An Introduction to Electrospinning and Nanofibres*. World Scientific.

Ramakrishna, S., Fujihara, K., Teo, W.-E., Yong, T., Ma, Z., & Ramaseshan, R. (2006). Electrospun nanofibres: Solving global issues. *Materials Today*, *9*(3), 40–50. https://doi.org/10.1016/S1369-7021(06)71389-X

Rinzler, A. G., Hafner, J. H., Nikolaev, P., Nordlander, P., Colbert, D. T., Smalley, R. E., Lou, L., Kim, S. G., & Tománek, D. (1995). Unraveling Nanotubes: Field Emission from an Atomic Wire. *Science*, *269*(5230), 1550–1553. https://doi.org/10.1126/science.269.5230.1550

Sada, K., Kokado, K., & Furukawa, Y. (2014). Polyacrylonitrile (PAN). In S. Kobayashi & K. Müllen (Eds.), *Encyclopedia of Polymeric Nanomaterials* (pp. 1–7). Springer Berlin Heidelberg. https://doi.org/10.1007/978-3-642-36199-9_249-1

Sadashiv Bubanale, M Shivashankar, & SIDDAGANGA INSTITUTE OF TECHNOLOGY. (2017). History, Method of Production, Structure and Applications of Activated Carbon. *International Journal of Engineering Research And*, *V6*(06). https://doi.org/10.17577/IJERTV6IS060277

Salles, V., Bernard, S., Brioude, A., Cornu, D., & Miele, P. (2010). A new class of boron nitride fibres with tunable properties by combining an electrospinning process and the polymer-derived ceramics route. *Nanoscale*, *2*(2), 215–217. https://doi.org/10.1039/B9NR00185A

Sarfraz, A., Raza, A. H., Mirzaeian, M., Abbas, Q., & Raza, R. (2020). Electrode Materials for Fuel Cells. In *Reference Module in Materials Science and Materials Engineering*. Elsevier. https://doi.org/10.1016/B978-0-12-803581-8.11742-4

Saufi, S. M., & Ismail, A. F. (2002). *Development and characterization of polyacrylonitrile (PAN) based carbon hollow fibre membrane*. *24*, 13.

Seoul, C., Kim, Y.-T., & Baek, C.-K. (2003). Electrospinning of poly(vinylidene fluoride)/dimethylformamide solutions with carbon nanotubes. *Journal of Polymer Science Part B: Polymer Physics*, *41*(13), 1572–1577. https://doi.org/10.1002/polb.10511

Sevilla, M., & Mokaya, R. (2014). Energy storage applications of activated carbons: Supercapacitors and hydrogen storage. *Energy Environ. Sci.*, *7*(4), 1250–1280. https://doi.org/10.1039/C3EE43525C

Shahzad, S., Shah, A., Kowsari, E., Iftikhar, F. J., Nawab, A., Piro, B., Akhter, M. S., Rana, U. A., & Zou, Y. (2019). Ionic Liquids as Environmentally Benign Electrolytes for High-Performance Supercapacitors. *Global Challenges*, *3*(1), 1800023. https://doi.org/10.1002/gch2.201800023

Shao, Y., El-Kady, M. F., Sun, J., Li, Y., Zhang, Q., Zhu, M., Wang, H., Dunn, B., & Kaner, R. B. (2018). Design and Mechanisms of Asymmetric Supercapacitors. *Chemical Reviews*, *118*(18), 9233–9280. https://doi.org/10.1021/acs.chemrev.8b00252

Song, K., Zhang, Y., Meng, J., Green, E. C., Tajaddod, N., Li, H., & Minus, M. L. (2013). Structural Polymer-Based Carbon Nanotube Composite Fibres: Understanding the Processing–Structure–Performance Relationship. *Materials*, *6*(6), 2543–2577. https://doi.org/10.3390/ma6062543

Stan, A.-I., Swierczynski, M., Stroe, D.-I., Teodorescu, R., & Andreasen, S. J. (2014). Lithium ion battery chemistries from renewable energy storage to automotive and back-up power applications—An overview. *2014 International Conference on Optimization of Electrical and Electronic Equipment (OPTIM)*, 713–720. https://doi.org/10.1109/OPTIM.2014.6850936

Stojanovska, E., Pampal, E. S., Kilic, A., Quddus, M., & Candan, Z. (2019). Developing and characterization of lignin-based fibrous nanocarbon electrodes for energy storage devices. *Composites Part B: Engineering*, *158*, 239–248. https://doi.org/10.1016/j.compositesb.2018.09.072

Stoller, M. D., & Ruoff, R. S. (2010). Best practice methods for determining an electrode material's performance for ultracapacitors. *Energy & Environmental Science*, *3*(9), 1294. https://doi.org/10.1039/c0ee00074d

Suresh, R., Tamilarasan, K., & Vadivu, D. S. (2017). *Effect of Electrolyte on the Supercapacitor Behaviour of CuO Nanostructures*. *4*(12), 4.

Surianarayanan, M., Vijayaraghavan, R., & Raghavan, K. V. (1998). Spectroscopic investigations of polyacrylonitrile thermal degradation. *Journal of Polymer Science Part A: Polymer Chemistry*, *36*(14), 2503–2512. https://doi.org/10.1002/(SICI)1099-0518(199810)36:14<2503::AID-POLA9>3.0.CO;2-T

Tee, E., Tallo, I., Kurig, H., Thomberg, T., Jänes, A., & Lust, E. (2015). Huge enhancement of energy storage capacity and power density of supercapacitors based on the carbon dioxide activated microporous SiC-CDC. *Electrochimica Acta*, *161*, 364–370. https://doi.org/10.1016/j.electacta.2015.02.106

Tõnurist, K., Vaas, I., Thomberg, T., Jänes, A., Kurig, H., Romann, T., & Lust, E. (2014). Application of multistep electrospinning method for preparation of electrical double-layer capacitor half-cells. *Electrochimica Acta*, *119*, 72–77. https://doi.org/10.1016/j.electacta.2013.11.155

Torop, J., Palmre, V., Arulepp, M., Sugino, T., Asaka, K., & Aabloo, A. (2011). Flexible supercapacitor-like actuator with carbide-derived carbon electrodes. *Carbon*, *49*(9), 3113–3119. https://doi.org/10.1016/j.carbon.2011.03.034

Tucker, N., Stanger, J. J., Staiger, M. P., Razzaq, H., & Hofman, K. (2012). The History of the Science and Technology of Electrospinning from 1600 to 1995. *Journal of Engineered Fibres and Fabrics*, *7*(2_suppl), 155892501200702. https://doi.org/10.1177/155892501200702S10

Ue, M., Shima, K., & Mori, S. (1994). Electrochemical properties of quaternary ammonium borodiglycolates and borodioxalates. *Electrochimica Acta*, *39*(18), 2751–2756. https://doi.org/10.1016/0013-4686(94)E0187-5

Vatamanu, J., Hu, Z., Bedrov, D., Perez, C., & Gogotsi, Y. (2013). Increasing Energy Storage in Electrochemical Capacitors with Ionic Liquid Electrolytes and Nanostructured Carbon Electrodes. *The Journal of Physical Chemistry Letters*, *4*(17), 2829–2837. https://doi.org/10.1021/jz401472c

Wallace, P. R. (1947). The Band Theory of Graphite. *Physical Review*, *71*(9), 622–634. https://doi.org/10.1103/PhysRev.71.622

Wan, Y.-Q., He, J.-H., & Yu, J.-Y. (2007). Carbon nanotube-reinforced polyacrylonitrile nanofibres by vibration-electrospinning. *Polymer International*, *56*(11), 1367–1370. https://doi.org/10.1002/pi.2358

Wang, F. (2017). *Electrochemical Capacitor Performance: Influence of Aqueous Electrolytes*. https://doi.org/10.5772/intechopen.70694

Wang, Y., Song, Y., & Xia, Y. (2016). Electrochemical capacitors: Mechanism, materials, systems, characterization and applications. *Chemical Society Reviews*, *45*(21), 5925–5950. https://doi.org/10.1039/C5CS00580A

Wei, K., & Kim, I. S. (2014). Application of Nanofibres in Supercapacitors. In B. Ding & J. Yu (Eds.), *Electrospun Nanofibres for Energy and Environmental Applications* (pp. 163–181). Springer Berlin Heidelberg. https://doi.org/10.1007/978-3-642-54160-5_7

Wei, L., & Yushin, G. (2012a). Nanostructured activated carbons from natural precursors for electrical double layer capacitors. *Nano Energy*, *1*(4), 552–565. https://doi.org/10.1016/j.nanoen.2012.05.002

Wei, L., & Yushin, G. (2012b). Nanostructured activated carbons from natural precursors for electrical double layer capacitors. *Nano Energy*, *1*(4), 552–565. https://doi.org/10.1016/j.nanoen.2012.05.002

Weingarth, D., Noh, H., Foelske-Schmitz, A., Wokaun, A., & Kötz, R. (2013). A reliable determination method of stability limits for electrochemical double layer capacitors. *Electrochimica Acta*, *103*, 119–124. https://doi.org/10.1016/j.electacta.2013.04.057

Weinstein, L., & Dash, R. (2013). Supercapacitor carbons. *Materials Today*, *16*(10), 356–357. https://doi.org/10.1016/j.mattod.2013.09.005

Welham, N. J., Berbenni, V., & Chapman, P. G. (2002). Increased chemisorption onto activated carbon after ball-milling. *Carbon*, *40*(13), 2307–2315. https://doi.org/10.1016/S0008-6223(02)00123-9

Winter, M., & Brodd, R. J. (2004). What Are Batteries, Fuel Cells, and Supercapacitors? *Chemical Reviews*, *104*(10), 4245–4270. https://doi.org/10.1021/cr020730k

Wortmann, M., Frese, N., Sabantina, L., Petkau, R., Kinzel, F., Gölzhäuser, A., Moritzer, E., Hüsgen, B., & Ehrmann, A. (2019). New Polymers for Needleless Electrospinning from Low-Toxic Solvents. *Nanomaterials*, *9*(1), 52. https://doi.org/10.3390/nano9010052

Wu, Y., & Cao, C. (2018). The way to improve the energy density of supercapacitors: Progress and perspective. *Science China Materials*, *61*(12), 1517–1526. https://doi.org/10.1007/s40843-018-9290-y

Xu, K. (1999). Toward Reliable Values of Electrochemical Stability Limits for Electrolytes. *Journal of The Electrochemical Society*, *146*(11), 4172. https://doi.org/10.1149/1.1392609

Xue, J., Wu, T., Dai, Y., & Xia, Y. (2019). Electrospinning and Electrospun Nanofibres: Methods, Materials, and Applications. *Chemical Reviews*, *119*(8), 5298–5415. https://doi.org/10.1021/acs.chemrev.8b00593

Yan, X., Tai, Z., Chen, J., & Xue, Q. (2011). Fabrication of carbon nanofibre–polyaniline composite flexible paper for supercapacitor. *Nanoscale*, *3*(1), 212–216. https://doi.org/10.1039/C0NR00470G

Ye, H., Lam, H., Titchenal, N., Gogotsi, Y., & Ko, F. (2004). Reinforcement and rupture behavior of carbon nanotubes–polymer nanofibres. *Applied Physics Letters*, *85*(10), 1775–1777. https://doi.org/10.1063/1.1787892

Yu, A., Chabot, V., & Zhang, J. (2017). *Electrochemical Supercapacitors for Energy Storage and Delivery: Fundamentals and Applications*. CRC Press.

Yu, L., & Chen, G. Z. (2019). Ionic Liquid-Based Electrolytes for Supercapacitor and Supercapattery. *Frontiers in Chemistry*, *7*. https://doi.org/10.3389/fchem.2019.00272

Yushin, G., Nikitin, A., & Gogotsi, Y. (2006). 8 Carbide-Derived Carbon. *Carbon Nanomater*. https://doi.org/10.1201/9781420004014.ch8

Zaharaddeen, S., Subramani, C., & Dash, S. S. (2016). A Brief Review on Electrode Materials for Supercapacitor. *International Journal of Electrochemical Science*, 10628–10643. https://doi.org/10.20964/2016.12.50

Zahmatkeshan, M., Adel, M., Bahrami, S., Esmaeili, F., Rezayat, S. M., Saeedi, Y., Mehravi, B., Jameie, S. B., & Ashtari, K. (2018). Polymer Based Nanofibres: Preparation, Fabrication, and Applications. In A. Barhoum, M. Bechelany, & A. Makhlouf (Eds.), *Handbook of Nanofibres* (pp. 1–47). Springer International Publishing. https://doi.org/10.1007/978-3-319-42789-8_29-2

Zhan, C., Lian, C., Zhang, Y., Thompson, M. W., Xie, Y., Wu, J., Kent, P. R. C., Cummings, P. T., Jiang, D., & Wesolowski, D. J. (2017). Computational Insights into Materials and Interfaces for Capacitive Energy Storage. *Advanced Science*, *4*(7), 1700059. https://doi.org/10.1002/advs.201700059

Zhang, L. L., & Zhao, X. S. (2009). Carbon-based materials as supercapacitor electrodes. *Chemical Society Reviews*, *38*(9), 2520–2531. https://doi.org/10.1039/B813846J

Zhang, S., & Pan, N. (2015). Supercapacitors Performance Evaluation. *Advanced Energy Materials*, *5*(6), 1401401. https://doi.org/10.1002/aenm.201401401

Zheng, J.-Y., Zhuang, M.-F., Yu, Z.-J., Zheng, G.-F., Zhao, Y., Wang, H., & Sun, D.-H. (2014, June 24). *The Effect of Surfactants on the Diameter and Morphology of Electrospun Ultrafine Nanofibre* [Research Article]. Journal of Nanomaterials; Hindawi. https://doi.org/10.1155/2014/689298

Zhong, C., Deng, Y., Hu, W., Qiao, J., Zhang, L., & Zhang, J. (2015). A review of electrolyte materials and compositions for electrochemical supercapacitors. *Chemical Society Reviews*, *44*(21), 7484–7539. https://doi.org/10.1039/C5CS00303B

Acknowledgements

Firstly, I would like to thank my first and second supervisors, Prof. Andres Krumme and Dr. Mati Arulepp, respectively, for their continued support and patience throughout my PhD studies. I am deeply grateful to all my colleagues in the Laboratory of Polymers and Textile Technology and at Skeleton Technologies OÜ for fruitful discussions, advice, and support. I express special gratitude to Skeleton Technologies OÜ for giving me the opportunity, support, and encouragement to continue my studies alongside my job in the company.

This work has been partially supported by the ASTRA "TUT Institutional Development Programme for 2016–2022" Graduate School of Functional Materials and Technologies (2014-2020.4.01.16-0032). In addition, institutional research funding was received from the Estonian Ministry of Education and Research (IUT34-14 and IUT19-28) and from the European Space Agency, ESA contract number 4000119258/16/NL/CBi, for the project "Fully electrospun durable electrode and electrochemical double-layer capacitor for high frequency".

Furthermore, I would like to thank my family for their endless support and encouragement through all these years.

Abstract

Development of electrospun nanostructured electrochemical double-layer capacitor electrodes

The main aim of this study was to develop carbide-derived carbon (CDC) containing fibrous, electrospun, thin-layered composite electrodes for supercapacitors. Fibrous electrospun electrodes for energy storage applications have a major benefit in terms of their strong mechanical properties and lower thickness compared to powder-based, pressure-rolled, or slurry-cast electrodes used in most commercially available supercapacitors. Several studies have been carried out with fibrous materials of different carbon allotropes and applying high-temperature post-treatment processes, but not with directly electrospun CDC materials without using any expensive or destructive post-treatment processes. Furthermore, the effect of various aqueous and organic electrolytes on the electrochemical performance of fibrous electrodes has not been fully assessed. To fill this gap, the effect of various electrolytes on the electrochemical performance of fibrous electrospun supercapacitor electrodes was investigated.

To optimise the CDC-based fibrous electrospun electrodes, various electrode compositions were studied in order to achieve the highest possible double-layer capacitance. A PAN solution in dimethylformamide (DMF) was electrospun with various ratios of CDC and carbon black (CB). Ionic liquid (IL) 1-ethyl-3-methylimidazolium tetrafluoroborate (EMIm-BF_4) was added at 10 wt%. The influence of densification pressure and temperature on the mechanical and electrochemical properties of electrospun electrodes was determined. The highest specific capacitance of 114 F g^{-1} was achieved with a CDC/CB ratio of 80/20 by applying a densification pressure of 2.5 MPa at 75 °C.

Tensile tests and scanning electron microscopy were used to characterise the mechanical and morphological properties of the fibrous, CDC-based, thin-layered electrodes. According to the present research, the mechanical and morphological properties of fibrous electrodes are strongly dependent on the applied densification pressure and temperature. The highest specific stress of 3.12×10^{-4} $NTEX^{-1}$ was obtained when sample heating was omitted during the densification process. Compared to the classical cast porous carbon electrode, the specific stress was approximately 20-fold higher in the case of electrospun fibrous CDC-based electrodes.

The effect of various electrolytes on the electrochemical performance of electrospun fibrous electrodes was analysed in aqueous, organic, and IL-based electrolytes. For this purpose, three different aqueous electrolytes (1.0M sodium nitrate ($NaNO_3/H_2O$), 1.0M potassium nitrate (KNO_3/H_2O), and 1.0M sodium sulphate (Na_2SO_4/H_2O)), two organic electrolytes (1.5M spiro-(1,1)-bipyrrolidinium tetrafluoroborate in acetonitrile (SBP-BF_4/ACN) and 1.8M triethylmethyl-ammonium tetrafluoroborate in acetonitrile (TEMA-BF_4/ACN)), and two IL-based electrolytes (1.5M 1-ethyl-3-methylimidazoliumbis(trifluoromethyl-sulphonyl)imide in acetonitrile (EMIm-TFSI/ ACN) and 1.5M 1-ethyl-3-methylimidazolium tetrafluoroborate in acetonitrile (EMIm-BF_4/ACN)) were studied in asymmetrical test-cell configuration. The widest potential window (3.5 V) was achieved with a 1.5M EMIm-TFSI/ACN electrolyte with a specific capacitance of 89.9 F g^{-1} for both positively and negatively charged electrodes. The highest capacitance was achieved with the aqueous 1.0M $NaNO_3/H_2O$ electrolyte, and 182.8 F g^{-1} and 295.1 F g^{-1} were achieved for the positively and negatively charged electrodes, respectively.

The best candidates from each electrolyte type were also analysed in a symmetrical test-cell configuration to characterise the energy and power performance for various electrolyte types. The highest energy density of 72.9 J g^{-1} and 0.63 W g^{-1} with no remarkable losses in cycle stability were achieved with the 1.5 M SBP-BF_4/ACN electrolyte, which indicates that fibrous CDC-based electrodes are more suitable for more mechanically demanding and high-energy applications.

To conclude, a novel approach for producing directly electrospun CDC-based fibrous electrodes for energy storage applications is proposed. Thin-layered, CDC-based fibrous electrodes were optimised to enhance the electrochemical performance and mechanical properties of the electrode materials. The CDC/CB ratio and electrode densification strongly influenced the morphological, mechanical, and electrochemical properties of the fibrous electrode. The results of the current research pave the way for further studies to improve the properties of fibrous composite electrodes for energy storage applications.

Lühikokkuvõte
Elektrilise kaksikkihi kondensaatori elektrokedratud nanostruktuursete elektroodide arendus

Doktoritöö keskendub elektrokedratud karbiidsel süsinikul (CDC) baseeruvate kiuliste elektroodide arendamisele. Kiulistel elektroodidel on mitmeid eeliseid pulber-kaetud kommertsiaalsete elektroodide ees nagu näiteks oluliselt väiksem paksus, parem painduvus ning paremad mehaanilised omadused. Varasemalt on uuritud kiulisi membraane superkondensaatorite elektroodidena kasutades erinevaid süsiniku allotroope ning rakendades neile järeltöötlus protsesse. Käesoleva töö eesmärgiks on arendada CDC osakesi sisaldavaid elektrokerdatud kiulisi elektroode, mis ei vajaks kõrgel temperatuuril kasutavaid järeltöötlus protsesse. CDC eeliseks teiste süsinike allotroopide ees on kõrge eripind, kõrge mikropooride hulk ja optimaalne mikropooride jaotus. Samuti pole varasemalt põhjalikult hinnatud erinevate vesilahustel ja orgaanilistel lahustel baseeruvate elektrolüütide mõju kiuliste elektroodide elektrokeemilistele omadustele.

CDC-l baseeruvate kiuliste elektrokedratud elektroodide koostise optimeerimiseks uuriti erinevaid CDC ja juhtiva lisandi - tahma (CB) vahekordi, lisaks ka elektroodide mehaanilisi omadusi, saavutamaks materjalis võimalikult kõrge kaksikkihi mahtuvus. Püstitatud eesmärgi saavutamiseks elektrokedrati polüakrüülnitriili (PAN) ja dimetüülformamiidi (DMF) lahusest kiulised elektroodid erinevate CDC/CB massivahekordadega. Kiuliste elektroodide juhtivuse suurendamiseks kasutati 10 massi% ioonvedelikku 1-etüül-3-metüülimidasoolium-tetrafluoroboraati ($EMImBF_4$). Lisaks uuriti kiuliste elektroodide pressimise käigus kasutatava temperatuuri ja rõhu mõju kiudude mehaanilistele ja elektrokeemilistele omadustele. Kõrgeim erimahtuvus 114 F g^{-1} saavutati CDC/CB suhtega 80/20 rakendades kiulise elektroodi pressimisel temperatuuri 75°C ja rõhku 2.5 MPa. Õhukeste kiuliste elektroodide morfoloogia ja mehaaniliste omaduste uurimiseks kasutati skaneerivat elektronmikroskoopiat ning suhtelist katkekoormust. Antud katsetuste tulemusena selgus, et kiuliste elektroodide morfoloogia ja mehaanilised omaduse sõltuvad tugevalt pressimisel rakendatavast temperatuurist ja rõhust. Kõrgeim suhteline katkekoormuse väärtus $3.12 \times 10{-}4$ N TEX^{-1} saavutati toatemperatuuril.

Käesolevas töös uuriti ka erinevate elektrolüüdi tüüpide mõju CDC-l baseeruvate kiuliste elektroodide elektrokeemilistele omadustele. Täpsemalt uuriti kolme vesilahuse (1.0M $NaNO_3/H_2O$, 1.0M KNO_3/H_2O ja 1.0M Na_2SO_4/H_2O, kahe mitte-vesilahuse (1.5M SBP-BF_4/ACN ja 1.8M TEMA-BF4/ACN) ja kahe ioonvedeliku (1.5M EMIm-TFSI/ ACN ja 1.5M EMIm-BF4/ACN) elektrolüüdi mõju elektrokeemilistele omadustele, kolme elektroodsetes katserakkudes. Kõige laiem potentsiaali aken 3.5 V, positiivselt ja negatiivselt laetud elektroodi erimahtuvusega 89.9 F g^{-1}, saavutati ioonsel vedelikul baseeruva elektrolüüdiga 1.5M EMIm-TFSI/ACN. Kõrgeim erimahtuvus 182.8 F g^{-1} ja 295.1 F g^{-1} vastavalt positiivselt ja negatiivselt laetud elektroodil, saavutati 1.0M $NaNO_3/H_2O$ elektrolüüdiga.

Kolme-elektroodsete katserakkude analüüsi tulemusel valiti igast elektrolüüdi tüübist parim kandidaat kahe-elektroodsete kondensaator - rakkude analüüsiks, hindamaks elektrokeemilise süsteemi energia- ja võimsus tihedusi. Kõrgeim energia 72.9 J g^{-1} ja võimsus 0.63 W g^{-1} saavutati mitte-vesilahuse elektrolüüdis 1.5M SBP-BF_4/ACN. Eelmainitud elektrolüüdiga ei täheldatud mahtuvuse vähenemist täis-tühjakslaadimise tsükleerimise testi käigus. Kokkuvõttes võib käesolevas töös saavutatud tulemuste põhjal

järeldada, et CDC-l baseeruvad kiulised elektroodid on eelkõige mõeldud kasutamaks rakendustes, kus on oluline kõrge energia ja head mehaanilised omadused.

Käesoleva doktoritöös pakuti välja uudne lahendus süsinikul baseeruvate kiuliste elektroodide kasutamiseks energia salvestamise rakendustes. Õhukeste kiuliste elektroodide mehaaniliste ja elektrokeemilste omaduste parendamiseks kasutati nenede koostise optimeerimist. Süsinike CDC/CB massivahekord ning elektroodide pressimise parameetrid omasid suurt mõju kiudude morfoloogiale, mehaanilistele ja elektrokeemilistele omadustele. Käesolevas töös saavutatud tulemused loovad eeldused uutele uuringutele, parendamaks kiuliste komposiit-elektroodide omadusi energia salvestus valdkonnas.

Appendix

Publication I

Malmberg, S., Arulepp, M., Savest, N., Tarasova, E., Vassiljeva, E., Krasnou, I., Käärik, M., Mikli, V., Krumme, A. (2020) Directly electrospun electrodes for electrical double-layer capacitors from carbide-derived carbon. *Journal of Electrostatics.* vol 103. 103396

Journal of Electrostatics 103 (2020) 103396

Contents lists available at ScienceDirect

Journal of Electrostatics

journal homepage: http://www.elsevier.com/locate/elstat

Directly electrospun electrodes for electrical double-layer capacitors from carbide-derived carbon

Siret Malmberg [a,b,*], Mati Arulepp [b], Natalja Savest [a], Elvira Tarasova [a], Viktoria Vassiljeva [a], Illia Krasnou [a], Maike Käärik [c], Valdek Mikli [a], Andres Krumme [a]

[a] Department of Materials and Environmental Technology, Tallinn University of Technology, Ehitajate Tee 5, 19086, Tallinn, Estonia
[b] Skeleton Technologies OÜ, Valukoja 8, 11415, Tallinn, Estonia
[c] Institute of Chemistry, University of Tartu, Ravila 14a, Tartu, 50411, Estonia

ARTICLE INFO

Keywords:
EDL capacitance
Specific energy
Carbide-derived carbon
Electrospinning
Supercapacitor
Polyacrylonitrile
Ionic liquid

ABSTRACT

This work aims towards the optimization of porous carbon saturated nanofibres composition for electrical-double layer (EDL) electrode's preparation. The properties of microporous carbide-derived carbon (CDC) based electrospun electrodes are discussed. The variable electrode composition and their mechanical properties were observed to obtain the highest EDL capacitance. Effect of densification pressure and -temperature of electrospun electrodes are discussed. Thin electrode layer enables faster charge-discharge capability and perform higher power with same consumption of electrode materials. The EDL capacitance of 114 Fg^{-1}, determined by cyclic voltammetry method within the voltage range of 0–2.7 V, was achieved.

1. Introduction

Electrochemical capacitors, also called as supercapacitors or ultra-capacitors, are energy storage devices with short time charge-discharge capability and long cycle life [1]. Supercapacitors are categorized as pseudocapacitors or electric double-layer capacitors (EDLC) [2]. The categorization depends on the charge storage mechanism and used electroactive materials [3]. Supercapacitors can be used in different applications, for example in automotive industry, electronics and energy recovery, *etc.* [4,5].

Electrospinning is a well-known fibre forming process, which is drawn significant attention in energy storage devices like in fuel cells, lithium ion batteries and dye-sensitized solar cells [6–9]. In last twenty years, the EDLC is gaining more and more attention alongside with batteries [10]. Their main advantages over secondary batteries are long cycle life, high power density and fast charge-discharge capability [1,6,11]. To achieve good EDL capacitance, carbon material with high surface area combined with polymer substance are required. Traditional capacitor electrodes are produced in the form of film, activated carbon paste or carbon fabric [12]. However, in recent years, electrodes of electrochemical capacitors have been also produced from electrospun nanofibres and electrosprayed mats [6,13–16].

Electrochemical double-layer system consists mainly of carbonaceous electrodes, separator and electrolyte. The EDL is formed on the surface of carbon/electrolyte interface [13].

The optimal electrode composition, thickness, wettability, porous structure and the mass transfer rate of ions in micro-mesoporous carbon material and separator are important parameters for development of supercapacitors [11]. One of the main advantages of electrospun electrode material is the thickness near 20 μm, which is several times lower compared to the conventional capacitor electrodes, including good flexibility of the electrode [17–19]. The decrease in thickness improves kinetics of electrolyte ions into the carbon electrode.

There have been several attempts to produce fibre-based supercapacitor electrodes for testing in aqueous and non-aqueous electrolytes [14–17,20]. The highest specific capacitance 120 Fg^{-1} in non-aqueous electrolyte and 155 Fg^{-1} in aqueous electrolyte are achieved [14,15].

With binder bonded fibrous electrodes the biggest problem is the relatively high polymer content, which is needed for mechanical strength of the electrodes. In order to decrease the effect of polymer isolating matrix, usage of conductive polymers [21,22] or activation processes such as pyrolysis and carbonization [14–16] are needed. However, fibrous electrodes electrospun directly from a carbon saturated solution have yet to be achieved. The advantage of directly electrospun electrodes is the less complex steps in preparations, lower cost and better mechanical durability [23].

* Corresponding author. Department of Materials and Environmental Technology, Tallinn University of Technology, Ehitajate Tee 5, 19086, Tallinn, Estonia.
E-mail address: siret.malmberg@taltech.com (S. Malmberg).

https://doi.org/10.1016/j.elstat.2019.103396
Received 5 June 2019; Received in revised form 29 October 2019; Accepted 31 October 2019
Available online 18 November 2019

One key element for achieving high EDL capacitance is proper choice of microporous carbon, which must have high surface area and the micropores need to be readily available for electrolyte ions. Commonly, the activated carbon materials are used, which can be obtained from natural sources such as fruit shells like coconut shells, and from wood, pitch, coke, or from synthetic precursors such as selected polymers [24]. Main disadvantages of activated carbon materials are the broad pore size distribution and relatively low bulk density [25–27]. Promising candidates can be found among so-called carbide-derived carbon (CDC) [25,26,28]. CDC stands for a large family of carbon materials, which are synthesized from metal or non-metal carbide precursors, transformed into pure carbon by following chemical reaction:

$$MC_x + y/2\ Cl_2 = xC + MCl_y$$

CDC materials have gained great attention, due to their unique properties, most importantly a structurally high microporosity from amorphous carbon to graphite structure. Widely investigated EDL processes on microporous carbon-electrodes have shown opportunities for significantly increasing gravimetric and volumetric capacitance [25,28]. The increase in capacitance can be reached by choosing suitable electrolytes and combining them with optimal microporosity and micropore size of carbide-derived carbon, which are exhibiting optimized high surface areas [25,28,29].

Electrochemical properties of titanium carbide-based carbon materials have been investigated with non-aqueous solutions; the achieved capacitance was up to 125 Fg^{-1} [28]. Furthermore, the fine-tuning of pore size distribution and increasing the nano-porosity of CDC can increase specific capacitance up to 140 Fg^{-1} [30].

Recent studies have shown that electrochemical performance of CDC can be improved even more by applying the additional activation. Steam based post-treatment of TiC-derived carbon increased microporosity of CDC by up to 50%. It was also demonstrated that when the volume of micropores is optimally adjusted to the electrolyte ion, specific capacitances close to 160 Fg^{-1} in non-aqueous electrolyte solution can be reached [31].

Electrospinning is relatively simple and easily scalable technique to fabricate high surface area nanofibres. In general, electrospinning is a process where a polymer drop from the tip of a needle is drawn into nanofibres by using electrostatic force and evaporating the solvent under the electrical field on the way to the grounded collector [15,22].

For EDLC electrode fabrication by electrospinning it is important to use carbon with rather small particle size (e.g., ca 0.1 μm in this work). Therefore, the grinding of carbon particles is often used. Furthermore, the grinding process of active carbon material helps to form a good conductive network among carbon particles, binder and current collector [32]. There are several grinding methods for carbon, such as manual grinding in a mortar, ball-milling [33], planetary ball-milling [34], etc. The conditions of ball-milling have an influence on the pore structure of carbon particles as well as on the capacitance of the resulting supercapacitor electrode. It is known that longer grinding time increases capacitance due to reduced particle size of carbon [30,35].

In addition to grinding, the densification process is also used to improve the performance of electrospun electrodes [36]. Densification is a common post-treatment for electrode formation, during which the electrodes are mechanically pressed in more dense structure by applying static pressure. Densification of the electrode has substantial influence on its thickness, density and surface morphology, and therefore, has influence also on electrochemical performance of resulting capacitors. Lobo et al. has shown that reduction of electrode thickness below critical limit, ca. 25 μm, can potentially improve power and energy densities for a given electrolyte as the electrode kinetics can furthermore be controlled by diffusional geometry change from linear to radial or edge transport mechanism. Over-compacting must be avoided, because this can cause the decrease in macro-porosity and capacitance of the electrode [37].

The purpose of this work is to form CDC-based nanofibrous electrodes for supercapacitors. Electrospun fibers have been tried several times for energy storage, but in this work a combination of high EDL capacity CDC and polymer has been achieved without further processing.

2. Experimental section

2.1. Materials

Polyacrylonitrile (PAN) (Sigma-Aldrich, $M_w = 15000$ g/mol) was used as a polymer matrix and dimethylformamide (DMF) (Sigma-Aldrich), was used as solvent.

Carbide derived carbon and carbon black (CB) were used as carbon materials, which guarantee high specific surface area and on other hand good electrical conductivity of the produced electrodes. CDC has highly nonporous structure with large surface area [38]. Titanium carbide (TiC) was converted to CDC by using Cl_2 treatment at 900 °C. Thereafter carbon was purified with hydrogen gas at 800 °C in purpose to remove residues of chlorine. CDC was produced by Skeleton Technologies OÜ. The specific surface area of CDC was 1577 m^2g^{-1} and particle size around 1–5 μm of the initial sample. The Super-C carbon black was used as conductive additive, it was purchased from Timcal with particle size approximate 30 nm.

Ionic liquid 1-ethyl-3-methylimidazolium tetrafluoroborate ($EMImBF_4$) (Sigma-Aldrich, purity ≥99.9%) was used. The aim of using ionic liquids was to improve the dispersion of carbon additives and to increase the conductivity of membranes [39].

2.2. Grinding of carbide-derived carbon

Grinding of CDC was carried out with planetary ball mill, Retch PM 100. To avoid formation of highly responsive surface of CDC, the planetary grinder was vacuumed and thereafter filled with nitrogen. Two types of balls were used, 19 mm stainless steel balls and 3 mm zirconium oxide balls, whereas milling time varied from 0.5 h to 10 h. The ratio between CDC and balls was selected ¼ by volume.

2.3. Preparation of spinning solution

Solution of PAN in DMF with carbon saturated mixture of CDC and CB were prepared for electrospinning solution by using sonification and mechanical stirring methods. Firstly, CB and CDC were dispersed into DMF by using ultrasonic treatment for 2 h with Bendelin Sonapuls Ultrasonic device. Following ratios between CDC and CB were used: 80/20, 85/15, 90/10 and 100/0 respectively. During sonification the solution was cooled down by using ice bath, to avoid heating effect. Afterwards, formed dispersion was mechanically stirred at 40 °C for 24 h. Finally, 7 wt% of PAN was added to whole solution (the ratio between PAN and carbon were kept as constant 50/50), and the dispersion was mechanically stirred another 24 h at 40 °C before electrospinning process. Finally, 15 wt% of $EMImBF_4$ was added to the electrospinning solution directly before the electrospinning, continued with mechanical stirring for 30 min at 40 °C.

2.4. Electrospinning

Electrospinning process was carried out at room temperature with relative humidity ca 40%. Horizontal electrospinning system was used, which consisted of the high voltage power supply (Gamma High Voltage Research Ormond Beach), in-house built grounded drum collector and syringe pump (New area pump system, Inc). Pumping rate in range of 0.3–1.5 ml h^{-1} was used depending on the solution viscosity. Distance between spinneret (needle of syringe) and drum collector varied between 8 and 10 cm. The voltage was used between 15 and 18 kV.

2.5. Densification process for electrodes

Densification of fibrous electrospun electrodes carried out with hydraulic static press Scamia. Electrospun electrode samples were pressed with pressure up to 2.5 MPa at different temperatures, from room temperature (RT) up to 125 °C. Densification time was 1 min and kept as constant through all experiments.

2.6. Sample analysis

In order to evaluate morphology and distribution of carbon particles in formed fibre mats, produced electrodes were analysed by SEM TM-1000 Hitachi and Gemini Zeiss Ultra 55. No conductive coating was deposited onto the samples.

Specific surface area (S_{BET}) of CDC was determined by using NOVA touch LX2 (Quantachrome Instruments). Before S_{BET} measurement carbon were kept under vacuum for 1 h at 300 °C. Low-temperature adsorption was done at the boiling temperature of nitrogen (77 K). The specific surface areas of measured carbon samples were calculated from N_2 adsorption in the p/p_0 interval of 0.02–0.2 by the Brauner-Emmet- Teller (BET theory) [40]. N_2 adsorption isotherm was also used for obtaining values of total pore volume (V_{tot}), calculated at p/p_0 of 0.97. A volume of micropores (V_μ) calculated from t-plot by using DeBoer statistical thickness.

Mechanical properties of fibrous electrodes were tested with an Instron 5866 tensile testing machine. Sample ribbons were cut to rectangular shape with length of 10 mm and a width of 4.5 mm. Five specimens were cut from each electrospun sample of electrode. Maximum load values were measured. Specific stress at maximum load was used for describing strength of fibrous electrodes. Density of each specimen was found in order to calculate the specific stress. The density ρ, was calculated according to the following equation:

$$\boldsymbol{\rho} = \frac{\mathbf{m}}{\mathbf{V}} \tag{1}$$

where m is a weight of the electrode and V is the volume of the electrode. The specific stress σ_{sp} in ($Ntex^{-1}$) was calculated according to equation (2):

$$\boldsymbol{\sigma_{sp}} = \frac{\mathbf{F}}{\mathbf{A}} \times \frac{1}{\boldsymbol{\rho}} \tag{2}$$

where F is force, A is width of sample (in cm) and ρ is the density (gcm^{-3}) [41].

Electrochemical evaluation. The fibrous electrode was electrospun on top of a carbon coated aluminum collector. The same composition was used for both, positively and negatively charged electrodes. Electrodes were cut out from electrospun material in disk size (with diameter 15 mm). All electrodes were tested in two electrode test cells. By assembly of the cell, electrodes were interleaved with two layers of ion-permeable separator paper (Nippon Kodoshi). After assembly, the cells were kept under vacuum for 72 h at 100 °C to remove absorbed gases and water from the prepared electrode pack. Thereafter, dried EDLC cells were vacuum filled with electrolyte, 1.8 M triethylmethylammonium terafluorborate ($TEMABF_4$) in acetonitrile (Honeywell**)**.

The electrochemical evaluation of the assembled EDLC-s was carried out with cyclic voltammetry (CV), in voltage range from 0 to 2.3 V with voltage scan rate of 5 mV s^{-1}. The rate of voltage change over time during the electrode potential ramp is known as the voltage scan rate. The operating voltage range was determined from the CV curves, whereas for selected cells the maximum voltages was increased up to 2.7 V. All measurements were carried out by multi-channel potentiostat VMP3 (BioLogic Science Instruments). Capacitance and energy were evaluated from the cyclic voltammetry data. Capacitance was calculated by dividing the integrated current I (between 0 V and 2 V, the region was selected based on occurred plateau on discharge curve) with voltage scan rate v, according to formula (3):

$$\mathbf{C} = \frac{\int_0^2 \boldsymbol{IdU}}{v} \tag{3}$$

whereas the specific capacitance (C_g) was calculated by equation (4):

$$\boldsymbol{C_g} = \frac{4\mathbf{C}}{\mathbf{m}} \tag{4}$$

where m is the weight of the carbon in electrodes.

Energy was calculated according to equation (5):

$$\boldsymbol{E} = \frac{\boldsymbol{CU}^2}{2} \tag{5}$$

where U is the applied voltage and specific energy E_g was calculated by eq. (6):

$$\boldsymbol{E_g} = \frac{\boldsymbol{E}}{\boldsymbol{m}} \tag{6}$$

3. Results and discussion

Different grinding processes were used to decrease the carbon particle size down to 0.1 μm. The applied grinding showed decrease in aggregation and complete disruption of the carbon particle structure. The best results of grinding, in terms of high specific surface area, were achieved by using planetary ball mill, with zirconium oxide balls in inert atmosphere (N_2). The rotation direction of the pot was determined at a speed of 300 rpm, in counter to the rotational speed of the disk revolution. The milled CDC fraction was analysed by BET and SEM methods. The porosity characteristics of grinded CDC samples 1–4, are presented in Table 1.

Grinding process of carbon materials increases the effective conducting surface in-between the activated carbon, binder and current collector is well known phenomenon [34]. Properly ground carbon material also helps to form a good conductive network. The porosity characteristics analysis revealed that in certain conditions surface area of milled CDC was 1560 m^2g^{-1}, which only slightly less compared to the initial surface area of CDC (1637 m^2g^{-1}). Furthermore, with increasing milling time up to 6 h, surface area of CDC was decreasing rapidly, as was obtained by SEM analysis. Previous can be explained by exceeding the optimum time of the milling or in high energy mill catalytical effect between carbon and stainless-steel balls can take place [36]. SEM analysis of grinded CDC particles showed that during grinding process, particle size was decreased, and distribution of the carbon particle size got more uniform (see Fig. 1). Based on the particle size analysis, the average particle size after milling was 0.8 μm.

3.1. The influence of densification process on supercapacitor electrodes

Densification is a common preparation process for supercapacitor electrode formation and has a substantial influence on electrode thickness, -density, mechanical properties and surface morphology. Therefore, it has also influence on the electrochemical performance of capacitors.

After densification, electrospun electrodes (PAN + CDC/CB in DMF) were assembled in electrical double-layer capacitors, the ratio of CDC and CB were set as following CDC/CB = 80/20 with addition of ionic liquid, 1-ethyl-3-methylimidazolium tetrafluoroborate ($EMImBF_4$ 15 wt % per solution).

The density values were calculated for each electrode sample, which showed that electrode density increases with increasing densification temperature. For example, the density of electrode sample compacted at room temperature (~25 °C) was 0.75 gcm^{-3} and increased up to 0.93 gcm^{-3} by increasing the temperature to 125 °C. With increasing electrode density, higher volumetric capacitance is achieved, and kinetics of

Table 1
The porosity characteristics of grinded CDC samples 1–4.

Sample ID	Grinding Method	Material of balls	Milling Atmos-phere	Milling time (h)	Porosity characteristics		
					S_{BET} (m^2g^{-1})	Vμ (cm^3g^{-1})	Vtot (cm^3g^{-1})
1	non-grinded	-	-	-	1637	0.71	0.81
2	planetary ball mill	stainless steel	N_2	6	222	0.07	0.19
3	planetary ball mill	stainless steel	N_2	1	1422	0.61	0.72
4	planetary ball mill	zirconium oxide	N_2	1	1560	0.71	0.82

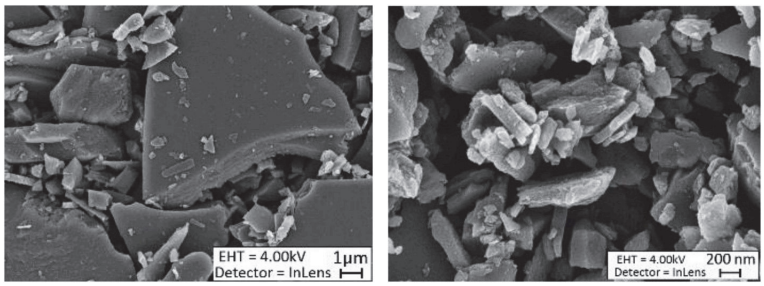

Fig. 1. SEM images of non-grinded CDC powder (left) and grinded CDC powder with planetary ball mill after 1 h (right).

electrochemical system is improved, as explain later. Furthermore, SEM analysis revealed that the fibrous structure of the electrodes was destroyed with densification at temperature higher than 95 °C (on Fig. 2). The loss of fibrous structure can be explained with exceeding the glass transition temperature of PAN (85 °C), weakening the binding effect and mechanical properties.

In order to study densification influence on mechanical properties, materials ribbons pressed in temperature range from room temperature to 95 °C were tested at 100 mm/min on extension for mechanical tests. Ribbons pressed at 125 °C were too weak for testing. The densification pressure was kept constant 2.5 MPa for all samples.

The influence of different densification temperatures on mechanical properties is presented in Fig. 3. As it can be seen, the electrodes become weaker with increasing temperature. Densification itself has no significant influence on the specific stress values of electrospun electrodes at RT. Densification of the electrospun electrodes under elevated temperature (up to 95 °C) decreases specific stress up to three times compared to the densification at room temperature. This effect is probably caused

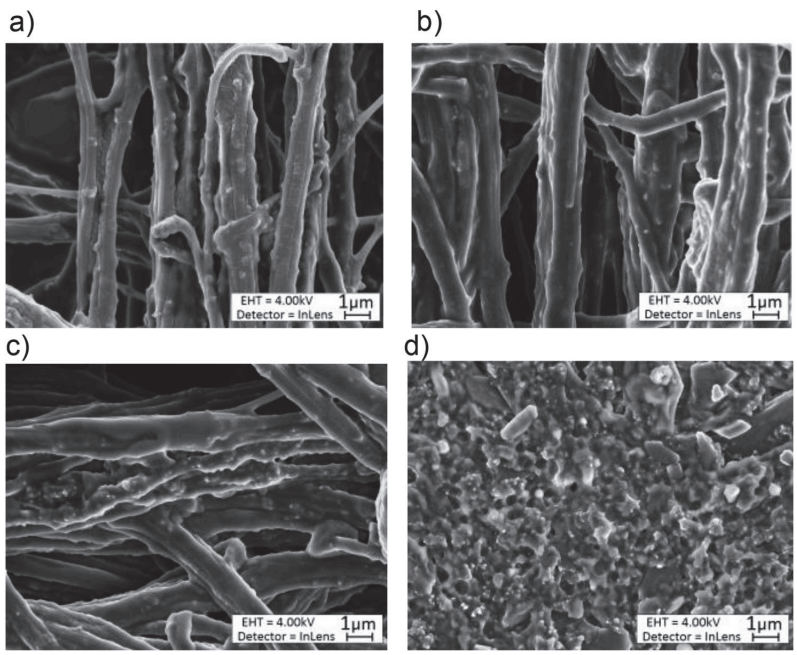

Fig. 2. SEM images of electrode samples: a) without densification b) at 75 °C c) at 95 °C and d) at 125 °C.

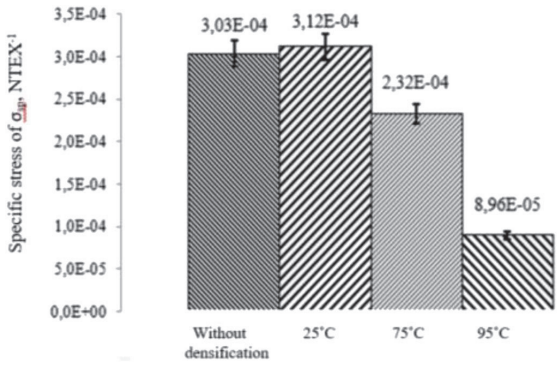

Fig. 3. Specific stress of electrospun electrodes.

by the fact that during hot-pressing fibres are losing macromolecular orientation. The highest specific stress 3.12×10^{-4} NTEX^{-1} was obtained when sample heating was not applied.

Tested ribbons were also analysed by SEM, in order to see fracture process of fibres. On Fig. 4, SEM images of fractured fibres are represented. As could be seen the fibres at break point are decreased in diameter, which is clear evidence of fibre necking before the break. This is typical behaviour of solid-state polymer materials at tensile deformation. Fibre necking phenomenon evidences strong interaction between fibres in material so that fibres are not drawn out of the material under extension load. The adhesion between current collector and electrodes became stronger after densification and it does not influence on the temperature. Densification helps to form crosslinking between fibre layers. Better contact between fibres inside of the electrospun matt, ensures higher conductivity and more effective charge transfer.

3.2. Results of electrochemical evaluation

The influence of densification pressure on electrochemical behaviour of four different pressures were tested: 0; 0.6; 1.25 and 2.5 MPa. For this purpose, the membrane of PAN in DMF with CDC and CB mixture was prepared. The polymer concentration was kept as constant (7% of PAN) and the ratio of CDC and CB was selected as 85/15. The 15% of ionic liquid $EMImBF_4$ was added to the electrospinning solution. After compaction of electrospun electrodes their electrochemical properties were evaluated in electrical-double layer capacitor with voltage range 0–2.3 V and scan rate of 5 mVs^{-1} (shown Fig. 5).

By increasing the densification pressure from 0 to 2.5 MPa specific capacitance increases from 11 to 100 Fg^{-1} per dry weight of CDC. Typical double-layer capacitor behaviour on CV in the pressure range of 1.2–2.5 MPa was achieved. One can suggest that better electrical contact

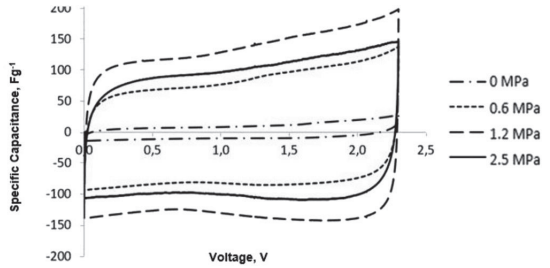

Fig. 5. Dependence of specific capacitance vs. voltage of electrodes after different densification ratios.

between the CDC and CB particles is achieved by applying pressure to the fibrous electrode.

For the optimal densification pressure of 2.5 MPa, the effect of temperature on capacitance was studied. The CV plots of various densification temperature electrodes are shown on Fig. 6a.

Achieved CV showed typical double-layer capacitor behaviour with nearly rectangular shape. The highest specific capacitance 114 Fg^{-1} for electrodes with densification temperature 75 °C was achieved. There is some delay in reaching the plateau of capacitance of the sample electrode at the applied compaction temperature of 95 °C, indicating its worse material kinetics due to the higher resistance. Most probably increase in electrical resistance due to partial bond breakage and on the other hand diffusion inhibition of electrolyte ions due to over compaction of material. This behaviour is clearly seen for electrode sample at temperature 125 °C showed decrease in specific capacitance (89 Fg^{-1}, in Fig. 6a). This is in correlation with SEM analysis, as the voltammogram of 125 °C electrode sample did not show as good rectangular shape as all other samples, probably due to destroyed fibrous structure. With the loss of the fibrous structure conductivity of the fibres is also decreased as the carbon particles were not in ordered structure anymore and partially blocked by polymer (see Fig. 2d). The fibrous electrode sample with densification temperature 75 °C was tested also at higher voltages from 2.3 V up to 2.7 V, (see Fig. 6b). Achieved cyclic voltammograms maintained good electrochemical stability also in wider voltage range as every next CV curve overlapped with previous one. Therefore, it can be concluded that the optimum densification parameters for CDC containing fibrous membranes is the 75 °C with compacting pressure in range of 1.2–2.5 MPa.

3.3. The influence of CDC ratios on specific capacitance

Four different CDC to CB ratios were tested for explaining optimized CDC and CB content in the electrospun electrodes. Weight ratios of CDC and CB were varied as following: CDC/CB 80/20, 85/15, 90/10 and

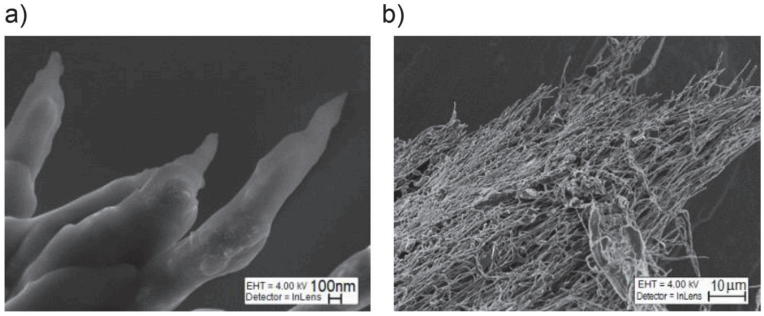

Fig. 4. SEM analysis of fracture ends of mechanical test ribbons at different magnification.

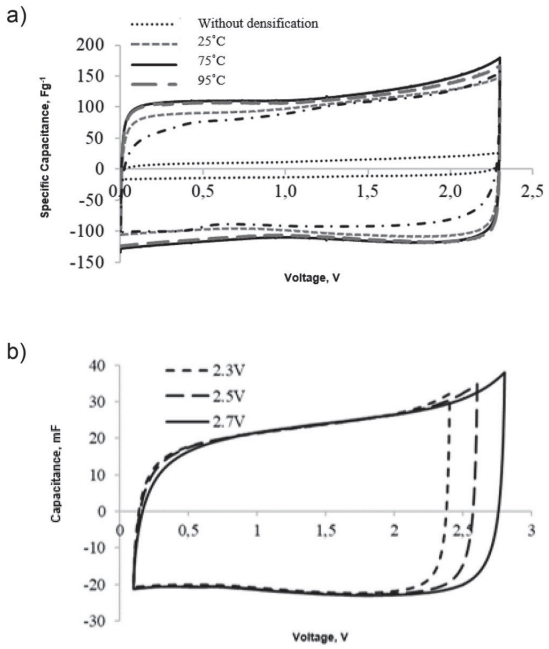

Fig. 6. a) The specific capacitance vs. voltage for different densification temperatures (2.5 MPa). **b)** The capacitance vs. voltage for fibrous electrode pressed at 75 °C, (2.5 MPa) at various voltage ranges.

100/0. The hypothesis was that higher specific capacitance will be achieved with increasing the CDC content in electrodes. The optimum densification parameters were applied, namely T = 75 °C and P = 2.5 MPa. The electrospun electrodes were tested with cyclic voltammetry in voltage range of 0–2.3 V. EDL characteristics of tested samples are presented in Fig. 7.

The ratio of the CDC and CB had significant influence on the capacitance values based on the achieved voltammograms. The highest specific capacitance of 114 Fg^{-1} and round-trip efficiency of 98% with CDC and CB ratio 80/20 was achieved, which is quite close to capacitance of conventional capacitors electrodes 120 Fg^{-1}. Based on the previous studies it is known that the specific capacitance and round-trip efficiency values starts decreasing when the CB content is increased above 20% [24]. This behaviour can be explained with the increase of the higher surface area of the particles as CDC has much higher surface area compared to carbon black. The surface area of CDC powder is 1637 m^2g^{-1} and the surface area of CB is 62 m^2g^{-1}. Therefore, with increasing the carbide-derived carbon content to certain level, the better accessibility to porous structure is ensured. However, the fine particles of conductive carbon are also needed to make electrical contacts (or bridges) between the carbide-derived carbon particles in fibrous structure. As the concentration of the polymer matrix (50%) is quite high in fibrous electrodes compared to the conventional EDLC electrodes (3–8%), the capacitive component CDC particles tend to be blocked. Therefore, when the CB amount is decreased below 20%, the specific capacitance value starts decreasing again due to the lack of conductivity between CDC particles in fibres. Specific energy of electrospun fibrous mats were also studied as supercapacitors are used for delivering and releasing energy. Similarly, to the specific capacitance, the highest specific energy value of 75 $kJkg^{-1}$ (at 2.3 V) was achieved with the CDC and CB ratio 80/20. The lowest energy value was obtained with pure CDC/PAN based electrode sample, where the energy value was two times lower.

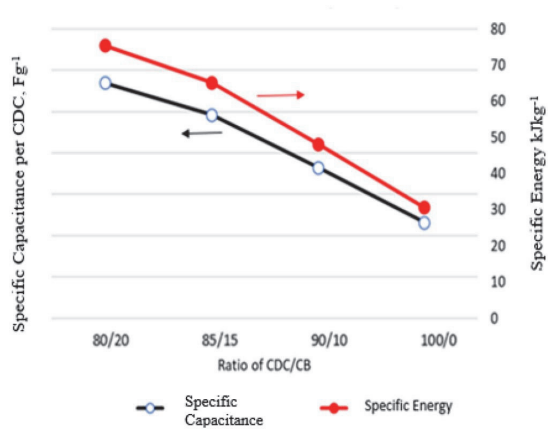

Fig. 7. The influence of CDC/CB ratio on the specific capacitance and specific energy.

4. Conclusions

This paper demonstrates an effective way to produce supercapacitor electrodes from carbon saturated polymer compounds. The combination of electrospinning and densification allows achieving fibrous electrodes with decent mechanical properties and high EDL capacitance. The optimized densification conditions were found as a temperature of 75 °C and a pressure between 1.2 and 2.5 MPa. It was shown that the densification of fibrous electrodes under elevated temperature above RT decreases the specific stress up to 24%, however, the capacitance therein increases by two times.

The electrospun fibrous carbon saturated electrodes in thickness range of 10–20 μm (with mass loading 2.13 $mgcm^{-2}$) after densification process applied show the EDL capacitance in the range of 46–114 Fg^{-1}. The highest specific capacitance value of 114 Fg^{-1} (yielding specific energy of 75.4 Jg^{-1}) at 2.3 V with CDC and CB ratio of 80/20, was achieved. The fibrous electrode based EDLC was successfully tested in voltage range up to 2.7 V and shows good electrochemical stability according to CV curves.

The advantage of directly electrospun fibrous electrodes is the elimination of pyrolysis-treatment, which currently is a routine procedure in the process for making conductive carbon fibres. Electrospun fibrous electrodes have relatively high binder content (50 wt% of solid material), which gives them outstanding mechanical properties. Nevertheless, their capacitance per carbon (*i.e.* per carbon weight in the electrode) compared to conventional supercapacitor electrode. The usage of fibrous electrodes in non-aqueous supercapacitors allows working at higher voltages and therefore to achieve higher energy densities.

Declaration of competing interest

The authors declare that they have no known competing financial interests or personal relationships that could have appeared to influence the work reported in this paper.

Acknowledgements

This work was financially supported by institutional research funding of the Estonian Ministry of Education and Research (IUT34-14 and IUT19-28). In addition, by the European Space Agency, ESA contract number 4000119258/16/NL/CBi “Fully electrospun durable electrode and electrochemical double-layer capacitor for high frequency

applications". We thank also Dr. Sebastian Pohlmann for consulting.

References

[1] S. Ymazaki, T. Ito, M. Ymagata, M. Ishikawa, Performance of non-aqueous electrochemical capacitor utilizing halogen redox reaction, Elec. Soc. S 41 (2012) 15–23.

[2] H. Su, H. Huang, H. Zhang, X. Chu, B. Zhang, B. Gu, X. Zheng, S. Wu, W. He, C. Yan, J. Chen, W. Yang, In Situ Direct Method to Massively prepare hydrophilic porous carbide-derived carbons for high- herformance supercapacitors, ACS Appl. Energy Mater. 1 (2018) 3544.

[3] H.A.A. Bashid, H.N. Lim, S.M. Hafiz, Y. Andou, M. Altrawneh, Z.T. Jiang, N. M. Huang, Modification of Carbon-Based Electroactive Materials for Supercapcitor Applications, Elsevier, Canada, 2018, p. 393.

[4] M. Xianwen, T. Hatton, G. Rutledge, A review of electrospun carbon fibers as electrode materials for energy storage, COC 17 (13) (2013) 1390–1401.

[5] J. Hwang, J. Muth, T. Gosh, Electrical and mechanical properties of carbon-black-filled, Adv. Poly Mat I 104 (2007) 2410–2417G.

[6] G. Sun, L. Xie, H. Liu, Electrospinning of nanofibers for energy applications, Nanomat 6 (2016) 129.

[7] N. Bahri-Laleh, A. Correa, S. Mehdipour-Atei, H. Arabi, M.N. Haghughi, G. Zohuri, L. Cavallo, Moving up and down the titanium oxidation state in ziegler- natta catalysis, Macromol 44 (2011) 7307.

[8] K. Liu, B. Kong, W. Liu, Y. Sun, M.-S. Song, J. Chen, Y. Liu, D. Lin, A. Pei, Y. Cui, Stretchable lithium metal anode with improved mechanical and electrochemical cycling stability, Joule 2 (2018) 1857.

[9] J. Chen, Y. Huang, N. Zhang, H. Zou, R. Liu, C. Tao, X. Fan, Z.L. Wang, Micro-cable structured textile for simultaneously harvesting solar and mechanical energy, Nat. Energy 1 (2016) 16138.

[10] Z. Wu, L. Li, J. Jan, X. Zhang, Materials and system construction for conventional new-concept supercapacitors, Adv. Sci. (2017) 4.

[11] K. Tõnurist, A. Jänes, T. Thomberg, H. Kurig, E. Lust, Influence of mesoporous separator properties on the parameters of double-layer capacitor single cells, J. Electrochem. Soc. 4 (2009) 156.

[12] T. Umemura, K. Abe, K. Akiyama, Y. Tanaka, All film power capacitor with folded electrode foil, Trans. Pow. Del. 1 (1987) 182–188.

[13] W. Xing, S.Z. Qiao, R.G. Ding, F. Li, G.Q. Lu, Z.F. Yan, H.M. Cheng, Superior electric double layer capacitors using ordered mesoporous carbons, Carbon 44 (2006) 216–224.

[14] J. Fang, X. Wang, T. Lin, in: Lin Tong (Ed.), Nanofibers - Production, Properties and Functional Applications, InTech, 2011.

[15] K. Liivand, I. Vaas, T. Thomberg, J. Jänes, E. Lust, Low Temperature Performance of electrochemical double-layer capacitor based on electrospun half-cells, J. Electrochem. Soc. 5 (2015) A5031–A5036.

[16] M. Tebyetrkerwa, S. Yang, S. Peng, Z. Xu, W. Shao, D. Pan, S. Ramakirshna, M. Zhu, Unveling polyindole: freestanding as- electrospun polyindole nanofibers and polyindole/carbon nanotubes composite as enhanced electrodes for flexible all solid-state supercapacitors, Electrochm Acta 247 (2017) 400–409.

[17] M.P. Chavhan, S. Ganguly, A novel carbon film electrode for supercapacitor by deposition of precursor sol on the collector, followed by carbonization and activation in situ, Ionics 25 (2019) 2373–2382.

[18] W. Song, X. Ji, W. Deng, Q. Chen, C. Shen, C.E. Banks, Graphene ultracapacitors: structural impacts, Phys. Chem. Chem. Phys. (2013) 13.

[19] E. Lust, A. Jänes, T. Pärn, P. Nigul, Influence of nanoporous carbon electrode thickness on the electrochemical characteristics of a nanoporous carbon|tetraethylamonium tetrafluoroborate in acetonitrile solution interface, J. Soild State Electrochem. 8 (2004) 224–237.

[20] X. Xiao, T. Li, P. Yang, Y. Gao, H. Jin, W. Ni, W. Zhan, X. Zhang, Y. Cao, J. Zhong, L. Gong, W. Yen, W. Mai, J. Chen, K. Huo, Y. Chueh, Z.L. Wang, J. Zhou, Fiber-base all-solid-state flexible supercapacitors for self-powered systems, ACS Nano 6 (2012) 9200–9206.

[21] Y. He, X. Wang, P. Zhang, B. Chen, Z. Guo, In-situ electropolymerization of porous xonduxting polyaniline fibrous network for solid- state supercapacitor, Appl. Surf. Sci. 469 (2019) 446–455.

[22] J. Liang, S. Su, D. Wang, S. Xu, Electrospun Fibrous Electrodes with Tunable Microstructure Made of Polyaniline/multi-Walled Carbon Nanotube Suspension for All-Solid-State Supercapacitors vol. 211, 2016, pp. 61–66.

[23] S. Malmberg, E. Tarasova, V. Vassiljeva, I. Krasnou, M. Arulepp, A. Krumme, Fully Electrospun Durable Electrode and Electrochemical Double-Layer Capacitor for High Frequency Applications, ESA SPCD, 2018. Symposium.

[24] P. Simone, A. Burke, Nanostructured Carbons: Double-Layer Capacitance and More, Electrochem Soc, 2008, pp. 38–40.

[25] J. Leis, A. Perkson, M. Arulepp, P. Nigu, G. Svensson, Catalytic effects of metals of the iron subgroup on the chlorination of titanium carbide to form nanostructural carbon, Carbon 40 (2002) 1559–1564.

[26] J. Leis, A. Perkson, M. Arulepp, M. Kaarik, G. Svensson, Carbon nanostructures produced by chlorinating aluminium carbide, Carbon 39 (2001) 2043–2048.

[27] M. Sevilla, R. Mokaya, Energy storage applications of active carbons: supercapacitors and hydrogen storage, Energy Environ. Sci. 4 (2014).

[28] R. Dash, J. Chimola, Y. Gogotsi, G. Laudisio, J. Singer, J. Fischer, S. Lucheyev, Titanium carbide derived nanoporous carbon for energy-related applications, Carbon 44 (2006) 2489–2497.

[29] A. Arulepp, L. Permann, J. Leis, A. Perkson, K. Rumma, A. Janes, E. Lust, Influence of the solvent properties on the characteristics of a double layer capacitor, J. Power Sources 133 (2004) 320–328.

[30] J. Chimola, G. Yushin, Y. Gogotsi, C. Portet, P. Simon, P.L. Taberna, Anomalous increase in carbon capacitance at pore sizes less than 1 nanometer, Sci. Magna 313 (2006) 1760–1763. ISSN 0036-8075.

[31] M. Käärik, A. Arulepp, M. Kook, U. Mäeorg, J. Kozlova, V. Sammelselg, A. Perkson, J. Leis, Characterisation of steam-treated nanoporous carbide-derived carbon of TiC origin: structure and enhanced electrochemical performance, J. Porous Mater. 25 (2018) 1057–1070, https://doi.org/10.1007/s10934-017-0517-8.

[32] L. Zhang, R. Zhang, L. Zhan, W. Qiao, X. Liang, L. Ling, Effect of Ball-Milling Technology of Pore Structure and Electrochemical Properties of Activated Carbon, vol. 12, J Shanghai University, 2008, pp. 372–376.

[33] B. Dyatkin, O. Gogotsi, B. Malinovskiy, Y. Zozulya, P. Simon, Y. Gogotsi, High capacitance of coarse-grained carbide derived carbon electrodes, J. Power Sources 306 (2016) 32–41.

[34] H. Lyu, B. Gao, F. He, C. Ding, J. Tang, J.C. Crittenden, Ball-milled crabon nanomaterials for energy and environmental applications, Sus. Chem. Eng. 11 (2007) 9568–9585.

[35] L.S. Godse, P.B. Karandikar, M.Y. Khaladkar, Study of Carbon Materials and effect of its ball milling on capacitance of supercapacitor, Energy Procedia 54 (2014) 302–309.

[36] D.E. Lobo, P. Chakraborty Banerjee, C.D. Easton, M. Majumder, Miniaturized supercapacitors: focused ion beam reduced graphene oxide supercapacitors with enhanced performance metrics, Adv. Energy Mat. (2005) 1–10.

[37] N.J. Welham, V. Berbenni, P.G. Chapman, Increased chemisorption onto activated carbon after ball milling, Carbon 40 (2002) 2307–2315.

[38] M. Arulepp, J. Leis, M. Käärik, A. Perkson, in: The 6th International Symposium on Large Ec Capacitor Technology and Applications, 2010.

[39] N. Savest, T. Plamus, K. Kütt, U. Kallavus, M. Viirsalu, E. Tarasova, V. Vassiljeva, I. Krasnou, A. Krumme, Electrospun conductive mats from PANi-ionic liquid blends, J. Electrost. 96 (2018) 40–44.

[40] S. Brunauer, P.H. Emmett, E. Teller, Adsorption of gases in multimolecular layers, J. Am. Chem. Soc. 60 (1938) 309–319.

[41] F.K. Ko, Introduction to Nanofiber Materials, Cambridge University Press, 2014.

Publication II

Malmberg, S., Arulepp, M., Tarasova, E., Vassiljeva, E., Krasnou, I., Krumme, A. (2020) Electrochemical evaluation of directly electrospun Carbide-derived carbon-based electrodes in different nonaqueous electrolytes for energy storage applications. *C - Journal of Carbon Research.* vol 6 (4). 59

C Journal of Carbon Research

MDPI

Article

Electrochemical Evaluation of Directly Electrospun Carbide-Derived Carbon-Based Electrodes in Different Nonaqueous Electrolytes for Energy Storage Applications

Siret Malmberg [1,2,*], Mati Arulepp [2], Elvira Tarasova [1], Viktoria Vassiljeva [1], Illia Krasnou [1] and Andres Krumme [1]

[1] Department of Materials and Environmental Technology, Tallinn University of Technology, Ehitajate tee 5, 19086 Tallinn, Estonia; elvira.tarsova@ttu.ee (E.T.); viktoria.vassiljeva@ttu.ee (V.V.); illia.krasnou@ttu.ee (I.K.); andres.krumme@ttu.ee (A.K.)

[2] Skeleton Technologies OÜ, Valukoja 8, 11415 Tallinn, Estonia; mati.arulepp@skeletontech.com

* Correspondence: siret.malmberg@ttu.ee

Received: 27 August 2020; Accepted: 17 September 2020; Published: 23 September 2020

Abstract: This study focuses on the electrochemical behavior of thin-layer fibrous carbide-derived carbon (CDC) electrospun electrodes in commercial and research and development stage organic-solvent and ionic liquid (IL) based electrolytes. The majority of earlier published works stated various electrolytes with asymmetric cells of powder-based pressure-rolled (PTFE), or slurry-cast electrodes, were significantly different from the presented CDC-based fibrous spun electrodes. The benefits of the fibrous structure are relatively low thickness (20 μm), flexibility and mechanical durability. Thin-layered durable electrode materials are gaining more interest and importance in mechanically more demanding applications such as the space industry and in wearable devices, and need to achieve a targeted balance between mechanical, electrical and electrochemical properties. The existing commercial electrode technologies lack compatibility in such applications due to their limited mechanical properties and high cost. The test results showed that the widest potential window dU ≤ 3.5 V was achieved in 1.5 M 1-ethyl-3-methylimidazoliumbis(trifluoromethyl-sulfonyl)imide (EMIm-TFSI) solution in acetonitrile (ACN). Gravimetric capacitance reached 105.6 F g^{-1} for the positively charged electrode. Cycle-life results revealed stable material capacitance and resistance over 3000 cycles.

Keywords: electrospinning; electrolyte; carbide-derived carbon; supercapacitor; double-layer capacitance; cycle-life

1. Introduction

Supercapacitors, also known as electrochemical double-layer capacitors (EDLC) are energy storage devices with the advantage over conventional capacitors of having significantly higher energy density in a wide range of power capabilities, combined with a long cycle-life [1]. In conventional supercapacitors there are no redox reactions and charge separation occurs upon polarization at the electrode/electrolyte interface, which is also called the electrochemical double layer [2]. The energy storage process in EDLCs is fast and reversible due to the physical adsorption process of electrolyte ions on the carbon surface. However, this is not the case with lithium ion batteries (LIBs), where energy is stored by chemical reactions [3]. Therefore, EDLCs are suitable for a large number of applications where large amounts of energy need to be stored or released in a short time-frame. For example, supercapacitors are primarily used in hybrid electric and fuel cell vehicles like buses [4], trains [5]

and trolley buses [6]. Batteries and fuel cells exhibit energy densities a few orders of magnitudes larger than supercapacitors. Therefore, it is not sufficient to use only supercapacitors as energy sources. Supercapacitors are more beneficial in situations where a great deal of power is needed in a short time, which batteries cannot provide so efficiently [3–6]. Therefore, the use of supercapacitors in combination with batteries provides significant advantages in terms of energy efficiency. For example, almost all the kinetic energy can be stored in the supercapacitor portion of the energy storage system during braking and can be further reused during accelerating. These high-power peaks would otherwise damage LIBs, while fuel cells do not offer any possibility for fast energy recuperation [1]. Other application areas of supercapacitors are energy harvesting systems [7], solar arrays [8] and windmill turbines [9], in which the supercapacitors' high energy efficiency and lifetime has proven to be advantageous [1].

The overall performance of supercapacitors is influenced by the interactions between the electrode and the electrolyte inside the cell. Besides the operative voltage, electrolytes have great influence on the other parameters of EDLCs such as equivalent series resistance and power density, cycling stability, operating temperature range and self-discharge rate. The electrostatic interactions between electrolyte ions and the surface of carbon electrodes thus play an important role in impacting the overall EDLC characteristics. Generally, a larger accessible surface area leads to higher energy density [10].

In general, an ideal electrolyte for EDLC applications should exhibit some critical characteristics: high electrochemical stability, i.e., broad electrochemical potential window; a wide working temperature range; high ionic conductivity; high polarity; low viscosity; environmental friendliness; low flammability and low cost [11]. Electrolytes are categorized into several groups such as aqueous; organic; IL; solid-state and redox-active electrolytes [11,12]. The most used type of electrolyte in industrial supercapacitors is a solution of quaternary ammonium salt in organic solvent, often acetonitrile (ACN) or propylene carbonate (PC) [1,6]. Acetonitrile-based electrolytes show higher conductivity and lower viscosity compared to PC-based electrolytes [13]. Therefore, EDLCs containing ACN-based electrolytes out-perform those containing propylene carbonate, especially regarding power density and specific energy at lower temperatures. However, PC-based electrolytes are considered safer alternatives compared to the acetonitrile-based electrolytes due to a lower level of toxicity and higher flash point [11]. The maximum operative voltage of the majority of nonaqueous electrolyte based commercial supercapacitors is between 2.5–3.0 V.

IL-based electrolytes are widely used for increasing the upper voltage limit of EDLCs [2,14]. Disadvantages of ILs are their sensitivity to moisture, moderate conductivity as a result of high molecular weight and viscosity [5], and high cost, impacting their cost per function [8,9]. In addition, moisture can easily affect the stability and conductivity of an IL. Even a small amount of water can dramatically reduce the electrochemical stability of ILs.

Typically, industrial supercapacitors utilize porous carbon electrodes with high specific surface areas. Over the last decade, several carbon candidates such as fullerenes [15], carbon nanotubes [16]; graphene [17] and CDCs [18], have been reported for electric double layer capacitor applications. Each of these compounds presents exceptional properties for capacitor electrodes. Their theoretical capacitance in a two electrode configuration ranges from 60 up to 360 F g^{-1} [19–22]. Carbide-derived carbons differ from other available carbon materials due to their unique nanoporous structure, narrow pore size distribution and the possibility of fine tuning of the pore size [10,21–24]. CDCs have been under increased attention over the past decade as high capacitance materials due to unique properties. Polytetrafluoroethylene or polyvinylidene fluoride binders based CDC electrodes have been tested with a variety of organic electrolytes including IL-based electrolytes [10,25–27]. The highest reported specific capacitance of CDC was up to 190 F g^{-1} with a 1-ethyl-3-methylimidazolium tetrafluoroborate (EMIm-BF_4)-based electrolyte [10]. As mentioned before, EDLCs store energy in the electrochemical double layer formed between the carbon electrode's surface and the electrolyte's ions. Generally, higher specific surface areas in carbon materials show higher gravimetric capacitances. However, carbon materials have natural limits to their possible capacitance, as their active surface area per weight is limited. Still, one can utilize the available surface most efficiently by matching carbon pore size with

the ion size of an electrolyte, ensuring access to the carbon surface by having enough transport channels and, with decreasing distance between charges, in the double-layer [12,22]. Otherwise, the electrical resistance of the electrode increases due to limited access of the electrolyte to the pores [28].

With porous carbon, the capacitance can depend on varying the different electrolytes with different ion sizes. To achieve high energy, it is important to know both the dominant pore size of the carbon and the size of the electrolyte ions. The N_2 adsorption method, or density functional method, are used for investigating pore sizes of carbon [21].

The ion sizes of electrolytes can be calculated by various methods, such as determining the bare molecular and solvated ion sizes [12]. It is important to note that the dimensions of the solvated ions depend on the concentration of the solution in the case of electrolyte solutions. This is particularly important in the case of ILs, where the electrolyte ions may also be unsolvated, such as in the case of pure IL. Lin et al. found that although the bare ion sizes of $EMIm^+$ and $TFSI^-$ were similar, they were nevertheless different for solvated ions in the acetonitrile solvent: (TFSI/ACN < $EMIm^+$/ACN) [29]. Quaternary ammonium salts' cation size decrease in the following order: tetraethylammonium, spiro-(1,1')-bipyrrolidinium and triethylmethyl-ammonium ($TEA^+ > SBP^+ > TEMA^+$), calculated for the solvated ion radii [2,30].

Carbon electrodes offer good electrical conductivity and a high surface area. Carbon-saturated electrospun fibrous electrodes can be used as alternatives to rolled or casted porous carbon electrodes. Recently, electrospun materials have been shown to also provide high EDL-capacitance with good flexibility and good mechanical properties [31].

Electrospinning is the process of forming fibers of submicrometer diameter by an electrical field. It is a scalable technique whereby a drop of polymer from the tip of a needle is drawn into fibers by electrostatic force. The solvent is evaporated and fibers are formed on their way to the current collector [32].

Numerous attempts have been made to increase the voltage stability range of carbonaceous electrodes in aqueous and nonaqueous electrolytes [18,19]. However, little is reported towards increasing the working potential of electrospun fibrous electrodes in supercapacitors [33,34]. Levitt et al. showed capacitance up to 205 mF cm^{-2} with composite MXene/PAN fibers, which is three times higher than pure carbonized PAN [33]. Another approach for making fibrous electrodes has been done with a PANi/carbonized polyimide combination [34]. However, the carbonization process itself is destructive and certainly it has a relatively high cost from a large-scale production point of view.

The present study analyzed the electrochemical behavior of electrospun fibrous electrodes saturated with CDC in different organic and IL-based electrolytes. A three-electrode test setup was used to explore the maximum working potential of the electrodes in different electrolytes as well as the respective electrodes' capacitances. The values presented herein can thus serve to design a two-electrode system utilizing the respective electrospun electrodes and investigated electrolytes. Moreover, the study also outlines the importance of electrolyte selection for the optimization of any EDLC's electrochemical performance.

2. Experimental Section

2.1. Materials and Processes

For analysis of the electrochemical behavior of the fibrous electrodes in various electrolytes, the best performing recipe from a previous study was used [31]. Titanium carbide (TiC) based CDC material was used as the main capacitive component. For this approach, a TiC precursor was converted to CDC by using Cl_2 treatment at 900 °C, followed by a hydrogen gas purification step at 800 °C to remove residues of chlorine. CDC was produced by the company Skeleton Technologies OÜ. The specific surface area of synthesized CDC was 1577 m^2 g^{-1} with an initial particle size around 1–5 μm. The CDC particles were milled according to the procedure described in our previous study [31].

A mixture of milled CDC particles and carbon black (CB, Timcal, Deutschland GmbH, Düsseldorf, Germany) with weight (wt) % ratio of 80/20, respectively, was dispersed by 2 h ultrasonic treatment in dimethylformamide (DMF, Sigma Aldrich, Tartu, Estonia). The resulting mixture of the solvent and carbon particles was mechanically stirred at 40 °C for 24 h. Thereafter, 7 wt% of polyacrylonitrile (PAN, Sigma Aldrich, Mw = 150,000 g mol^{-1}) was added to the solution, while the ratio of PAN and carbon was 50/50. The whole solution was mechanically stirred for another 24 h at 40 °C. As a last step before the electrospinning process, 15 wt% of IL EMIm-BF_4 was added to the solution and mixed for 0.5 h at 40 °C [31]. The purpose of IL was to increase the solution's conductivity for a successful electrospinning process.

The prepared solution was electrospun by using a horizontal electrospinning system. The electrospinning conditions were as follows: the pumping rate of the solution was 0.5 mL h^{-1}, the distance between the spinneret and drum collector was 8 cm and a DC voltage of 15 kV was applied [31]. Scanning electron microscopy (SEM) of the prepared electrode, with two different magnifications, was carried out with a Gemini Zeiss Ultra 55 and is presented in Figure 1. SEM analysis displayed the fibrous structure of the electrode. The distribution of CDC/CB particles was clearly observed on the surface and inside of the main PAN/DMF fibers. As seen on the SEM images the contact between the CDC/CB particles remained, which is important to achieve good conductivity of the fibers. More detailed SEM analysis of the samples is described in our previous work [31].

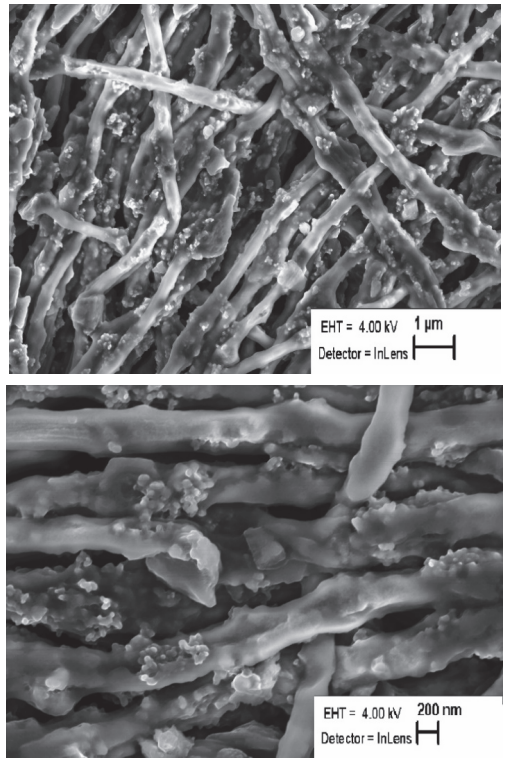

Figure 1. Different magnifications of scanning electron microscope (SEM) images of electrospun carbide-derived carbon (CDC) based fibrous electrode.

The thermal stability of the electrode was evaluated by thermal gravimetric analysis (TGA) by Labsys Evo TG DTA Omni Star. As shown in Figure 2, the electrospun fibrous electrode sample decomposed in three steps. The first mass loss stage is present between 247–317 °C, which has an

early shoulder at 290 °C, which indicates several parallel or competing reaction kinetics. The main reaction at this stage is the degradation of PAN, which occurs at 260 °C. This is comparable with PAN degradation found in V. Salles, etc. research, where pure polyacrylonitrile fibers decomposed between 250–300 °C [35]. The second mass loss stage starts at 318 °C and ends at 442 °C, indicating the degradation of ionic liquid $EMImBF_4$, which, based on the literature, has been found to occur between 333 and 455 °C [36].

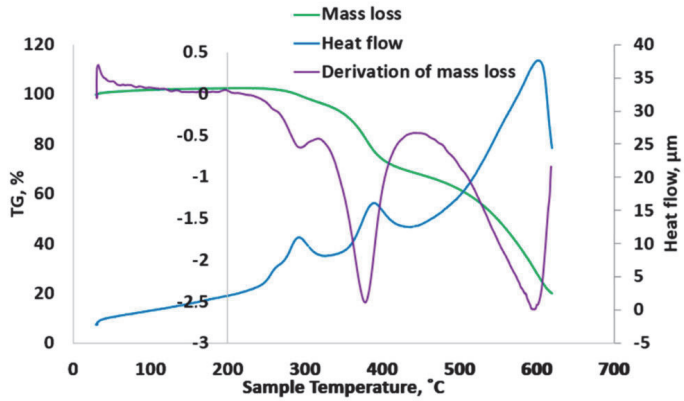

Figure 2. Decomposition characteristics of fibrous electrospun electrode material.

The degradation of ionic liquid also shows the highest heat flow. Third mass loss stage with the highest mass loss of 48.3%, which has a peak at 600 °C is the degradation of carbonous fillers CDC and CB. The porosity characteristics of the CDC powder was determined from N_2 adsorption at −196 °C using the NOVA touch LX2 (Quantachrome Instruments, Boynton Beach, FL, USA). Before measuring, the samples were dried for 12 h in vacuum at 300 °C. The Brunauer-Emmmet-Teller(BET) surface area was calculated from N_2 adsorption according to BET theory at a pressure interval P/P_0 of 0.02–0.2. The micropore volume (V_μ), calculated by a t-plot model and the total pore volume (V_{tot}) was calculated at P/P_0 of 0.97. Calculations of pore size distribution (PSD) were done by using a quenched solid density functional theory (QSDFT) equilibria model for slit type pores. Before measurement, the sample was degassed in a vacuum at 300 °C for 12 h. The porosity characteristics and PSD are presented in Table 1 and in Figure 3.

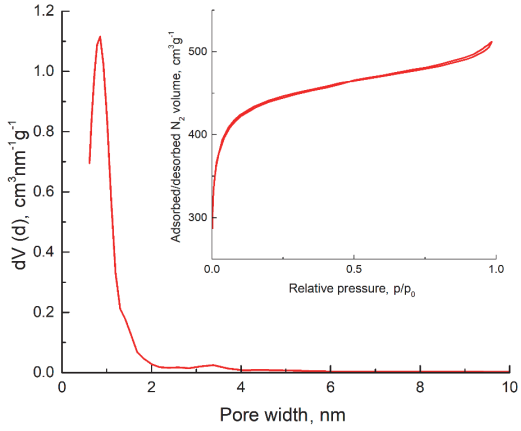

Figure 3. The pore size density (PSD) and N_2 absorption/desorption isotherm of tested CDC samples.

Table 1. Porosity characteristics of CDC particles.

Sample	S_{BET}, m^2 g^{-1}	V_μ, cm^3 g^{-1}	V_{tot}, cm^3 g^{-1}	APS nm
CDC	1560	0.71	0.82	0.95

For electrochemical tests, the prepared electrodes were cut with a diameter of 6 mm and an average coat weight of 1.86 g m^{-2} and dried under vacuum at 100 °C for 24 h to remove absorbed gases and water. For testing in various electrolytes, the weights of the electrodes were recorded after drying with an analytical scale (Mettler AE 163, Tallinn, Estonia). Afterwards, the prepared electrodes were assembled into three-electrode test cells with a glass fiber separator (purchased from VWR, Dresden, Germany), including a large carbon counter and carbon reference electrodes (RE).

2.2. Electrolytes

Commercial electrolytes 1.0 M TEA-BF4/ACN and 1.8 M TEMA-BF4/ACN were purchased from Honeywell. 1.5 M SBP-BF4/ACN was purchased from Japan Carlit Co., Ltd, Tokyo, Japan.

ILs, EMIm-TFSI and EMIm-BF_4 were purchased from Sigma Aldrich. Both conductive salts were mixed with acetonitrile in a 1.5 molar concentration in a dry box in a nitrogen atmosphere (O_2 < 0.5 ppm and H_2O < 0.5 ppm) to prevent contamination and to keep electrolytes dry. The physical properties and chemical structure of the electrolytes are presented in Table 2 and Figure 4.

Table 2. Physical properties of electrolytes and ions.

Acronym	Chemical Formula	Ionic Radii, nm	Concentration in Acetonitrile, M (in This Study)	Reference
TEA^+	$(C_2H_5)_4N^+$	0.670	1	[37]
$TEMA^+$	$(C_2H_5)_3CH_3N^+$	0.327	1.8	[38]
$EMIm^+$	$C_6H_{11}N_2^+$	0.326	1.5	[39]
SBP^+	$C_8H_{16}N^+$	0.420	1.5	[21]
BF_4^-	BF_4^-	0.480	variable	[29]
$TFSI^-$	$(CF_3SO_2)_2N^-$	0.227	1.5	[39]

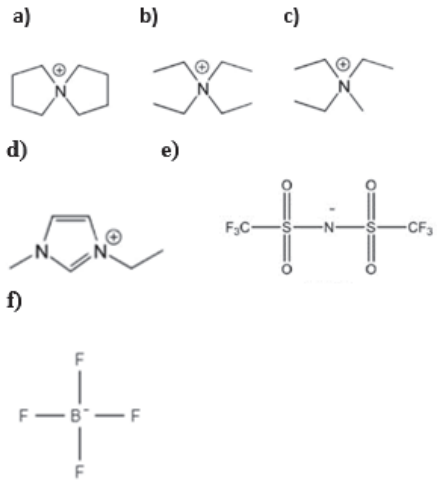

Figure 4. Chemical structures of cations and anions: (**a**) SBP, (**b**) TEA, (**c**) TEMA, (**d**) EMIm, (**e**) TFSI, (**f**) BF_4 [40,41].

2.3. Electrochemical Characterization

The electrochemical characteristics of the electrospun materials were measured using cyclic voltammetry (CV), constant-current charge-discharge (CC), and electrochemical impedance spectroscopy (EIS) methods, all carried out using a Gamry Interface 1010 E equipment, Warminster, Pennsylvania, United States of America.

The CV plots were measured at potential scan rates (v) of 50 mV s^{-1} to 1 mV s^{-1}. The EDL capacitance was calculated from CV data by dividing measured current values i by the voltage scan rate v, according to Formula (1):

$$C = \frac{i}{v} \tag{1}$$

In addition to the information about capacitance, CV represents information regarding electrochemical processes concerning kinetics, cycle efficiency and visible faradaic reactions [42,43]. The coulomb efficiency (E_q) is used to characterize charge-discharge cycle efficiency in a CV plot. An efficiency of more than 90% indicates a reversible charge-discharge cycle, where almost all applied charge is returned during discharge. Coulomb efficiency was calculated according to the following formula:

$$E_q = \frac{Q_{chrage}}{Q_{discharge}}, \tag{2}$$

where Q_{chrage} is the amount of electrical charge used during material recharging and $Q_{discharge}$ is the amount of charge received during discharging.

Current charge-discharge is the most common method for measuring integral capacitance. It also correlates most closely with the end application results [44]. The applied potential is selected based on the electrolyte's stability obtained from CV plots. The potential limits were selected for negatively and positively charged systems, −1.2 V and 1.2 V, respectively. For the positively charged electrode (C_A), and the negatively charged electrode (C_C), capacitance values from galvanostatic cycles were calculated at a discharge current density of 0.5 mA cm^{-2}. Since the discharge curves were not linear, the capacitance was calculated by integrating the charges in accordance with Equation (3).

$$C_A;\ C_C = \int_0^{E_{max}} \frac{idt}{\Delta E} \tag{3}$$

where ΔE is the potential range for oppositely charged electrodes, 1.2–0 V (positive) and −1.2–0 V (negative) vs. RE [43].

Electrochemical impedance spectra were measured in the AC frequency ranges 200 kHz to 5 mHz, at a fixed electrode potential of −0.5 V vs. carbon reference. To describe the impedance spectroscopy, complex Z'', Z' plots known as Nyquist plots are generally presented. Nyquist plots consist of three regions in the case of a porous electrode: the small depressed semicircle at higher AC frequencies, the porous region with a −45° or lower slope and the double-layer capacitance region with a slope of about −90°. In the case of series RC circuits, the total impedance (Z) can be described by Equation (4):

$$Z = Z' + Z'' = R + \frac{1}{j\omega C_s}, \tag{4}$$

where Z' is real impedance and Z'' imaginary impedance, j is the imaginary number $\sqrt{-1}$, C_s is series capacitance, ω is angular frequency, $\omega = 2\pi f$, and f is AC frequency in Hz.

The series capacitance values for each electrode material in different electrolytes were calculated by Equation (5).

$$C_s = -\frac{1/Z''}{\omega} \tag{5}$$

R_s can be determined by frequency response analysis based on Equation (6):

$$R_s = Z' \quad (6)$$

The R_s value, at $Z'' = 0$ is the impedance of the electrochemical system.

The phase angle response to frequency for an ideal capacitor is −90°. However, it is slightly below −90° in practice, which is frequency dependent, and, therefore, read at the lowest frequency [24,43].

A common method for evaluating long-term stability of a supercapacitor is cycling between maximum and minimum working voltages by the CV or constant current methods for longer periods of time [45]. Therefore, in this study, the cycle-life was carried out at a voltage range of 0 to 2.3 V at a voltage scan rate 20 mV s^{-1}. The capacitance retention was evaluated by CV, and resistance increase by EIS.

3. Results and Discussion

3.1. Galvanostatic Charge and Discharge

The galvanostatic charge-discharge method was performed in the four different electrolytes: two IL and two quaternary ammonium salt-based solutions. To reach the capacitance limits of the positively and negatively charged electrodes, the materials were held at a fixed potential for 5 min before being discharged. Thereafter, the material was recharged for the next cycle. The same profile was repeated five times, firstly at negative and, thereafter, at positive potential regions separately. The average DL capacitance values for the last three cycles are given in Table 3 and discharge curves are shown in Figure 5.

Table 3. Capacitance values obtained from constant current discharge plots at I = 0.5 mA cm^{-2}.

Electrolyte	Electrode Coat Weight	Positively Charged Electrode			Negatively Charged Electrode		
	g m^{-2}	mF cm^{-2}	F cm^{-3}	F g^{-1}	mF cm^{-2}	F cm^{-3}	F g^{-1}
EMIm-TFSI/ACN	2.29	20.6	10.3	89.8	20.6	10.3	89.8
SBP-BF_4/ACN	1.83	14.4	14.4	78.5	19.7	9.9	95.3
TEMA-BF_4/ACN	1.02	5.7	2.8	70.8	6.9	2.3	55.8
EMIm-BF_4/ACN	2.29	24.2	12.1	105.6	19.7	9.9	76.2

EMIm-TFSI/ACN: 1-ethyl-3-methylimidazoliumbis(trifluoromethyl-sulfonyl)imide in acetonitrile; SBP-BF4/ACN: spiro-(1,1')-bipyrrolidinium tetrafluoroborate in acetonitrile; TEMA-BF4/ACN: tetraethylammonium tetrafluoroborate in acetonitrile and EMIm-BF4/ACN: 1-ethyl-3-methylimidazolium tetrafluoroborate in acetonitrile.

The highest capacitance of 105.6 F g^{-1} for a positively charged electrode was achieved with an EMIm-BF_4/ACN electrolyte, whereas the capacitance for a negatively charged electrode was only 76.2 F g^{-1} and the difference between the capacitance for a positively and negatively charged electrode was 28%. The lowest capacitance at both potentials was measured in the TEMA-BF_4 electrolyte; the capacitance achieved for the negatively charged electrode was 55.8 F g^{-1} and for the positively charged electrode 70.8 F g^{-1}. Therefore, it seems that with similar BF_4^- anions, the counter ion still has influence on the material capacitance. ILs are also known to have lower conductivity, but somewhat higher capacitance, as measured for porous carbon electrodes [32]. A similar result was observed here. For SBP-BF_4/ACN the capacitance on the positive potential was 17% lower compared to the capacitance on the negative potential. However, the capacitance for the EMIm-TFSI/ACN electrolyte was equal for positive and negative potentials. The capacitance values on negative potentials in SBP-BF_4/ACN and for EMIm-TFSI/ACN electrolytes were rather similar, 95.3 F g^{-1} and 89.8 F g^{-1}, respectively, most probably due to the similar size of cations.

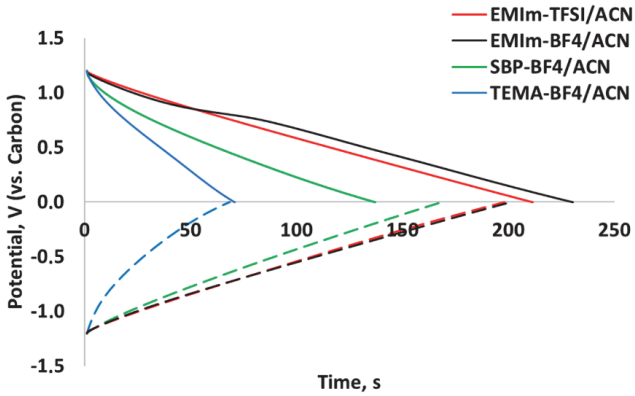

Figure 5. Discharge voltage profiles for positively and negatively charged electrodes at a current density of 0.5 mA cm^2.

3.2. Cyclic Voltammetry

Cyclic voltammetry was applied to investigate the electrochemical stability of fibrous electrodes in different electrolytes. CV plots were measured with voltage scan rates from 5 to 50 mV s^{-1} to evaluate the material stability over time and, more importantly, if the supercapacitor built from CDC-based fibrous electrodes was capable of fast charging rates. Figure 6 presents typical dependence of voltage scan rates for fibrous CDC-based electrodes. As shown on the graph, if the voltage scan rate was increased four times, there was no change in capacitance. In the case of the 10-times increase, capacitance was decreased around 20%.

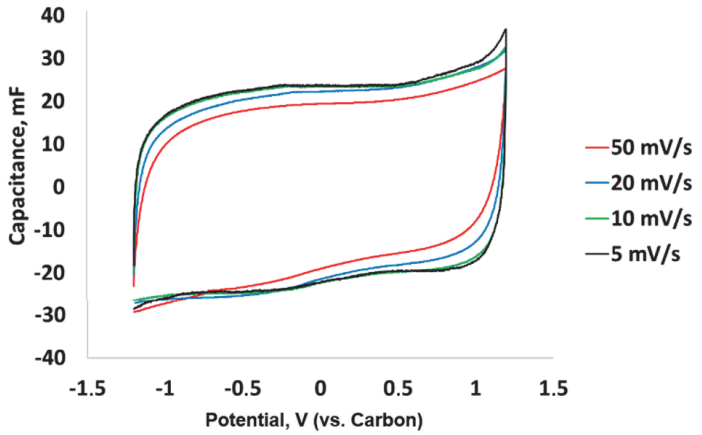

Figure 6. Capacitance dependence of voltage scan rates for fibrous CDC-based electrode material in 1.5 M EMIm-TFSI/ACN electrolyte.

The CV method also enabled us to investigate the positive and negative potential limits and coulombic efficiency at different electrode potential intervals of the system. The positive and negative potential limits were determined by the onset of the faradaic current from the nonfaradaic current. The method itself is well described by the studies of Xu [46], Ruschhaupt [45] and Weingarth [47]. The coulombic efficiency and potential windows for positively and negatively charged electrodes are presented in Figure 7A–D.

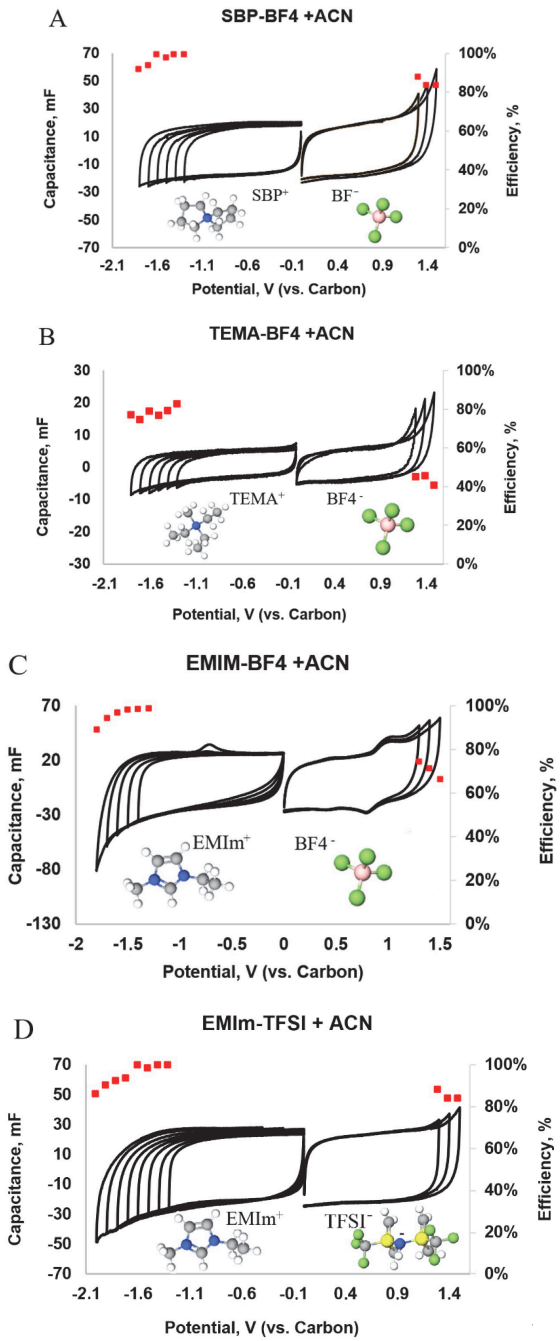

Figure 7. Cycling voltammograms expressed as capacitance vs. potential (black lines) and energy efficiency at respective potential (red dots) in electrolytes: (**A**) SBP-BF_4/ACN (**B**) TEMA-BF_4/ACN, (**C**) EMIm-BF_4/ACN and (**D**) EMIm-TFSI/ACN.

Generally, wider potential limits together with higher coulombic efficiency, were observed for negatively charged electrodes compared to the positive potentials (Figure 7). The widest potential window was achieved for the EMIm-TFSI/ACN electrolyte, where negative potential limit reached up to −2.0 V and the positive potential limit reached +1.5 V vs. RE, (total stability voltage dU ~ 3.5 V). The E_q values at negative electrode potentials did not drop below 90%, whereas at positive electrode potentials E_q was almost <85%. With the EMIm-BF_4/ACN electrolyte, the decrease of E_q was observed on negative potentials already at −1.6 V and on positive potentials at +0.8 V vs. RE, which is not close to potential limits for this ionic IL-based electrolyte. Furthermore, additional peaks were observed on the voltammogram of negative potentials, where the peak appeared at −0.5 V with the EMIm-BF_4/ACN electrolyte. Evolution of the negative discharge peak was observed when negative potential exceeded −1.7 V, which is most probably caused by surface compounds formed with negative overpotential. The peak was reversible on positive potentials close to 0.9 V vs. RE. The origin of this peak is not clear.

A smaller potential window was observed with the TEMA-BF_4/ACN electrolyte compared to the other tested electrolytes. The negative limit was −1.9 V, close to the EMIm-TFSI/ACN electrolyte. However, the stable positive potential was reached close to the +1.0 V vs. carbon reference. The efficiency for a positively charged electrode was lower than expected in the TEMA-BF_4/ACN electrolyte, probably because CV plots were recorded on a wider electrode potential limits than the EDLC region and also includes parasitic processes. The widest potential window of 3.0 V was observed for the SBP-BF_4/ACN electrolyte from the quaternary ammonium salt electrolytes.

3.3. Electrochemical Impedance Spectroscopy

The three-electrode experiments of pure ionic liquids and ILs diluted with acetonitrile were also performed by impedance spectroscopy. The fibrous electrodes with the studied electrolytes showed different behaviors at analyzed frequency regions (see in Figure 8A–C).

The Nyquist plot of fibrous electrodes are presented in Figure 7A. For typical carbonous EDL electrodes, the −45° slope should be observed immediately after the semicircle, followed by a vertical line, which is almost parallel to the imaginary impedance axis (Y-axis) in the lower frequency region [44].

The closest results to EDLC behavior of the fibrous electrodes were achieved for quaternary ammonium-based electrolytes and with the EMIm-TFSI/ACN electrolyte, where a near-vertical line at a low frequency area was achieved. A clear semicircle was observed for EMIm-TFI/ACN in the high frequency region, which points to several possible reasons; for example, interfacial impedance occurring at the current collector/active material interface, mass transfer resistance inside microporous electrode at high frequencies, and charge transfer resistance inside macro/mesopores [44,48]. No clear semicircle was observed with other IL-based electrolyte solutions, probably due to the lower conductivity and higher viscosity of the electrolyte [33,49]. For pure IL-based electrolytes, high impedance was seen in the low frequency range, indicating that processes with limited mass transfer predominate at f = 5 mHz, and even at 5 mHz; capacitive behavior was not ideal. This was caused by the much higher viscosity and much lower mobility of the electrolyte ions than in ACN-diluted solutions. A similar effect was also observed with $EMImBF_4$ by Zhang et al. when by diluting EMIm-BF_4 in ACN, the total resistance of the electrode decreased remarkably [43].

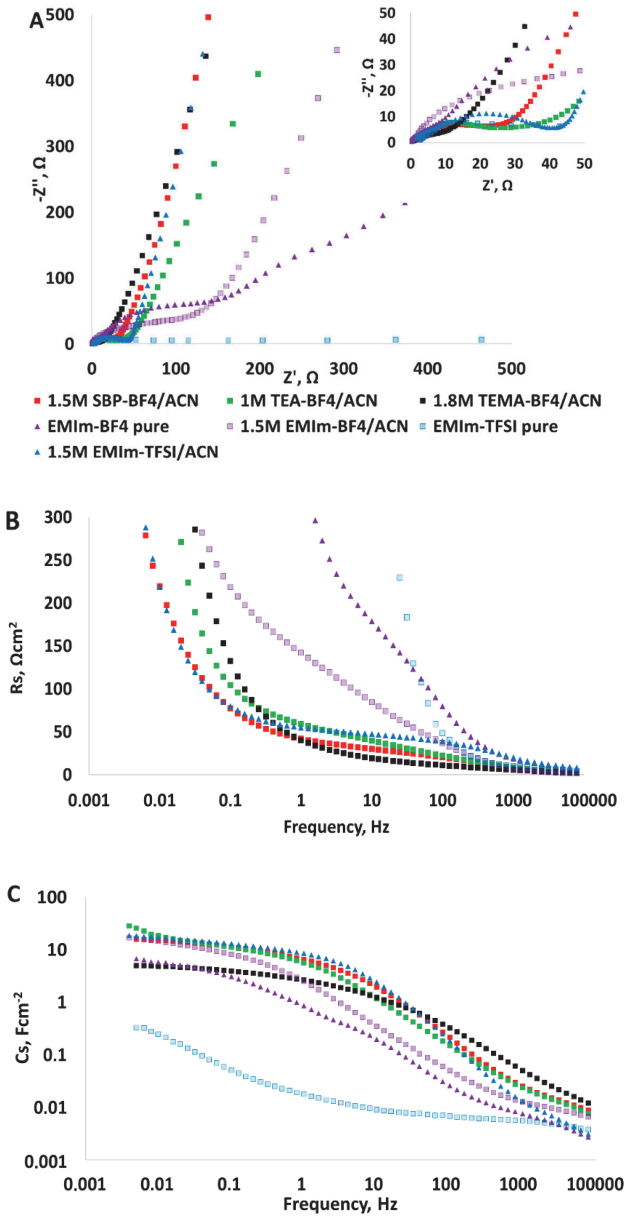

Figure 8. Electrochemical impedance spectroscopy (EIS) plots for electrolyte-carbon interface: (**A**) Nyquist plot, (**B**) R_s as a function frequency and (**C**) C_s as a function of frequency.

Series resistance and -capacitance, calculated by Equations (5) and (6) are shown in Figure 8B,C. According to the graph R_s vs. f, the electrolytes can be divided into two groups: (1) quaternary salt solutions and (2) pure ionic liquids with EMIm-BF4/ACN. Interestingly, EMIm-TFSI/ACN behaved similarly to the first group of electrolytes. At high frequency region (f > 1 Hz) for the first group and (f > 200 Hz) for the second group electrolytes, R_s values were much lower compared to the low-frequency region in Figure 7B. This was due to electrolyte ion migration speed and

their adsorption/desorption rate, which is maximum at low frequency of EDLCs [11]. The lowest resistance at the frequency region $10 < f < 100$ Hz was observed with TEMA-BF_4/ACN electrolyte. In addition, the resistance at 20 Hz increased in the following order: TEMA-BF_4 < SBP-BF_4 < TEA-BF_4 < EMIm-TFSI/ACN < EMImBF_4/ACN < EMIm-TFSI < EMIm-BF_4. This order correlates to the assumption that IL has a lower conductivity compared to organic electrolytes [12]. The lowest resistance among IL-based electrolytes of an electrode/electrolyte system was observed for EMIm-TFSI/ACN, as mentioned above. Also, the highest capacitance was achieved with the same IL-based electrolyte, EMIm-TFSI/ ACN. At high frequencies, the electrode material behaved more as a smooth surface and, therefore, electrolyte ions did not have enough time to migrate to carbon micropores, so the capacitance was very low. With decreased frequencies, the electrolyte ions started to migrate and adsorb into carbon pores, which resulted in an increase of the capacitance value. With a decrease in frequency ($f < 1$ Hz), capacitance reached the plateau for certain electrolytes. However, for pure IL-based electrolytes this plateau was not achieved even at very low frequencies ($f < 10$ mHz), due to their high viscosity, which can be observed in Figure 7C.

3.4. Cycle-Life

The cycle-life for electrospun fibrous CDC-based electrodes, was measured in a two-electrode set up by the CV method. The voltage scan rate was selected as 20 mV s^{-1}, due the electrode material previously showing steady capacitance behavior at this voltage scan rate. The cells were cycled between 0 V and 2.3 V. For the cycle-life measurements, SBP-BF_4/ACN and EMIm-TFSI/ACN electrolytes were selected. In the case of IL-based EMIm-TFSI/can, an exponential decrease in capacitance was observed during cycling, which may have been caused by the relatively high viscosity and high voltage scanning rate which disabled the effective ion transfer in the electrical double layer. Stable cycle stability was achieved with the SBP-BF_4/ACN electrolyte as shown in Figure 9. There was no significant capacitance loss (dC ~ 3%) and resistance increased by 21% during 3000 cycles.

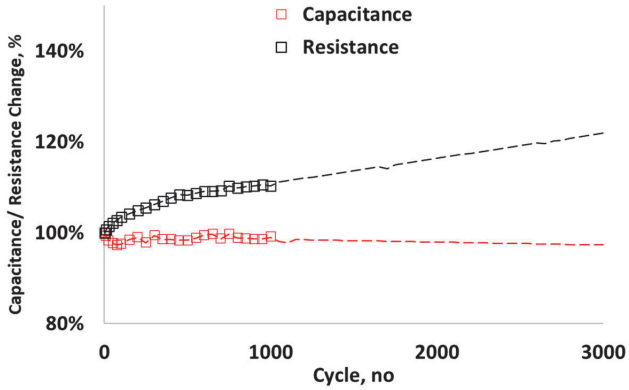

Figure 9. Cycle-life performance with SBP-BF_4/ACN electrolyte: capacitance retention and series resistance change during cycling.

4. Conclusions

The behavior of CDC containing flexible and mechanically durable fibrous electrodes was studied in various organic and IL-based electrolytes. The results of electrochemical evaluation showed that the widest potential range was achieved with a 1.5 M EMIm-TFSI/ACN electrolyte with a total voltage range of $dU \leq 3.5$ V. This electrolyte also showed identical gravimetric capacitance 89.8 F/g for positively and negatively charged electrodes. Among quaternary ammonium salt-based electrolytes, the largest potential window was reached in 1.5 M SBP-BF_4/ACN–3.0 V, with a gravimetric

capacitance of 95.3 F g^{-1} and 78.5 F g^{-1} for positively and negatively charged electrodes, respectively. Electrochemical impedance spectroscopy showed that pure ionic-liquids had very high resistance and low DL-capacitance, making them practically unsuitable as electrolytes in electrospun materials. However, capacitance was significantly increased by diluting pure ionic liquid with acetonitrile; for 1.5 M EMIm-TFSI/ACN, the capacitance was increased 15-fold compared to pure ionic liquid. Stable cycle-life of electrospun CDC-based electrodes was achieved with organic SBP-BF4/ACN electrolyte with only a 3% capacitance loss.

Author Contributions: Data curation, S.M.; Investigation, S.M. and E.T.; Methodology, S.M.; Resources, V.V.; Supervision, M.A.; Validation, S.M. and I.K.; Writing—original draft, S.M.; Writing—review & editing, A.K. All authors have read and agreed to the published version of the manuscript.

Funding: This study was financially supported by the European Space Agency, ESA contract number 4000119258/16/NL/CBi "Fully electrospun durable electrode and the electrochemical double-layer capacitor for high frequency applications" and Estonian Ministry of Education and Research (IUT19-28).

Acknowledgments: We thank Sebastian Pohlmann and Ann Laheäär for fruitful discussions and consulting. Furthermore, we also thank senior researcher Valdek Mikli for SEM, Maike Käärik for BET and Can Rüstü Yörük for TGA analysis.

Conflicts of Interest: The authors declare no conflict of interest.

References

1. Libich, J.; Máca, J.; Vondrák, J.; Čech, O.; Sedlaříková, M. Supercapacitors: Properties and applications. *J. Energy Storage* **2018**, *17*, 224–227. [CrossRef]
2. Pohlmann, S.; Lobato, B.; Centeno, T.A.; Balducci, A. The influence of pore size and surface area of activated carbons on the performance of ionic liquid based supercapacitors. *Phys. Chem. Chem. Phys.* **2013**, *15*, 17287. [CrossRef] [PubMed]
3. Stan, A.-I.; Swierczynski, M.; Stroe, D.-I.; Teodorescu, R.; Andreasen, S.J. Lithium ion battery chemistries from renewable energy storage to automotive and back-up power applications—An overview. In Proceedings of the 2014 International Conference on Optimization of Electrical and Electronic Equipment (OPTIM), Brasov, Romania, 22 May 2014; pp. 713–720. [CrossRef]
4. Burke, A.; Zhao, H. *Applications of Supercapacitors in Electric and Hybrid Vehicles*; Institute of Transportation Studies: Davis, CA, USA, 2015; p. 15.
5. Radu, P.; Szelag, A.; Steczek, M. On-Board Energy Storage Devices with Supercapacitors for Metro Trains—Case Study Analysis of Application Effectiveness. *Energies* **2019**, *12*, 1291. [CrossRef]
6. Brazis, V.; Latkovskis, L.; Grigans, L. Simulation of Trolleybus Traction Induction Drive with Supercapacitor Energy Storage System. *Latv. J. Phys. Technol. Sci.* **2010**, *47*, 33–47. [CrossRef]
7. Kim, S.; Chou, P.H. Energy Harvesting with Supercapacitor-Based Energy Storage. In *Smart Sensors and Systems*; Lin, Y.-L., Kyung, C.-M., Yasuura, H., Liu, Y., Eds.; Springer International Publishing: Cham, Germany, 2015; pp. 215–241, ISBN 978-3-319-14710-9.
8. Fahmi, M.I.; Rajkumar, R.K.; Arelhi, R.; Isa, D. Study on the effect of supercapacitors in solar PV system for rural application in Malaysia. In Proceedings of the 2015 50th International Universities Power Engineering Conference (UPEC), Stoke On Trent, UK, 1–4 September 2015; pp. 1–5. [CrossRef]
9. Liudvinavičius, L. *Supercapacitors: Theoretical and Practical Solutions*; BoD–Books on Demand: Norderstedt, Germany, 2018; ISBN 978-1-78923-352-0.
10. Käärik, M.; Arulepp, M.; Kook, M.; Kozlova, J.; Ritslaid, P.; Aruväli, J.; Mäeorg, U.; Sammelselg, V.; Leis, J. High-performance microporous carbon from deciduous wood-origin metal carbide. *Microporous Mesoporous Mater.* **2019**, *278*, 14–22. [CrossRef]
11. Béguin, F.; Presser, V.; Balducci, A.; Frackowiak, E. Carbons and Electrolytes for Advanced Supercapacitors. *Adv. Mater.* **2014**, *26*, 2219–2251. [CrossRef]
12. Zhong, C.; Deng, Y.; Hu, W.; Qiao, J.; Zhang, L.; Zhang, J. A review of electrolyte materials and compositions for electrochemical supercapacitors. *Chem. Soc. Rev.* **2015**, *44*, 7484–7539. [CrossRef]
13. Balducci, A.; Dugas, R.; Taberna, P.L.; Simon, P.; Plée, D.; Mastragostino, M.; Passerini, S. High temperature carbon–carbon supercapacitor using ionic liquid as electrolyte. *J. Power Sources* **2007**, *165*, 922–927. [CrossRef]

14. Martins, V.L.; Rennie, A.J.R.; Sanchez-Ramirez, N.; Torresi, R.M.; Hall, P.J. Improved Performance of Ionic Liquid Supercapacitors by using Tetracyanoborate Anions. *ChemElectroChem* **2018**, *5*, 598–604. [CrossRef]
15. Keypour, H.; Noroozi, M.; Rashidi, A. An improved method for the purification of fullerene from fullerene soot with activated carbon, celite, and silica gel stationary phases. *J. Nanostructure Chem.* **2013**, *3*. [CrossRef]
16. Arepalli, S.; Fireman, H.; Huffman, C.; Moloney, P.; Nikolaev, P.; Yowell, L.; Kim, K.; Kohl, P.A.; Higgins, C.D.; Turano, S.P.; et al. Carbon-nanotube-based electrochemical double-layer capacitor technologies for spaceflight applications. *JOM* **2005**, *57*, 26–31. [CrossRef]
17. Cai, Y.; Qin, Z.; Chen, L. Effect of electrolytes on electrochemical properties of graphene sheet covered with polypyrrole thin layer. *Prog. Nat. Sci. Mater. Int.* **2011**, *21*, 460–466. [CrossRef]
18. Arulepp, M.; Leis, J.; Lätt, M.; Miller, F.; Rumma, K.; Lust, E.; Burke, A.F. The advanced carbide-derived carbon based supercapacitor. *J. Power Sources* **2006**, *162*, 1460–1466. [CrossRef]
19. Inamuddin; Boddula, R.; Ahamed, M.I.; Asiri, A.M. *Supercapacitor Technology: Materials, Processes and Architectures*; Materials Research Forum LLC: Millersville, PA, USA, 2019; ISBN 978-1-64490-049-9.
20. Vatamanu, J.; Hu, Z.; Bedrov, D.; Perez, C.; Gogotsi, Y. Increasing Energy Storage in Electrochemical Capacitors with Ionic Liquid Electrolytes and Nanostructured Carbon Electrodes. *J. Phys. Chem. Lett.* **2013**, *4*, 2829–2837. [CrossRef]
21. Käärik, M.; Arulepp, M.; Käärik, M.; Maran, U.; Leis, J. Characterization and prediction of double-layer capacitance of nanoporous carbon materials using the Quantitative nano-Structure-Property Relationship approach based on experimentally determined porosity descriptors. *Carbon* **2019**. [CrossRef]
22. Käärik, M.; Arulepp, M.; Kook, M.; Mäeorg, U.; Kozlova, J.; Sammelselg, V.; Perkson, A.; Leis, J. Characterisation of steam-treated nanoporous carbide-derived carbon of TiC origin: Structure and enhanced electrochemical performance. *J. Porous Mater.* **2018**, *25*, 1057–1070. [CrossRef]
23. Leis, J.; Arulepp, M.; Kuura, A.; Lätt, M.; Lust, E. Electrical double-layer characteristics of novel carbide-derived carbon materials. *Carbon* **2006**, *44*, 2122–2129. [CrossRef]
24. Torop, J.; Palmre, V.; Arulepp, M.; Sugino, T.; Asaka, K.; Aabloo, A. Flexible supercapacitor-like actuator with carbide-derived carbon electrodes. *Carbon* **2011**, *49*, 3113–3119. [CrossRef]
25. Ewert, J.-K.; Weingarth, D.; Denner, C.; Friedrich, M.; Zeiger, M.; Schreiber, A.; Jäckel, N.; Presser, V.; Kempe, R. Enhanced capacitance of nitrogen-doped hierarchically porous carbide-derived carbon in matched ionic liquids. *J. Mater. Chem. A* **2015**, *3*, 18906–18912. [CrossRef]
26. Dyatkin, B.; Gogotsi, O.; Malinovskiy, B.; Zozulya, Y.; Simon, P.; Gogotsi, Y. High capacitance of coarse-grained carbide derived carbon electrodes. *J. Power Sources* **2016**, *306*, 32–41. [CrossRef]
27. Krüner, B.; Odenwald, C.; Tolosa, A.; Schreiber, A.; Aslan, M.; Kickelbick, G.; Presser, V. Carbide-derived carbon beads with tunable nanopores from continuously produced polysilsesquioxanes for supercapacitor electrodes. *Sustain. Energy Fuels* **2017**, *1*, 1588–1600. [CrossRef]
28. Beguin, F.; Frackowiak, E. *Supercapacitors: Materials, Systems, and Applications*; John Wiley & Sons: Hoboken, NJ, USA, 2013; ISBN 978-3-527-64668-5.
29. Lin, R.; Taberna, P.-L.; Chmiola, J.; Guay, D.; Gogotsi, Y.; Simon, P. Microelectrode Study of Pore Size, Ion Size, and Solvent Effects on the Charge/Discharge Behavior of Microporous Carbons for Electrical Double-Layer Capacitors. *J. Electrochem. Soc.* **2009**, *156*, A7. [CrossRef]
30. Cheng, W.; Yu, Q.; Qiu, Z.; Yan, Y. Effects of different ionic liquids on the electrospinning of a polyacrylonitrile polymer solution. *J. Appl. Polym. Sci.* **2013**, *130*, 2359–2368. [CrossRef]
31. Malmberg, S.; Arulepp, M.; Savest, N.; Tarasova, E.; Vassiljeva, V.; Krasnou, I.; Käärik, M.; Mikli, V.; Krumme, A. Directly electrospun electrodes for electrical double-layer capacitors from carbide-derived carbon. *J. Electrost.* **2020**, *103*, 103396. [CrossRef]
32. Yang, T.; Yao, Y.; Lin, Y.; Wang, B.; Xiang, R.; Wu, Y.; Wu, D. Electrospinning of polyacrylonitrile fibers from ionic liquid solution. *Appl. Phys. A* **2010**, *98*, 517–523. [CrossRef]
33. Levitt, A.S.; Alhabeb, M.; Hatter, C.B.; Sarycheva, A.; Dion, G.; Gogotsi, Y. Electrospun MXene/carbon nanofibers as supercapacitor electrodes. *J. Mater. Chem. A* **2018**, *7*, 269–277. [CrossRef]
34. Miao, Y.-E.; Yan, J.; Huang, Y.; Fan, W.; Liu, T. Electrospun polymer nanofiber membrane electrodes and an electrolyte for highly flexible and foldable all-solid-state supercapacitors. *RSC Adv.* **2015**, *5*, 26189–26196. [CrossRef]

35. Salles, V.; Bernard, S.; Brioude, A.; Cornu, D.; Miele, P. A new class of boron nitride fibers with tunable properties by combining an electrospinning process and the polymer-derived ceramics route. *Nanoscale* **2010**, *2*, 215–217. [CrossRef]
36. Hao, F.; Lin, H. Recent molecular engineering of room temperature ionic liquid electrolytes for mesoscopic dye-sensitized solar cells. *RSC Adv.* **2013**, *3*, 23521. [CrossRef]
37. Prabaharan, S.R.S.; Michael, M.S. *Nanotechnology in Advanced Electrochemical Power Sources*; CRC Press: Boca Raton, FL, USA, 2014; ISBN 978-981-4241-43-4.
38. Saito, M.; Kawaharasaki, S.; Ito, K.; Yamada, S.; Hayamizu, K.; Seki, S. Strategies for fast ion transport in electrochemical capacitor electrolytes from diffusion coefficients, ionic conductivity, viscosity, density and interaction energies based on HSAB theory. *RSC Adv.* **2017**, *7*, 14528–14535. [CrossRef]
39. Cho, J.; Shin, W.-K.; Kim, D.-W.; Kim, Y.R.; Lee, B.J.; Kim, S.-G. Electrochemical characterization of electric double layer capacitors assembled with pyrrolidinium-based ionic liquid electrolytes. *J. Electrochem. Sci. Technol.* **2016**, *7*, 199–205. [CrossRef]
40. Bashid, H.A.A.; Lim, H.N.; Hafiz, S.M.; Andou, Y.; Altarawneh, M.; Jiang, Z.T.; Huang, N.M. 16-Modification of Carbon-Based Electroactive Materials for Supercapacitor Applications. In *Carbon-Based Polymer Nanocomposites for Environmental and Energy Applications*; Ismail, A.F., Goh, P.S., Eds.; Elsevier: Amsterdam, The Netherlands, 2018; pp. 393–413, ISBN 978-0-12-813574-7.
41. Zhang, E.; Fulik, N.; Paasch, S.; Borchardt, L.; Kaskel, S.; Brunner, E. Ionic liquid—Electrode materials interactions studied by NMR spectroscopy, cyclic voltammetry, and impedance spectroscopy. *Energy Storage Mater.* **2019**, *19*, 432–438. [CrossRef]
42. Gualous, H.; Louahlia-Gualous, H.; Gallay, R.; Miraoui, A. Supercapacitor thermal modeling and characterization in transient state for industrial applications. *IEEE Trans. Ind. Appl.* **2009**, *45*, 1035–1044. [CrossRef]
43. Stoller, M.D.; Ruoff, R.S. Best practice methods for determining an electrode material's performance for ultracapacitors. *Energy Environ. Sci.* **2010**, *3*, 1294. [CrossRef]
44. Tõnurist, K.; Vaas, I.; Thomberg, T.; Jänes, A.; Kurig, H.; Romann, T.; Lust, E. Application of multistep electrospinning method for preparation of electrical double-layer capacitor half-cells. *Electrochim. Acta* **2014**, *119*, 72–77. [CrossRef]
45. Ruschhaupt, P.; Pohlmann, S.; Varzi, A.; Passerini, S. Determining realistic electrochemical stability windows of electrolytes for electrical double layer capacitors. *Batter. Supercaps* **2020**, *3*, 698–707. [CrossRef]
46. Xu, K. Toward Reliable Values of Electrochemical Stability Limits for Electrolytes. *J. Electrochem. Soc.* **1999**, *146*, 4172. [CrossRef]
47. Weingarth, D.; Noh, H.; Foelske-Schmitz, A.; Wokaun, A.; Kötz, R. A reliable determination method of stability limits for electrochemical double layer capacitors. *Electrochim. Acta* **2013**, *103*, 119–124. [CrossRef]
48. Kreczanik, P.; Venet, P.; Hijazi, A.; Clerc, G. Study of Supercapacitor Aging and Lifetime Estimation According to Voltage, Temperature, and RMS Current. *IEEE Trans. Ind. Electron.* **2014**, *61*, 4895–4902. [CrossRef]
49. Gao, Q. Optimizing Carbon/Carbon Supercapacitors in Aqueous and Organic Electrolytes. Ph.D. Thesis, Université d'Orléans, Orléans, France, 2013.

Publication III

Malmberg, S., Arulepp, A., Laanemets, K., Käärik, M., Laheäär, A., Tarasova, E., Vassiljeva, E., Krasnou, I., Krumme, A. (2021) The Performance of Fibrous CDC Electrodes in Aqueous and Non-Aqueous Electrolytes. *C - Journal of Carbon Research,* vol 7 (2), 46

C Journal of Carbon Research

MDPI

Article

The Performance of Fibrous CDC Electrodes in Aqueous and Non-Aqueous Electrolytes

Siret Malmberg [1,2,*], Mati Arulepp [2], Krista Laanemets [1], Maike Käärik [3], Ann Laheäär [2], Elvira Tarasova [1], Viktoria Vassiljeva [1], Illia Krasnou [1] and Andres Krumme [1]

[1] Department of Materials and Environmental Technology, Tallinn University of Technology, Ehitajate tee 5, 19086 Tallinn, Estonia; krista.laanemets@gmail.com (K.L.); elvira.tarasova@ttu.ee (E.T.); viktoria.vassiljeva@ttu.ee (V.V.); illia.krasnou@taltech.ee (I.K.); andres.krumme@taltech.ee (A.K.)
[2] Skeleton Technologies OÜ, Valukoja 8, 11415 Tallinn, Estonia; mati.arulepp@skeletontech.com (M.A.); ann.laheaar@skeletontech.com (A.L.)
[3] Institute of Chemistry, University of Tartu, Ravila 14a, 50411 Tartu, Estonia; maike.kaarik@ut.ee
* Correspondence: siret.malmberg@taltech.com

Abstract: The aim of this study was to investigate the electrochemical behaviour of aqueous electrolytes on thin-layer (20 µm) nanoporous carbide-derived carbon (CDC) composite fibrous directly electrospun electrodes without further carbonisation. There have been previously investigated fibrous electrodes, which are produced by applying different post-treatment processes, however this makes the production of fibrous electrodes more expensive, complex and time consuming. Furthermore, in the present study high specific capacitance was achieved with directly electrospun nanoporous CDC-based fibrous electrodes in different neutral aqueous electrolytes. The benefit of fibrous electrodes is the advanced mechanical properties compared to the existing commercial electrode technologies based on pressure-rolled or slurry-cast powder mix electrodes. Such improved mechanical properties are preferred in more demanding applications, such as in the space industry. Electrospinning technology also allows for larger electrode production capacities without increased production costs. In addition to the influence of aqueous electrolyte chemical composition, the salt concentration effects and cycle stability with respect to organic electrolytes are investigated. Cyclic voltammetry (CV) measurements on electrospun electrodes showed the highest capacitance for asymmetrical cells with an aqueous 1 M $NaNO_3$-H_2O electrolyte. High CV capacitance was correlated with constant current charge–discharge (CC) data, for which a specific capacitance of 191 F g^{-1} for the positively charged electrode and 311 F g^{-1} for the negatively charged electrode was achieved. The investigation of electrolyte salt concentration on fibrous electrodes revealed the typical capacitance dependence on ionic conductivity with a peak capacitance at medium concentration levels. The cycle-life measurements of selected two-electrode test cells with aqueous and non-aqueous electrolytes revealed good stability of the electrospun electrodes.

Keywords: electrospun electrode; EDL capacitance; carbide-derived carbon; supercapacitor; aqueous electrolytes

Citation: Malmberg, S.; Arulepp, M.; Laanemets, K.; Käärik, M.; Laheäär, A.; Tarasova, E.; Vassiljeva, V.; Krasnou, I.; Krumme, A. The Performance of Fibrous CDC Electrodes in Aqueous and Non-Aqueous Electrolytes. *C* **2021**, *7*, 46. https://doi.org/10.3390/c7020046

Academic Editor: Bruno C. Janegitz

Received: 19 April 2021
Accepted: 12 May 2021
Published: 14 May 2021

1. Introduction

With the need to decrease CO_2 emissions, enormous effort has been put into the development of electrochemical energy storage devices such as batteries, fuel cells, and supercapacitors, supporting the shift to more extensive incorporation of renewable energy sources. Supercapacitors, also called electrical double layer capacitors (EDLCs), are energy storage devices with high power density and long cycle stability [1–3]. From the application requirements perspective, supercapacitors bridge the gap between lithium-ion batteries and electrolytic capacitors [4]. EDLCs are mostly attractive for further development due to their possible use as load levelling devices in renewable energy technology [5] and to further enhance electrical vehicle performance [6–8].

The energy storage mechanism of supercapacitors relies on the electrochemical double layer (EDL), which forms between the electrode material and the electrolyte [9–11]. Liquid electrolytes can typically be classified as non-aqueous, aqueous and ionic liquids (ILs) [12]. In general, the requirements for an ideal electrolyte are high ionic conductivity, chemical and electrochemical stability (wide potential window), wide operating temperature range, low volatility and flammability, environmental friendliness, and feasible cost at scale [13]. However, in real applications, few of the parameters often need to be compromised. The specific performance of an EDL depends on the interactions between the carbon with a high surface area and the electrolyte ions [4,14–16]. Therefore, it is important that the properties of the electrolyte meet the demands from the pore structure of the carbon.

The effect of various aqueous electrolytes has been extensively studied with various carbon powder composite electrodes [17–19]. A few studies have been performed with fibrous electrodes [20] or electrospun carbon-containing electrodes [21] in aqueous electrolytes but, to our knowledge, no studies have directly electrospun fibrous electrodes of CDCs. The most fundamental studies have been performed with H_2SO_4-H_2O and KOH-H_2O electrolytes, but these electrolytes are corrosive and have a working voltage range up to 1.0 V [22–24]. Therefore, neutral aqueous solutions such as Li_2SO_4-H_2O, Na_2SO_4-H_2O and K_2SO_4-H_2O are preferred to avoid the harmful effects of acidic and alkaline environments [22]. Furthermore, the activated carbons were tested for operating voltages up to 1.6 V in symmetrical cells of aqueous Na_2SO_4-H_2O and long-term stability (<10,000 cycles) [22,25].

To achieve high EDL capacitance, the size of the electrolyte ions must correspond to the pore size of carbon [26]. Cai et al. showed the effects of anions and cations with graphene-based nanocomposite electrodes, where 0.5 M aqueous solutions of sodium salts displayed a specific capacity of the SO_4^{2-} anion that was 21% higher than that of the NO_3^- anions [27]. In monovalent cation electrolytes, the specific capacitance increases under the influence of the corresponding cationic radius. In common aqueous electrolyte solutions, the ionic radii of cations decrease as follows: $Li^+ > Na^+ > K^+$ (0.69, 1.2 and 1.5 Å, respectively) [27–29].

Electrospinning is a versatile fibre forming process for generating ultra-fine fibres from different materials, such as polymers, ceramics and composites [30]. Electrospun fibres can be used in many applications, such as filtering materials [31,32], sensors [33] or energy storage [34]. In the case of energy storage, electrospun fibrous electrodes have been mainly used with a combination of post-treatment processes [35,36] or with a multi-step electrospinning method [37]. The benefit of directly electrospun nanofibres is the simplicity of the process, as it does not include any post-treatment methods, such as pyrolysis and thermal treatment. Such post-treatments have been proven to be effective in eliminating the negative performance impacts of the relatively high content of non-capacitive polymer in the spun layer matrix, which is necessary for efficient fibre formation [37,38]. However, the carbonisation process itself is destructive to the fibrous structure, which in turn decreases the mechanical durability and certainly has a relatively high cost impact from a large-scale production point of view.

Our research group has previously shown that the advanced mechanical durability and flexibility of electrospun electrodes is related to their fibrous structure [38]. Furthermore, despite the relatively high polymer content, the capacitance per carbon contained remains almost constant compared to tape-casted and rolled pressed (PTFE) technologies [39].

In our previous work, electrospun carbide-derived carbon (CDC) nanofibre electrodes were studied with a focus on non-aqueous electrolytes, out of which the best performance was achieved in combination with 1.5 M spiro-(1,1′)-bipyrrolidinium tetrafluoroborate in acetonitrile (SBP-BF_4-ACN), with a potential window of 3.0 V and gravimetric capacitance of 95.3 F g^{-1} and 78.5 F g^{-1} for positively and negatively charged electrodes, respectively [39,40]. The advantages of applying non-aqueous electrolytes are a wider operative temperature range and wide potential stability range, leading to a higher energy density than aqueous electrolytes [4,12,26,41,42]. Thus, the major drawback of aqueous electrolytes

is the lower operative voltage, which is limited by the water decomposition voltage of 1.23 V [4,12,43–45]. However, the benefit of using aqueous electrolytes comes from low cost [45,46], environmental friendliness, [13,41] and higher ionic conductivity [13], leading to low resistance and superior power performance [3,41,44].

Therefore, goal of this study is to investigate the effect of aqueous electrolytes on the EDL capacitance, resistance and cyclability of electrospun fibrous CDC-based electrodes. The specific effects of cations and anions in aqueous solutions are evaluated in a three-electrode system configuration, and the cycle-life performance of both aqueous and non-aqueous electrolytes is studied in two-electrode systems.

The stability during charge–discharge cycling of post-treated fibrous electrodes in aqueous media has been tested by Stojanovska et al., where stable performance was achieved for more than 1000 cycles [47]. Furthermore, T. He et al. showed good cycle stability and a high capacitance retention of ~99.3% after 1000 cycles of polyacrylonitrile/polyvinyl-pyrrolidone electrospun composite fibres in an IL-based electrolyte in 1-butyl-3-methylimidazolium hexafluorophosphate [36]. Compared to fibrous electrodes, activated carbon-based cast electrodes have also shown long and stable cycle stability in aqueous and non-aqueous electrolytes [25,48,49]. In addition, L. Demarconnay et al. showed stable cycle stability up to 10,000 cycles at different voltage limits with cast electrodes in a 0.5 M aqueous Na_2SO_4-H_2O system [25]. However, the effect of different electrolytes on the cycle-life performance of directly electrospun electrodes has not been studied to our knowledge.

2. Experimental Section

2.1. Materials and Processes

The electrodes for electrochemical analysis of cation and anion influence on EDL performance in aqueous electrolytes were prepared by the electrospinning method, according to a similar electrode process and recipe from our previous studies [39,40]. The carbide-derived carbon active material was purchased from Skeleton Technologies OÜ (Tallinn, Estonia). Titanium carbide was converted to porous CDC carbon by applying Cl_2 treatment at 900 °C. A hydrogen gas purification step at 800 °C was applied to remove residues of chlorine in the converted CDC. The CDC material initial particle size was 1–5 μm, which was further milled to reduce the size of particles to ~100 nanometres. The detailed milling procedure is described in our previous work [40] and more detailed carbon surface chemistry is discussed by M. Käärik et al. [15] The resulting milled CDC particles were mixed with a carbon conductive additive (Super C, Timcal, Deutschland GmbH, Düsseldorf, Germany) at a ratio of 80/20 (wt %). The carbon mixture was sonicated in dimethylformamide (DMF, Sigma Aldrich, Tartu, Estonia) for 2 h. After sonication, mechanical stirring was applied for another 24 h at 40 °C, after which polyacrylonitrile (PAN, Sigma Aldrich, Tartu, Estonia M_w = 150,000 g mol^{-1}) was added to the solution at 7% weight, and the solution was stirred for an additional 24 h at 40 °C. The weight ratio of polymer to total mass of carbon was 50/50 in the solution. Finally, 15% by weight of 1-ethyl-3-methylimidazolium tetrafluoroborate (EMIm-BF_4, Sigma Aldrich, Tartu, Estonia, purity $\geq$ 99.9%) ionic liquid (IL) was added to the electrospinning solution and stirred for 0.5 h before the electrospinning process was initiated. The addition of IL is necessary to increase the conductivity of the solution for a stable electrospinning process. The electrospinning parameters were set as constant: solution pumping rate of 0.5 mL h^{-1}, applied DC voltage of 15 kV, and a distance between spinneret and rotating drum of 8 cm. After electrospinning, the fibrous electrodes were mechanically compressed by a hydraulic static press (Scamia) to achieve better electrical contacts between the fibres. The morphology of the CDC-based fibrous electrode was evaluated by scanning electron microscopy (SEM, Gemini Zeiss Ultra 55, Graz, Austria), as shown in Figure 1.

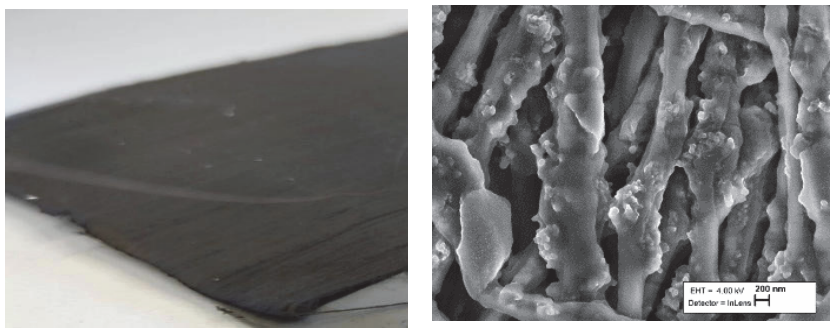

(a) (b)

Figure 1. (**a**) Electrospun electrode 3 × 4 cm^2 sheet and (**b**) morphology of the fibres by examined SEM.

The porosity characteristics of the CDC powder before and after milling and of the electrospun electrode were determined from the N_2 adsorption method at −196 °C using the NOVA touch LX2 (Quantachrome Instruments, Boynton Beach, FL, USA). Before gas adsorption measurement, the carbon samples were dried for 12 h under a vacuum at 300 °C, and the electrode sample was dried at 100 °C to avoid strongly exceeding the glass transition temperature of PAN. The Brunauer–Emmmet–Teller surface area (S_{BET}) was calculated from N_2 adsorption data according to BET theory [50] at a pressure interval P/P_0 of 0.02–0.2, and the total pore volume (V_{tot}) was calculated at a P/P_0 of 0.97. Calculations of the pore size distribution (PSD), micropore volume (V_μ) and specific surface area (S_{dft}) were performed by using the quenched solid density functional theory (QSDFT) equilibria model for slit-type pores. The N_2 adsorption–desorption isotherms are shown in Figure 2, and the porosity characteristics are presented in Table 1. The isotherms of CDCs appear as Type I, corresponding to microporous materials [51]. One can see from the porosity analysis that both the specific surface area of carbon and the amount of micropores slightly decreased during the milling process.

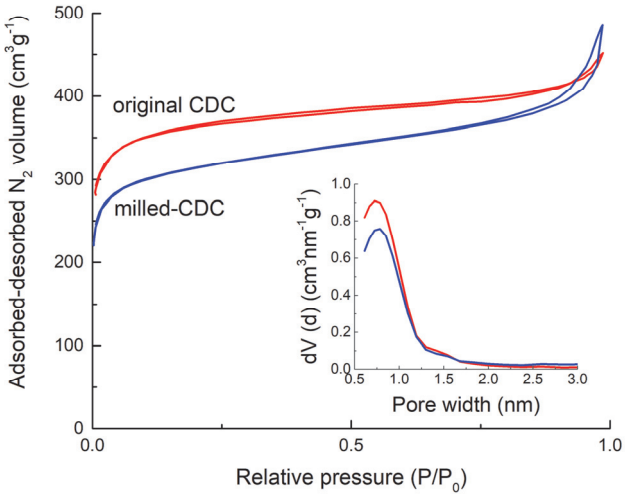

Figure 2. N_2 absorption–desorption isotherms and pore size distribution of the CDC before and after milling.

Table 1. Porosity characteristics of CDC.

Material	Sa_{BET}	Sa_{dft}	V_{tot}	$V_{\mu\ dft}$
	$m^2\ g^{-2}$	$m^2\ g^{-2}$	$cm^3\ g^{-2}$	$cm^3\ g^{-2}$
Non-milled	1282	1390	0.67	0.53
Milled	1098	1173	0.66	0.44

The thermal stability of the electrode was evaluated by thermal gravimetric analysis (Labsys EVO TG DTA 1600 °C, Ankara, Turkey). The temperature increase rate was set to 5 °C min^{-1}, and the sample was heated to 600 °C. The start of degradation of the electrode was observed at ~250 °C.

The mechanical properties of the electrospun CDC-based fibrous electrodes were evaluated by an Instron 5866 (Norwood, MA, USA) tensile testing machine. For optimal mechanical properties, morphology, and capacitance (tested after the stress test), a specific stress of 2.32×10^{-4} N TEX^{-1} was determined. More detailed porosity analysis, TGA and mechanical strength analysis can be found in our previous works [38–40].

The intermolecular interactions within the nanofibrous mats treated with Na_2SO_4-H_2O, $NaNO_3$-H_2O and KNO_3-H_2O aqueous electrolytes were analysed by Fourier transform infrared spectroscopy (FTIR). FTIR spectra obtained by means of Interspec 200-X (Tartu, Estonia) instrument with attenuated total reflection (ATR) unit. A wavenumber range a 400–4000 cm^{-1} with a 0.5 cm^{-1} resolution was used. IR absorption spectra show significant stability of electrospun PAN fibres in electrolytes and strong absorption of anions on the fibre surface. The measured FTIR spectra are presented in Figure 3. To analyse the influence of electrolytes on the intermolecular interactions of PAN/DMF fibres, electrospun samples were kept in the electrolytes for 48 h and thereafter washed with distilled water to remove the salt residues. Afterwards, the samples were dried under a vacuum at 95 °C for 24 h. The reference data in Figure 3 show the peaks of pure electrospun PAN fibre. Bands attributed to main chain groups, C-C stretching vibrations (1245 cm^{-1}), C-H symmetric vibrations (2936 cm^{-1} and 1360 cm^{-1}), and in- and out-of-plane bending vibrations (1450 cm^{-1} and 1071 $cm^{-1,}$ respectively), demonstrate neither polymer decomposition nor macromolecular structure changes after exposure to the electrolyte [52–55]. The most common PAN undergoes hydrolysis and thermal oxidation in the dissolved state. However, no corresponding peaks were observed. Furthermore, the absorption band of the nitrile side group (C≡N, 2245 cm^{-1}) shows no significant change in intensity or peak area, which means no hydrogen bond formation between the nitrogen atom of the nitrile group and anions, NO_3^- or SO_4^{2-}, was observed. At the same time, peaks corresponding to the above-mentioned anions were present in the spectra of PAN electrodes exposed to the electrolyte. For nitrate-based electrolytes, a strong peak at 1356 cm^{-1} and a small peak at 835 cm^{-1} were observed, corresponding to asymmetric and symmetric stretching of the NO_3^- group, respectively [53]. For the sulphate-based electrolyte, the peaks were located at 1123 cm^{-1} and 615 cm^{-1}, indicating asymmetric stretching of SO_4^{2-} groups [54]. This can be explained by the absorption of salt anions via electrostatic interactions with dipoles formed on the fibre surface by the -C≡N group of PAN [56]. Thus, one could conclude the chemical stability of electrospun fibres in the studied electrolytes together with the ability to absorb anions on the fibre surface.

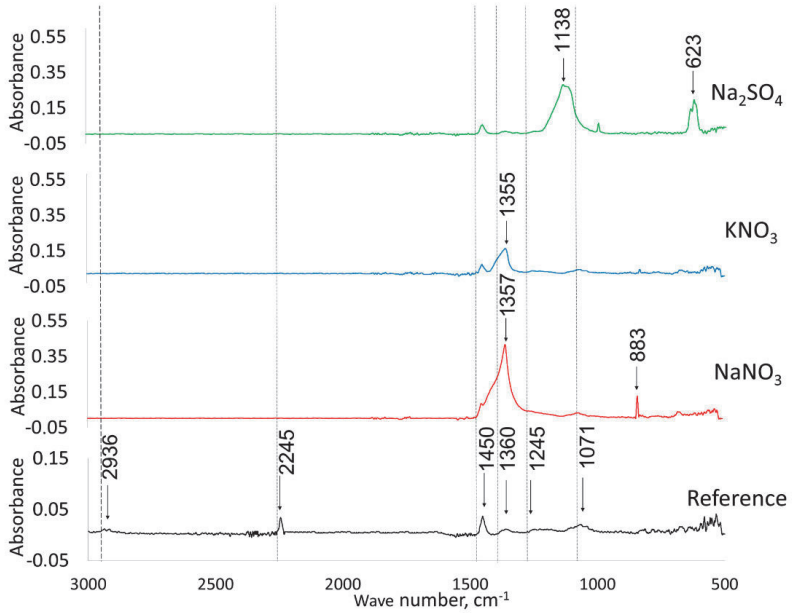

Figure 3. FTIR spectra of PAN/DMF fibre (reference) and the fibres soaked in aqueous 1.0 M electrolytes: Na_2SO_4-H_2O, KNO_3-H_2O, KNO_3-H_2O.

Two- and three-electrode test cells were used for electrochemical testing. Electrospun fibrous mats with a coating weight of 1.86 g m^{-2} were used in all experimental cells. A working electrode (WE) with a diameter of 6 mm was cut for the 3-electrode cells, and identical electrodes of 15 mm diameter were cut for the 2-electrode set-up. For 3-electrode systems, a 15 mm diameter counter electrode (CE) and Ag | AgCl (3.5 M KCl) reference electrode (RE) were used. Prior to cell assembly, the cut electrodes were dried in a vacuum oven at 100 °C for 24 h. The electrodes were then contacted with gold current collectors in electrochemical test cells. The WE and CE were interleaved by a 1 mm thick glass fibre separator membrane (purchased from VWR, Dresden, Germany). The 2-electrode test cells applied a cellulosic separator (purchased Nippon Kodoshi, Kochi, Japan).

Three aqueous electrolyte solutions from different salts—$NaNO_3$-H_2O (Lach-Ner, Neratovice, Czech Republic), KNO_3-H_2O (Sigma-Aldrich, Tartu, Estonia) and Na_2SO_4-H_2O (Sigma-Aldrich, Tartu, Estonia)—were prepared to study the EDLC of CDC-based electrospun fibrous electrodes. For the analysis of the electrolyte ionic composition effect, the concentration of the electrolyte solutions was kept constant at 1.0 M. To additionally investigate the effect of electrolyte concentration on the capacitance and resistance, the $NaNO_3$-based electrolyte concentration was altered from 0.2 M to 5.0 M. The electrolyte conductivity was measured at room temperature with a Benchtop conductivity metre (SevenCompactTM S230, Columbus, OH, USA). Electrolyte pH was measured by a standard Ag | AgCl double junction pH combination electrode (Sigma-Aldrich, Tartu, Estonia). The physical parameters of the selected salts and electrolyte solutions are presented in Table 2.

Table 2. Conductivity, pH values and ion sizes [30] for used aqueous electrolytes.

Salt	Molarity, M	Conductivity, mS cm^{-1}	pH	Ion Radius, nm	
				Cation	Anion
Na_2SO_4	1.0	78.2	7.13	0.12	0.24
KNO_3	1.0	73.2	7.34	0.15	0.17
$NaNO_3$	0.2	73.0	6.85		
$NaNO_3$	1.0	89.2	7.10	0.12	0.17
$NaNO_3$	2.5	103.0	7.08		
$NaNO_3$	5.0	117.2	7.02		

The 3-electrode studies were conducted with all electrolyte alternatives, while 2-electrode stability studies were performed with two aqueous and two organic electrolytes: 1 M $NaNO_3$-H_2O, 1 M KNO_3-H_2O, and 1.5 M 1-ethyl-3-methylimidazolium-bis (trifluoromethyl sulfonyl) imide in acetonitrile (EMIm-TFSI-ACN) and SBP-BF_4-ACN. The selection of aqueous electrolytes for cycle life analysis was based on the results of 3-electrode cells. The choice of organic electrolytes was made based on the results of our previous work, where the maximum potential window of $dU \leq 3.5$ V was determined in 1.5 M EMIm-TFSI-ACN, showing an identical gravimetric capacitance of 89.8 F g^{-1} for positively and negatively charged electrodes. Second, the largest potential window of 3.0 V was reached in 1.5 M SBP-BF_4-ACN-type quaternary ammonium salt-based electrolytes, with a gravimetric capacitance of 95.3 F g^{-1} and 78.5 F g^{-1} for positively and negatively charged electrodes, respectively [16].

2.2. Electrochemical Evaluation Methods

Cyclic voltammetry (CV), constant current cycling (CC) and electrochemical impedance spectroscopy (EIS) tests were performed to electrochemically evaluate the electrospun fibrous electrodes. All electrochemical measurements were performed at room temperature with Gamry Interface 1010 E equipment (Warminster, PA, USA).

CV plots were obtained from 3-electrode measurements in the potential range of +0.6 V to −0.7 V (vs. AgIAgCl RE) at potential scan rates of 200 to 5 mV s^{-1}. The capacitance was calculated by dividing the measured current i by the applied potential scan rate v, according to Equation (1):

$$C = \frac{i}{v} \tag{1}$$

A constant current charge–discharge study was performed between the potential limits of +0.6 V to 0 V and −0.6 V to 0 V for positively and negatively charged electrodes, respectively, (vs. AgIAgCl RE). The experiments were performed with different polarisation potentials to determine the DL- properties of the cation and anion of different electrolytes. To achieve the maximum capacitance limits for positively and negatively charged electrodes, the cells were held at fixed potential for 5 min and then discharged; thereafter, the next cycle was started as shown in Figure 4.

Similar charge–discharge profiles were repeated five times in both positive and negative potential regions. EDL capacitance values were counted from the last three cycles. The current density was varied between 0.1 and 2 mA cm^{-2}. The capacitance values for positively (C_+) and negatively (C_-) charged electrodes were calculated by integrating the discharge curves according to Equation (2):

$$\begin{aligned} C_+ &= \int_{0.6}^{0} \frac{|I|dt}{\Delta E} \\ C_- &= \int_{-0.6}^{0} \frac{|I|dt}{\Delta E} \end{aligned} \tag{2}$$

where I is the current density, dt is the discharge time, and ΔE is the potential range of the positively or negatively charged electrodes (0.6 V) [42].

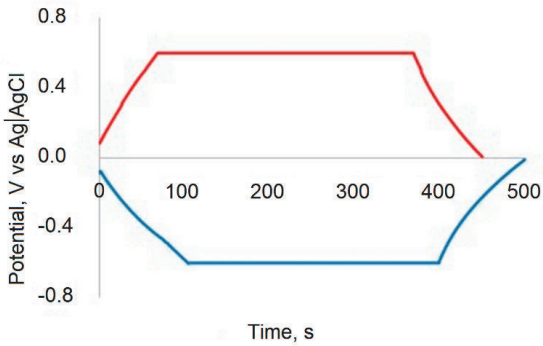

Figure 4. Constant current discharge curve at 0.25 mA cm^{-2}.

The EIS spectra were measured in the AC frequency range from 1 MHz to 50 mHz at an amplitude of the sinusoidal voltage of 5 mV. The total impedance (*Z*) of RC circuits was described by Equation (3):

$$Z = Z' + Z'' = R + \frac{1}{j\omega C_s} \quad (3)$$

where Z' is described as the real impedance, Z'' is the imaginary impedance, j is the imaginary number $\sqrt{-1}$, ω is the angular frequency $\omega = 2\pi f$, and C_s is the series capacitance.

R_s values were determined by frequency response analysis and are equal to real impedance, $R_s = Z'$.

The series capacitance C_S values of the EIS were calculated from Equation (4) [57,58]:

$$C_s = -\frac{1}{\omega Z''} \quad (4)$$

The specific capacitance values were obtained by dividing the capacitance value from different methods by the mass of carbon in the working electrode.

The CV method was used to evaluate the cycle stability of electrospun electrodes in various organic and aqueous electrolytes in a two-electrode test cell configuration. The cycling test was performed at a potential scan rate of v = 20 mV s^{-1} for <3000 cycles. The applied voltage range for organic electrolytes was 0 to 2.3 V and, for the aqueous electrolytes, the voltage limit was reduced to 1.0 V to prevent water decomposition. The capacitance decrease was monitored via the CV method, while the resistance (R_s) increase was evaluated by the EIS method at 0 V (DC), at f = 1 kHz.

3. Results and Discussion

3.1. Electrochemical Evaluation of Fibrous Electrodes in Aqueous Electrolytes

The stability and ideal polarisation region of fibrous CDC-based electrodes in the selected aqueous electrolytes was evaluated by cyclic voltammetry [59], for which three-electrode cell curves are as shown in Figure 5.

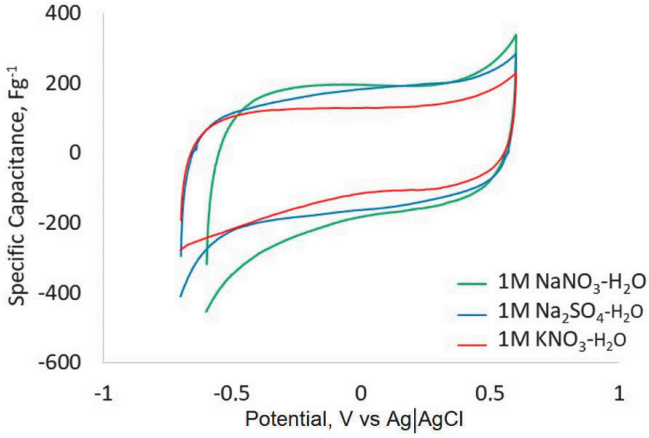

Figure 5. Cyclic voltammograms expressed as capacitance per CDC weight in fibrous electrodes in 1 M aqueous electrolytes (v = 20 mV s^{-1}).

Aqueous electrolyte solutions are known to cause reduction reactions at higher negative electrode potentials, leading to the formation of hydrogen gas and water oxidation reactions at the positive electrode potential limits, resulting in the formation of oxygen. In the case of the KNO_3-H_2O electrolyte, the oxidation and reduction processes are somewhat less evident in Figure 5, as the potential limits have not yet been reached or exceeded significantly. When the cation is replaced from K^+ to Na^+, an exponential increase in current at potentials close to −0.5 V was observed, indicating the possible competing hydrogen ion adsorption and reduction on the carbon surface in parallel with adsorption of Na^+, being more pronounced compared to the K^+ based electrolyte. Furthermore, differences in the capacitance of nitrate-based electrolytes were observed for both positive and negative electrode potential regions, being lower for the KNO_3 electrolyte. This can be explained by the different cation sizes of Na^+/K^+, and during such measurements, cation and anion adsorption are still slightly affected by the reduction and oxidation processes. According to the CV curves presented in Figure 5, no difference in capacitance was observed in the positively charged region by the exchange of anions from NO_3^- to SO_4^{2-}, although the nitrate ion was much smaller than the sulphate ion. To further study the ion-related capacitance effects, the CC method was applied at current densities between 0.1 and 2 mA cm^{-2}, with the results presented in Figure 6a–c and in Table 3.

Table 3. Gravimetric capacitance values for positively and negatively charged electrodes evaluated by CC tests at a current density of 0.5 mA cm^{-2} in 1 M solutions.

Electrolyte	C^+ Electrode, F g^{-1}	C^+ CDC, F g^{-1}	C^- Electrode, F g^{-1}	C^- CDC, F g^{-1}
$NaNO_3$-H_2O	40.8	177.5	63.5	276.1
KNO_3-H_2O	47.7	132.0	57.0	157.6
Na_2SO_4-H_2O	34.6	150.7	51.0	221.9

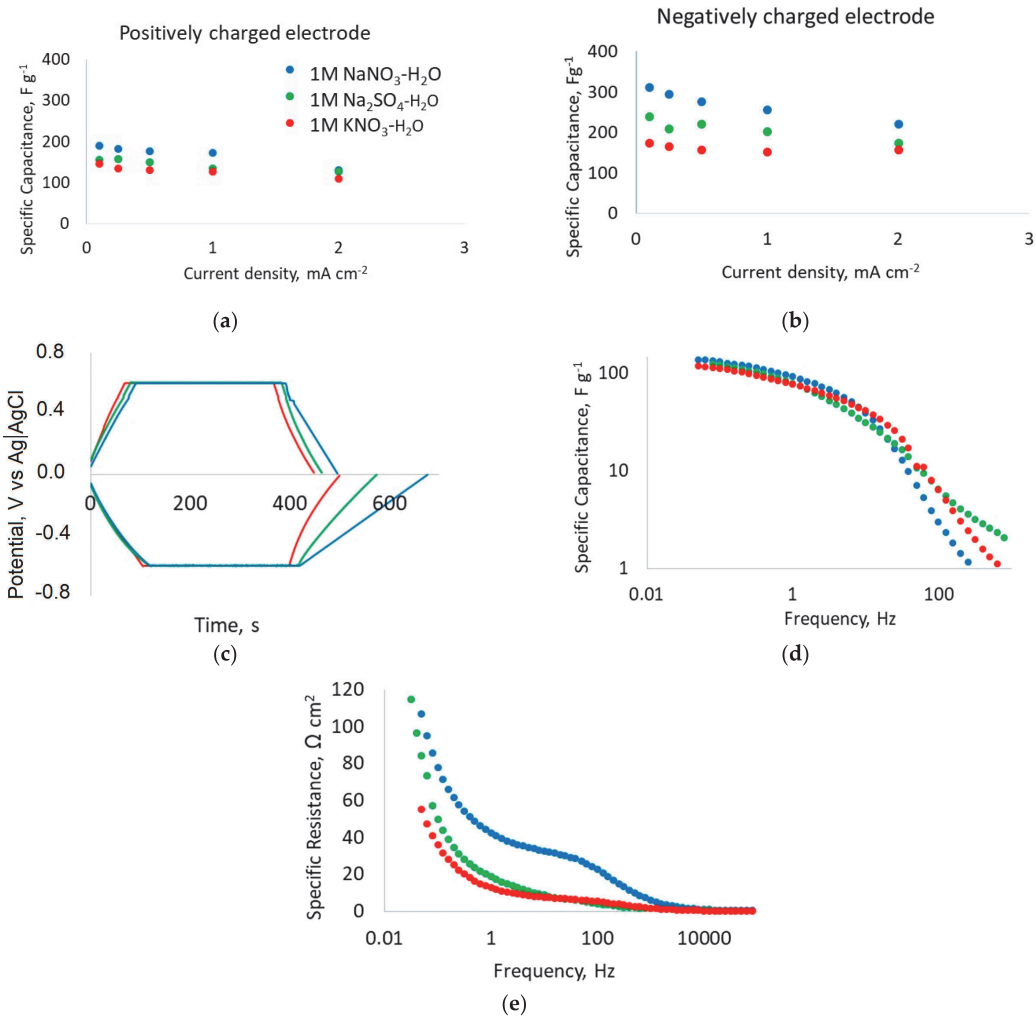

Figure 6. Electrochemical performance of "electropsun" CDC based fibrous electrodes in aqueous electrolytes: (**a**,**b**) specific capacitance values from CC discharge plots at I = 0.5 mA cm^{-2} for positively and negatively charged electrodes, (**c**) CC charge–discharge, curves I = 0.5 mA cm^{-2} (**d**) specific capacitance, C_s as a function of frequency and (**e**) resistance, R_s as a function of frequency from EIS measurements at 0 V vs. Ag | AgCl.

The capacitance dependence of the negatively charged electrode (Figure 6b) shows that Na^+, with an ion size 20% smaller than the K^+ ion, increases the specific capacitance up to 30% at a current density of 2 mA cm^{-2}. By reducing the applied current density, the ions have a longer time to migrate and adsorb onto the carbon surface and, thus, the specific capacitance increases even more. When the NO_3^- anion was replaced by SO_4^{2-}, the specific capacitance at 2 mA cm^{-2} was practically equal, although the ion radius of the SO_4^{2-} anions was significantly larger than that of NO_3^- (Figure 6a). This result is in line with the previously described CV measurements. However, by reducing the applied current density, the specific capacitance in NaNO3-H2O increased compared to SO_4^{2-}, as expected according to the ion size comparison.

The effect of the aqueous electrolytes on the capacitance and resistance of fibrous CDC-based electrodes was further evaluated by electrochemical impedance spectroscopy

measurements recorded at DC = 0 V (vs. ref) to characterise the uncharged surface properties. Based on these measurements, the series capacitance values were calculated using Equation (4), and the results are shown in Figure 6d. In all three studied electrolyte solutions, the adsorption of ions into carbon pores begins at frequencies f < 100 Hz, with a steep increase in capacitance. At f < 1 Hz, a capacitance plateau begins to form when most ions are adsorbed to carbon micropores (Figure 6d). The capacitance in different 1.0 M solutions did not differ significantly, which can be explained by the uncharged (E_{DC} = 0 V) electrode surface. In the frequency range of 10–100 kHz, much lower *Rs* values were obtained compared to the low-frequency ranges (Figure 6e) due to electrolyte ion migration and adsorption/desorption rate effects, i.e., At high frequency, ions do not have enough time to migrate to the carbon pores, and the electrode behaves like a smooth surface. Ion adsorption reaches maximum levels only at low frequencies, which is reflected by the significant increase in capacitance and resistance [2,40]. Surprisingly, the highest resistance was observed in the low frequency region of the $NaNO_3$-H_2O solution, although it has the smallest anion/cation size and slightly higher conductivity compared to other electrolytes.

3.2. Effect of Electrolyte Concentration on Fibrous Electrode Performance

The effect of electrolyte salt concentration on the electrochemical performance of fibrous CDC-based electrodes was evaluated in $NaNO_3$-H_2O solutions of 0.2 M, 1.0 M, 2.5 M, and 5.0 M molarity. The conductivity and pH values of the prepared electrolytes are shown in Table 1. The specific capacitance of positively and negatively charged electrodes was determined at different current densities of CC, presented in Figure 7a,b. The areal capacitance as a function of frequency and Nyquist plots are presented in Figure 7c,d, respectively.

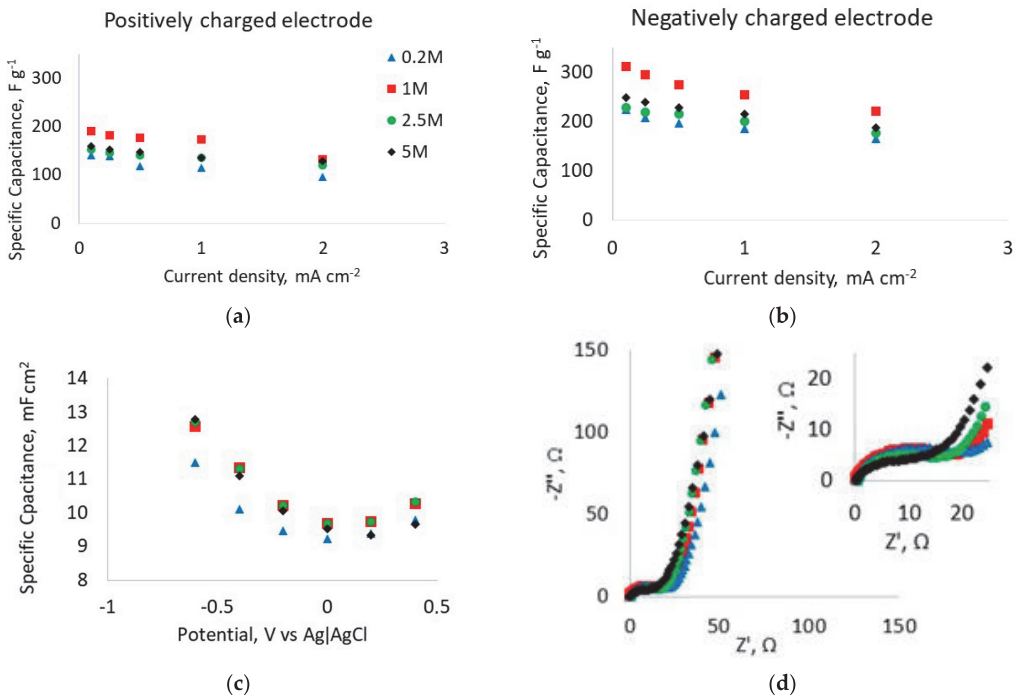

Figure 7. Electrochemical performance of "electropsun" CDC-based fibrous electrodes in xM NaNO3 electrolytes: (**a**,**b**) capacitance values obtained from CC discharge plots at I = 0.5 mA cm-2 for positively and negatively charged electrodes, (**c**) Cs (at I = 50 mHz) as a function of potential from EIS measurements and (**d**) Nyquist plot at 0 V (vs. Ag | AgCl).

The rate capability analysis (*C* vs. *I* in Figure 7a,b) gave the highest capacitance at a concentration of 1.0 M of $NaNO_3$. However, it is generally known that by increasing the concentration of electrolyte salt, the charge-transfer resistance of EDLC cells is decreased while the capacitance and rate capability are increased [60,61]. However, there are no major differences in the obtained capacitance values, as higher salt concentrations also increase the viscosity of the electrolyte and promote the saturation of active ions on the carbon surface [60,61].

The capacitance-potential dependency was additionally analysed with the EIS method at different fixed electrode potentials (Figure 7c). It was confirmed that negatively charged electrodes have higher capacitance over the electrode area, as also observed by the CC measurements. The change in capacitance as a function of the electrode potential is precisely defined, where it has a clear minimum for all solution concentrations close to zero charge potential of 0 V vs. Ag | AgCl, with marginal effects from the concentration. Some differences in the absolute capacitance values from CC and EIS measurements are mainly due to the differences in the measurement methodology. The capacitance from the EIS technique is calculated at relatively high frequencies (~50 mHz) at which the boundary diffusion of different electrolyte ions has not yet been reached, while constant current measurements at very low current densities of 0.1 mA cm^{-2} allow for the finite ion diffusion to occur.

The Nyquist plots (Figure 7d) show the highest impedance for the cells with the lowest ionic conductivity electrolyte of 0.2 M concentration. Figure 7d also shows a small decrease in charge-transfer resistance (semi-circle) for uncharged electrodes by increasing the salt concentration. Additionally, the differences in capacitance and resistance decreased at higher concentrations because enough electrolyte ions were adsorbed on the carbon electrode. However, due to the increase in viscosity at higher concentrations, the expected increase in capacitance and decrease in resistance were less evident. Such results are well in accordance with the CC measurement data.

3.3. Cycle-Stability Analysis for Full Cells

Two-electrode systems were applied to analyse the long-term cycle stability of fibrous CDC-based electrode materials. Cycle-life tests in selected aqueous and non-aqueous electrolytes were performed using the CV method (v = 20 mVs^{-1}) in voltage ranges of 0–1.0 V and 0–2.3 V, respectively, where the change in capacitance was assessed during CV discharge cycles, and the change in resistance was evaluated by EIS at f = 1 kHz. The capacitance and resistance change over the cycles is shown in Figure 8a,b. Stable results over ~1000 cycles were observed for both aqueous electrolytes and the organic 1.5 M SBP-BF_4-ACN electrolyte. An exponential decrease in capacitance and increase in resistance during cycling was observed in the 1.5 M EMIm-TFSI-ACN electrolyte. Such unstable behaviour can be caused by the relatively high viscosity of the electrolyte and possibly an excessively high voltage scanning rate, which does not support efficient ion transfer and adsorption on the electrodes [40]. For the SBP-BF_4-ACN and KNO_3-H_2O electrolytes, no significant change in capacitance was observed over the cycles. The increase in SBP-BF_4-ACN cell resistance was typical of EDL capacitors and increased by only 21% over 3000 cycles, while the resistance of the KNO_3 capacitor was almost constant.

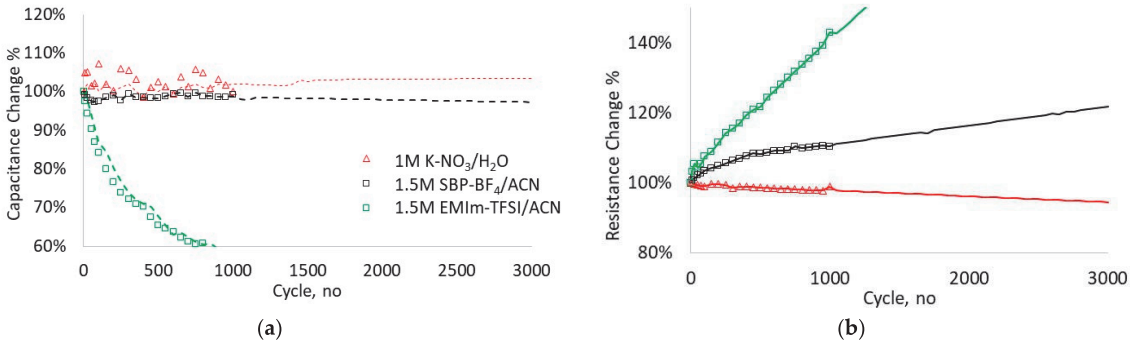

Figure 8. Cycle-life performance of fibrous CDC-based electrodes of 1000 cycles (shapes) with extrapolation of 3000 cycles (lines): (**a**) capacitance retention by CV at 20 mV s^{-1} and (**b**) series resistance change during cycling by EIS.

4. Conclusions

The present study investigated the influence of aqueous $NaNO_3$-H_2O, KNO_3-H_2O and Na_2SO_4-H_2O electrolyte ionic composition and concentration on the electrochemical behaviour of directly electrospun carbide-derived carbon electrodes. The highest gravimetric capacitances of 191 F g^{-1} and 311 F g^{-1} for positively and negatively charged electrodes, respectively, were achieved in 1 M $NaNO_3$-H_2O at 0.1 mA cm^{-2}. The capacitance values in 1 M Na_2SO_4-H_2O and 1 M KNO_3-H_2O electrolyte solutions were 23% and 30% lower than that of $NaNO_3$-H_2O, respectively. The results correlate well with the electrolyte ion sizes.

A salt concentration effect study on the fibrous electrodes showed that a $NaNO_3$-H_2O concentration of 1.0 M is optimum for capacitive performance. On the other hand, a higher salt concentration (>1 M) slightly improved the cell resistance at the expense of increased electrolyte conductivity.

Based on the analysis of the two-electrode cells, a stable cycle life was achieved with both non-aqueous SBP-BF_4-ACN and aqueous $NaNO_3$-H_2O and Na_2SO_4-H_2O electrolytes. In the case of aqueous electrolyte solutions, some further ion absorption effects were observed in the first few hundred cycles of the cycle-life test, leading to an increase in capacitance, followed by a generally expected declining trend.

Author Contributions: Data curation, S.M., K.L., M.K.; investigation, S.M., K.L., M.K. and E.T.; methodology, S.M. and M.A.; resources, V.V.; supervision, M.A. and A.K.; validation, S.M., K.L., M.K. and I.K.; writing—original draft, S.M.; writing—review and editing, A.K., M.A. and A.L. All authors have read and agreed to the published version of the manuscript.

Funding: This work was financially supported by the European Space Agency, ESA contract number 4000119258/16/NL/CBi "Fully electrospun durable electrode and electrochemical double-layer capacitor for high frequency applications" and the European Union European Regional Development Fund through Foundation Archimedes (TK143).

Institutional Review Board Statement: Not applicable.

Acknowledgments: We thank senior researcher Valdek Mikli for SEM analyses and Can Rüstü Yörük for TGA analyses.

Conflicts of Interest: The authors declare no conflict of interest.

References

1. Yu, A.; Chabot, V.; Zhang, J. *Electrochemical Supercapacitors for Energy Storage and Delivery: Fundamentals and Applications*; CRC Press: Boca Raton, FL, USA, 2017.
2. Beguin, F.; Frackowiak, E. *Supercapacitors: Materials, Systems, and Applications*; John Wiley & Sons: Hoboken, NJ, USA, 2013.
3. Zhong, C.; Deng, Y.; Hu, W.; Qiao, J.; Zhang, L.; Zhang, J. A review of electrolyte materials and compositions for electrochemical supercapacitors. *Chem. Soc. Rev.* **2015**, *44*, 7484–7539. [CrossRef]

4. Menzel, J.; Fic, K.; Frackowiak, E. Hybrid aqueous capacitors with improved energy/power performance. *Prog. Nat. Sci. Mater. Int.* **2015**, *25*, 642–649. [CrossRef]
5. Guerrero-Martínez, M.Á.; Romero-Cadaval, E.; Minambres-Marcos, V.; Milanés-Montero, M.I. Supercapacitor Energy Storage System for Improving the Power flow in Photovoltaic Plants. *Electron. Compon. Mater.* **2014**, *44*, 3. [CrossRef]
6. Zhao, C.; Zheng, W. A Review for Aqueous Electrochemical Supercapacitors. *Front. Energy Res.* **2015**, *3*, 1–5. [CrossRef]
7. Horn, M.; MacLeod, J.; Liu, M.; Webb, J.; Motta, N. Supercapacitors: A new source of power for electric cars? *Econ. Anal. Policy* **2019**, *61*, 93–103. [CrossRef]
8. Burke, A.; Zhao, H. *Applications of Supercapacitors in Electric and Hybrid Vehicles*; 5th European Symposium on Supercapacitor and Hybrid Solutions (ESSCAP): Brasov, Romania, 2015; p. 15.
9. Weingarth, D.; Noh, H.; Foelske-Schmitz, A.; Wokaun, A.; Kötz, R. A reliable determination method of stability limits for electrochemical double layer capacitors. *Electrochim. Acta* **2013**, *103*, 119–124. [CrossRef]
10. Käärik, M.; Arulepp, M.; Käärik, M.; Maran, U.; Leis, J. Characterization and prediction of double-layer capacitance of nanoporous carbon materials using the Quantitative nano-Structure-Property Relationship approach based on experimentally determined porosity descriptors. *Carbon* **2020**, *158*, 494–504. [CrossRef]
11. Arulepp, M.; Leis, J.; Lätt, M.; Miller, F.; Rumma, K.; Lust, E.; Burke, A. The advanced carbide-derived carbon based supercapacitor. *J. Power Sources* **2006**, *162*, 1460–1466. [CrossRef]
12. Ramachandran, R.; Wang, F. Electrochemical Capacitor Performance: Influence of Aqueous Electrolytes. *Supercapacitors Theor. Pract. Solut.* **2017**. [CrossRef]
13. Pal, B.; Yang, S.; Ramesh, S.; Thangadurai, V.; Jose, R. Electrolyte selection for supercapacitive devices: A critical review. *Nanoscale Adv.* **2019**, *1*, 3807–3835. [CrossRef]
14. Dyatkin, B.; Mamontov, E.; Cook, K.M.; Gogotsi, Y. Capacitance, charge dynamics, and electrolyte-surface interactions in functionalized carbide-derived carbon electrodes. *Prog. Nat. Sci.* **2015**, *25*, 631–641. [CrossRef]
15. Käärik, M.; Arulepp, M.; Kook, M.; Mäeorg, U.; Kozlova, J.; Sammelselg, V.; Perkson, A.; Leis, J. Characterisation of steam-treated nanoporous carbide-derived carbon of TiC origin: Structure and enhanced electrochemical performance. *J. Porous Mater.* **2017**, *25*, 1057–1070. [CrossRef]
16. Käärik, M.; Arulepp, M.; Kook, M.; Kozlova, J.; Ritslaid, P.; Aruväli, J.; Mäeorg, U.; Sammelselg, V.; Leis, J. High-performance microporous carbon from deciduous wood-origin metal carbide. *Microporous Mesoporous Mater.* **2019**, *278*, 14–22. [CrossRef]
17. Lota, K.; Sierczynska, A.; Acznik, I. Effect of aqueous electrolytes on electrochemical capacitor capacitance. *Chemik* **2013**, *67*, 1138–1145.
18. Barzegar, F.; Momodu, D.Y.; Fashedemi, O.O.; Bello, A.; Dangbegnon, J.K.; Manyala, N. Investigation of different aqueous electrolytes on the electrochemical performance of activated carbon-based supercapacitors. *RSC Adv.* **2015**, *5*, 107482–107487. [CrossRef]
19. Ibukun, O.; Jeong, H.K. Effects of Aqueous Electrolytes in Supercapacitors. *New Phys. Sae Mulli* **2019**, *69*, 154–158. [CrossRef]
20. Lang, A.W.; Ponder, J.F.; Österholm, A.M.; Kennard, N.J.; Bulloch, R.H.; Reynolds, J.R. Flexible, aqueous-electrolyte supercapacitors based on water-processable dioxythiophene polymer/carbon nanotube textile electrodes. *J. Mater. Chem. A* **2017**, *5*, 23887–23897. [CrossRef]
21. Mao, X.; Hatton, T.A.; Rutledge, G.C. A Review of Electrospun Carbon Fibers as Electrode Materials for Energy Storage. *Curr. Org. Chem.* **2013**, *17*, 1390–1401. [CrossRef]
22. Frackowiak, E.; Abbas, Q.; Béguin, F. Carbon/carbon supercapacitors. *J. Energy Chem.* **2013**, *22*, 226–240. [CrossRef]
23. Ruiz, V.; Santamaría, R.; Granda, M.; Blanco, C. Long-term cycling of carbon-based supercapacitors in aqueous media. *Electrochim. Acta* **2009**, *54*, 4481–4486. [CrossRef]
24. Khomenko, V.; Raymundo-Piñero, E.; Béguin, F. A new type of high energy asymmetric capacitor with nanoporous carbon electrodes in aqueous electrolyte. *J. Power Sources* **2010**, *195*, 4234–4241. [CrossRef]
25. Demarconnay, L.; Raymundo-Piñero, E.; Béguin, F. A symmetric carbon/carbon supercapacitor operating at 1.6V by using a neutral aqueous solution. *Electrochem. Commun.* **2010**, *12*, 1275–1278. [CrossRef]
26. Béguin, F.; Presser, V.; Balducci, A.; Frackowiak, E. Carbons and Electrolytes for Advanced Supercapacitors. *Adv. Mater.* **2014**, *26*, 2219–2251. [CrossRef] [PubMed]
27. Cai, Y.-M.; Qin, Z.-Y.; Chen, L. Effect of electrolytes on electrochemical properties of graphene sheet covered with polypyrrole thin layer. *Prog. Nat. Sci.* **2011**, *21*, 460–466. [CrossRef]
28. Xu, C.; Wei, C.; Li, B.; Kang, F.; Guan, Z. Charge storage mechanism of manganese dioxide for capacitor application: Effect of the mild electrolytes containing alkaline and alkaline-earth metal cations. *J. Power Sources* **2011**, *196*, 7854–7859. [CrossRef]
29. Jenkins, H.D.B.; Thakur, K.P. Reappraisal of thermochemical radii for complex ions. *J. Chem. Educ.* **1979**, *56*, 576. [CrossRef]
30. Park, J.-S. Electrospinning and its applications. *Adv. Nat. Sci. Nanosci. Nanotechnol.* **2010**, *1*, 043002. [CrossRef]
31. Sundarrajan, S.; Tan, K.L.; Lim, S.H.; Ramakrishna, S. Electrospun Nanofibers for Air Filtration Applications. *Procedia Eng.* **2014**, *75*, 159–163. [CrossRef]
32. Rahman, M.M.; Tahkar, A.I. Use of Nano Fibers in Filtration—A review. *IJSRD-Int. J. Sci. Res. Dev.* **2016**, *4*, 7.
33. Ding, B.; Wang, M.; Wang, X.; Yu, J.; Sun, G. Electrospun nanomaterials for ultrasensitive sensors. *Mater. Today* **2010**, *13*, 16–27. [CrossRef]

34. Sun, G.; Sun, L.; Xie, H.; Liu, J. Electrospinning of Nanofibers for Energy Applications. *Nanomaterials* **2016**, *6*, 129. [CrossRef] [PubMed]
35. Li, X.; Zhao, Y.; Bai, Y.; Zhao, X.; Wang, R.; Huang, Y.; Liang, Q.; Huang, Z. A Non-Woven Network of Porous Nitrogen-doping Carbon Nanofibers as a Binder-free Electrode for Supercapacitors. *Electrochim. Acta* **2017**, *230*, 445–453. [CrossRef]
36. He, T.; Fu, Y.; Meng, X.; Yu, X.; Wang, X. A novel strategy for the high performance supercapacitor based on polyacrylonitrile-derived porous nanofibers as electrode and separator in ionic liquid electrolyte. *Electrochim. Acta* **2018**, *282*, 97–104. [CrossRef]
37. Tõnurist, K.; Vaas, I.; Thomberg, T.; Jänes, A.; Kurig, H.; Romann, T.; Lust, E. Application of multistep electrospinning method for preparation of electrical double-layer capacitor half-cells. *Electrochim. Acta* **2014**, *119*, 72–77. [CrossRef]
38. Malmberg, S.; Tarasova, E.; Vassiljeva, V.; Krasnou, I.; Arulepp, M.; Krumme, A. *Fully Elecrospun Durable Electrode and Electrochemical Double-Layer Capacitor for High Frequency Applications*; ESA SPCD: Lanskroun, Czech Republic, 2018; p. 10.
39. Malmberg, S.; Arulepp, M.; Savest, N.; Tarasova, E.; Vassiljeva, V.; Krasnou, I.; Käärik, M.; Mikli, V.; Krumme, A.; Malmberg, S. Directly electrospun electrodes for electrical double-layer capacitors from carbide-derived carbon. *J. Electrost.* **2020**, *103*, 103396. [CrossRef]
40. Malmberg, S.; Arulepp, M.; Tarasova, E.; Vassiljeva, V.; Krasnou, I.; Krumme, A. Electrochemical Evaluation of Directly Electrospun Carbide-Derived Carbon-Based Electrodes in Different Nonaqueous Electrolytes for Energy Storage Applications. *C J. Carbon Res.* **2020**, *6*, 59. [CrossRef]
41. Balbuena, P.B. Electrolyte Materials-Issues and Challenges. In Proceedings of the AIP Conference Proceedings, Freiberg, Germany, 17 February 2014; pp. 82–97. [CrossRef]
42. Conway, B.E. Behavior of the Double Layer in Nonaqueous Electrolytes and Nonaqueous Electrolyte Capacitors. In *Electrochemical Supercapacitors*; Springer: Boston, MA, USA, 1999; pp. 169–181.
43. Balducci, A. Electrolytes for high voltage electrochemical double layer capacitors: A perspective article. *J. Power Sources* **2016**, *326*, 534–554. [CrossRef]
44. Tomiyasu, H.; Shikata, H.; Takao, K.; Asanuma, N.; Taruta, S.; Park, Y.-Y. An aqueous electrolyte of the widest potential window and its superior capability for capacitors. *Sci. Rep.* **2017**, *7*, srep45048. [CrossRef]
45. Bu, X.; Su, L.; Dou, Q.; Lei, S.; Yan, X. A low-cost "water-in-salt" electrolyte for a 2.3 V high-rate carbon-based supercapacitor. *J. Mater. Chem. A* **2019**, *7*, 7541–7547. [CrossRef]
46. Lee, M.H.; Kim, S.J.; Chang, D.; Kim, J.; Moon, S.; Oh, K.; Park, K.-Y.; Seong, W.M.; Park, H.; Kwon, G.; et al. Toward a low-cost high-voltage sodium aqueous rechargeable battery. *Mater. Today* **2019**, *29*, 26–36. [CrossRef]
47. Stojanovska, E.; Pampal, E.S.; Kilic, A.; Quddus, M.; Candan, Z. Developing and characterization of lignin-based fibrous nanocarbon electrodes for energy storage devices. *Compos. Part B Eng.* **2019**, *158*, 239–248. [CrossRef]
48. Khosrozadeh, A.; Singh, G.; Wang, Q.; Luo, G.; Xing, M. Supercapacitor with extraordinary cycling stability and high rate from nano-architectured polyaniline/graphene on Janus nanofibrous film with shape memory. *J. Mater. Chem. A* **2018**, *6*, 21064–21077. [CrossRef]
49. Jia, Z.; Liu, D.Q.; Yang, S.Y. Electrochemical Insight into Cycle Stability of Organic Electrolyte Supercapacitors. *Adv. Mater. Res.* **2011**, *347–353*, 467–471. [CrossRef]
50. Brunauer, S.; Emmett, P.H.; Teller, E. Adsorption of Gases in Multimolecular Layers. *J. Am. Chem. Soc.* **1938**, *60*, 309–319. [CrossRef]
51. Thommes, M.; Kaneko, K.; Neimark, A.V.; Olivier, J.P.; Rodriguez-Reinoso, F.; Rouquerol, J.; Sing, K.S. Physisorption of gases, with special reference to the evaluation of surface area and pore size distribution (IUPAC Technical Report). *Pure Appl. Chem.* **2015**, *87*, 1051–1069. [CrossRef]
52. Lee, S.; Kim, J.; Ku, B.-C.; Kim, J.; Joh, H.-I. Structural Evolution of Polyacrylonitrile Fibers in Stabilization and Carbonization. *Adv. Chem. Eng. Sci.* **2012**, *2*, 275–282. [CrossRef]
53. Li, J.; Su, S.; Zhou, L.; Kundrát, V.; Abbot, A.M.; Mushtaq, F.; Ouyang, D.; James, D.; Roberts, D.; Ye, H. Carbon nanowalls grown by microwave plasma enhanced chemical vapor deposition during the carbonization of polyacrylonitrile fibers. *J. Appl. Phys.* **2013**, *113*, 024313. [CrossRef]
54. Surianarayanan, M.; Vijayaraghavan, R.; Raghavan, K.V. Spectroscopic investigations of polyacrylonitrile thermal degradation. *J. Polym. Sci. Part Polym. Chem.* **1998**, *36*, 2503–2512. [CrossRef]
55. Conley, R.T.; Bieron, J.F. Examination of the oxidative degradation of polyacrylonitrile using infrared spectroscopy. *J. Appl. Polym. Sci.* **1963**, *7*, 1757–1773. [CrossRef]
56. Henrici-Olivé, G.; Olivé, S. Molecular interactions and macroscopic properties of polyacrylonitrile and model substances. In *Chemistry*; Springer: Berlin/Heidelberg, Gemany, 1979; Volume 32, pp. 123–152. [CrossRef]
57. Torop, J.; Palmre, V.; Arulepp, M.; Sugino, T.; Asaka, K.; Aabloo, A. Flexible supercapacitor-like actuator with carbide-derived carbon electrodes. *Carbon* **2011**, *49*, 3113–3119. [CrossRef]
58. Barsoukov, E.; Macdonald, J.R. (Eds.) *Impedance Spectroscopy: Theory, Experiment, and Applications*, 2nd ed.; Wiley-Interscience: Hoboken, NJ, USA, 2005.

59. Feng, X. *Nanocarbons for Advanced Energy Storage, Volume 1*; John Wiley & Sons: Hoboken, NJ, USA, 2015.
60. Fic, K.; Lota, G.; Meller, M.; Frackowiak, E. Novel insight into neutral medium as electrolyte for high-voltage supercapacitors. *Energy Environ. Sci.* **2012**, *5*, 5842–5850. [CrossRef]
61. He, M.; Fic, K.; Frąckowiak, E.; Novák, P.; Berg, E.J. Influence of aqueous electrolyte concentration on parasitic reactions in high-voltage electrochemical capacitors. *Energy Storage Mater.* **2016**, *5*, 111–115. [CrossRef]

Curriculum vitae

Personal data

Name:	Siret Malmberg
Date of birth:	26.03.1993
Place of birth:	Estonia
Citizenship:	Estonia

Contact data

E-mail:	siret.malmberg@ttu.ee

Education

2017–2021	Tallinn University of Technology, Chemical and Materials Technology, PhD student
2015–2017	Tallinn University of Technology, Technology of Materials (minor field of study: Plastic Technology), Master of Sciences *(cum laude)*
2012–2015	Tallinn University of Technology, Technology of Materials (minor field of study: Plastic technology), Bachelor of Science Engineering
2004–2012	High school, “Vesiroosi” Gymnasym, Rapla

Language competence

Estonian	native speaker
English	fluent
Russian	basic skills

Professional employment

2019–...	Skeleton Technologies OÜ, Electrochemist (1.0)
2017–2019	Skeleton Technologies OÜ, Electrochemist (0.80)
2015–2016	Skeleton Technologies OÜ, Laboratory assistant (0.70)

Defended Thesis

Siret Malmberg. Master’s Diploma. 2017. (sup) Dr. Natalja Savest; Dr. Mati Arulepp. Development of supercapacitor electrodes by electrospinning Tallinn University of Technology, Faculty of Chemical and Materials Technology Department of Polymer Materials. Chair of Polymer Technology.

Elulookirjeldus

Isikuandmed

Nimi:	Siret Malmberg
Sünniaeg:	26.03.1993
Sünnikoht:	Eesti
Kodakondsus:	Eesti

Kontaktandmed

E-post:	siret.malmberg@ttu.ee

Hariduskäik

2017–...	Tallinna Tehnikaülikool, keemia- ja materjalitehnoloogia eriala, doktorantuur
2015–2017	Tallinna Tehnikaülikool, materjalitehnoloogia eriala spetsialiseerumisega plastitehnoloogiale, loodusteaduste magistrikraad *(cum laude)*
2012–2015	Tallinna Tehnikaülikool, materjalitehnoloogia erialaplastitehnoloogiale, tehnikateaduse bakalaureuse kraad
2004–2012	Rapla Vesiroosi Gümnaasium

Keelteoskus

Eesti keel	emakeel
Inglise keel	kõrgtase
Vene keel	algtase

Teenistuskäik

2019–...	Skeleton Technologies OÜ, elektrokeemik (1.0)
2017–2019	Skeleton Technologies OÜ, elektrokeemik (0.80)
2015–2016	Skeleton Technologies OÜ, laborant (0.70)

Kaitstud väitekirjad

Siret Malmberg. Magistrikraad. 2017. (juh) Dr. Natalja Savest; Dr. Mati Arulepp. Superkondensaatorite elektroodide arendus elektroketrus meetodil. Tallinna Tehnikaülikool. Keemia ja materjalitehnoloogia teaduskond. Polümeermaterjalide instituut. Polümeeride tehnoloogia õppetool.

ISSN 2585-6901 (PDF)
ISBN 978-9949-83-723-6 (PDF)